Identifying novel substrates of Salt-inducible kinase 2



David Mannion

Keble College

Nuffield Department of Obstetrics & Gynaecology,

University of Oxford

Thesis submitted for the degree of Doctor of Philosophy

2016

ABSTRACT

Salt-inducible kinase 2 (SIK2) has previously been identified as a potential therapeutic target in high-grade serous ovarian cancer. Depletion of SIK2 sensitises ovarian cancers to paclitaxel treatment both *in vitro* and in xenograft models. In patients, increased tumour SIK2 expression is associated with paclitaxel resistance and correlates with increased risk of cancer progression following paclitaxel treatment. Although high-grade serous tumours are highly chemosensitive, 80 – 90% of patients with advanced stage disease eventually relapse due to recurrent chemotherapy-resistant disease, so there is a pressing need for novel therapeutic targets. Inhibition of SIK2 is a plausible strategy to augment existing chemotherapy in ovarian cancer, but signalling downstream of SIK2 has not been well studied.

Here, I present the optimisation and results of a chemical genetic screen to identify novel SIK2 substrates to facilitate its development as a therapeutic target. The screen used a SIK2 gatekeeper mutant engineered to utilise a 'bulky' A*TPγS analogue to specifically label its substrates in lysates from an ovarian cancer cell line. A covalent capture approach was then used to isolate labelled peptides for identification by tandem mass spectrometry. Between four independent screen experiments, 73 putative substrate proteins were identified, 18 of which were present in multiple replicates.

SIK2 was found to phosphorylate the p85α regulatory subunit of PI3 kinase at S154, resulting in activation of the PI3K/AKT signalling pathway. Furthermore, PI3K/AKT signalling was stimulated in ovarian cancer cells upon incubation with primary adipocytes extracted from the omentum, a key site of ovarian cancer metastasis, in a SIK2 dependent manner. Finally, overexpression of wild-type SIK2, but not a kinase-inactive mutant, in ovarian cancer cell lines promoted tumour growth and metastasis in a xenograft model. Together, this evidence suggests that in addition to its role in chemotherapy resistance, SIK2 also promotes the establishment of omental metastases in ovarian cancer.

TABLE OF CONTENTS

List of Tables iv
List of Figures v
List of Abbreviations vii
Acknowledgements ix
Declaration x
Chapter 1: Introduction 1
1.1 Ovarian cancer 1
1.2 Salt-inducible kinase 2 3
1.2.1 SIK2 is a potential therapeutic target in HGSOC 3
1.2.2 SIK2 regulates energy balance and cellular metabolism 5
1.2.3 SIK2 regulates a variety of other processes 9
1.3 Protein kinases and kinase inhibitors 11
1.3.1 Structure and function 11
1.3.2 Kinases as therapeutic targets in cancer 12
1.4 Investigating protein phosphorylation 13
1.4.1 Kinase-substrate mapping 14
1.5 Aims & Objectives 16
Chapter 2: Materials & methods 18
2.1.1 *In vitro* kinase assays 18
2.1.2 MALDI-TOF/TOF 18
2.1.3 SDS-PAGE and western blotting 18
2.1.4 Plasmid preparations 19
2.1.5 Site-directed mutagenesis 19
2.1.6 Agarose gel electrophoresis 20
2.1.7 Cell culture 20
2.1.8 Plasmid transfection 20
2.1.9 Immunoprecipitation 21
2.1.10 Substrate labelling in live cells 21
2.1.11 Substrate labelling in cell lysates 21

2.1.12 Covalent capture of model thiophosphorylated peptide 22
2.1.13 Gateway cloning 22
2.1.14 Lentiviral transduction 23
2.1.15 Kinase-substrate mapping 23
2.1.16 LC-MS/MS 24
2.1.17 LC-MS/MS data analysis 24
2.1.18 Gene ontology analysis 24
2.1.19 PI3K Activity Assay 25
2.1.20 Xenograft model 25
2.1.21 RNAi 25
2.1.22 Immunofluorescence microscopy 25
2.1.23 Time-lapse microscopy 26
2.1.24 Software 26
Chapter 3: Optimising a screen for novel SIK2 substrates 27
3.1 Introduction 27
3.2 Results 30
3.2.1 Wild-type SIK2 can utilise ATPγS 30
3.2.2 The SIK2 gatekeeper residue is threonine 96 32
3.2.3 Wild-type SIK2 cannot utilise 'bulky' ATPγS analogues 34
3.2.4 SIK2 T96G can utilise 'bulky' ATPγS analogues *in vitro* 36
3.2.5 SIK2 T96G can utilise 'bulky' ATPγS analogues in live cells and cell lysates 38
3.2.6 Thiophosphorylated peptides can be specifically captured 42
3.2.7 Generation of SK-OV-3-SIK2 cell lines 43
3.2.8 Preliminary screen data 44
3.3 Discussion 45
Chapter 4: Screening and analysis 47
4.1 Introduction 47
4.2 Results 49
4.2.1 Labelling of SIK2 substrates 49
4.2.2 Identification of putative SIK2 phosphorylation sites 49
4.2.3 Gene ontology analysis 53

4.2.4 Canonical and non-canonical phosphorylation sites 54
4.3 Discussion 56
Chapter 5: SIK2 activation promotes tumour growth and metastasis 63
5.1 Introduction 63
5.2 Results 65
5.2.1 SIK2 undergoes autophosphorylation at serine 358 65
5.2.2 SIK2 S358 phosphorylation increases in response to adipocytes 68
5.2.3 Phosphorylation of p85α by SIK2 increases PI3K activity 70
5.2.4 SIK2 overexpression affects cell spreading 72
5.2.5 Overexpression of SIK2 promotes peritoneal metastasis *in vivo* 74
5.3 Discussion 77
Chapter 6: Preliminary investigation of CLASPs and p120 Catenin 79
6.1 Introduction 79
6.2 Results 81
6.2.1 Mutagenesis of CLASP1 S600 does not affect localisation 81
6.2.2 SIK2 does not influence p120 S268 phosphorylation 84
6.3 Discussion 86
Chapter 7: Discussion & Conclusion 88
7.1 Overview 88
7.2 Future directions 90
7.3 Conclusions 92
References 93
Appendix I: *In silico* Screen Results 112
Appendix II: Additional Screen Data 115
Appendix III: MS/MS Spectra 117
Appendix IV: Gene Ontology Analysis 121
GO over-representation test (72 proteins) 121
GO over-representation test (18 proteins) 123

LIST OF TABLES

Table 1.1. Previously identified SIK2 substrates....10
Table 2.1. Site directed mutagenesis primers....19
Table 2.2. Sequencing primers....20
Table 2.3. *att*B primers....22
Table 2.4. siRNA sequences....25
Table 3.1. Preliminary screen hits....44
Table 4.1. Screen hits from four independent experiments....52
Table 4.2. Selected biological processes enriched in 72 putative substrates....53
Table 4.3. Selected molecular functions enriched in 72 putative substrates....53
Table 4.4. Selected cellular components enriched in 72 putative substrates....53
Table 4.5. Sites containing a canonical SIK consensus sequence....54
Table 4.7. SIK2 autophosphorylation sites....58

LIST OF FIGURES

Figure 1.1. SIK2 signalling pathways 7
Figure 1.2. Domain structure of AMPK-related kinases 8
Figure 1.3. Schematic representation of the ATP binding pocket 15
Figure 3.1. Chemical genetic screening techniques 28
Figure 3.2. Retention of cysteine-containing peptides 29
Figure 3.3. Mass spectra following *in vitro* kinase reactions (CEP250) 30
Figure 3.4. Mass spectra following *in vitro* kinase reactions (p85α) 31
Figure 3.5. Gatekeeper sequence alignment and MARK3 structure 33
Figure 3.6. Western blot detection of thiophosphorylated proteins 35
Figure 3.7. Western blots following incubation with 'bulky' analogues 37
Figure 3.8. Western blot following labelling in intact cells 39
Figure 3.9. Western blots following labelling in 293T lysates 40
Figure 3.10. Western blots following labelling using recombinant SIK2 41
Figure 3.11. Mass spectra showing peptide enrichment following covalent capture 42
Figure 3.12. Western blot following labelling in SK-OV-3-SIK2 lysates 43
Figure 3.13. Western blot following preliminary screen labelling 44
Figure 4.1. Revised screen workflow 48
Figure 4.2. Labelling of SIK2 substrates in four independent experiments 49
Figure 4.3. Amino acid bias in putative SIK2 phosphorylation sites 55
Figure 4.4. Site identifications and reproducibility 61
Figure 5.1. SIK2 domain structure 63
Figure 5.2. p85α domain structure 64
Figure 5.3. *In vitro* kinase assays with immunoprecipitated SIK2 and ATP 66
Figure 5.4. *In vitro* kinase assays with immunoprecipitated SIK2 and ATPγS 67
Figure 5.5. Isolation of primary omental adipocytes 68
Figure 5.6. Western blots following incubation of SK-OV-3-SIK2 cells with primary adipocytes 69
Figure 5.7. Phosphorylation of p85α and PI3K activity 71
Figure 5.8. Cell spreading in SK-OV-3-SIK2 cell lines 73
Figure 5.9. An *in vivo* model of ovarian cancer metastasis 74
Figure 5.10. Overexpression of SIK2 in OVCA432 cells 74
Figure 5.11. Metastatic tumour burden following orthotopic transplantation 75
Figure 5.12. SIK2 overexpression and survival *in vivo* 76
Figure 6.1. CLASP1 and CLASP2 domain structures 80
Figure 6.2. p120 domain structure 80
Figure 6.3. Expression of CLASP mutants 82
Figure 6.4. Immunofluorescence staining in SK-OV-3-CLASP1 cells 83

Figure 6.5. SIK2 overexpression, depletion, and p120 phosphorylation.....85
Figure 7.1. A model of SIK2 activation by omental adipocytes.....89

LIST OF ABBREVIATIONS

AMPK	AMP-activated protein kinase
ANCOVA	Analysis of covariance
ATP	Adenosine 5’-triphosphate
ATPγS	Adenosine 5’-(γ-thio)-triphosphate
BCA	Bicinchoninic acid
BSA	Bovine serum albumin
Bn-ATPγS	N^6-Benzyladenosine 5’-(γ-thio)-triphosphate
cAMP	Cyclic AMP
CLASP1	CLIP-associating protein 1
CLASP2	CLIP-associating protein 2
C-NAP1	Centrosome-associated protein CEP250
CREB	cAMP response element-binding protein
CRTC	CREB-regulated transcription coactivator
DAPI	4',6-diamidino-2-phenylindole
DTT	Dithiothreitol
DMEM	Dulbecco’s minimal essential medium
DMSO	Dimethyl sulfoxide
EB1	End-binding protein 1, also known as MAPRE1
EDTA	Ethylenediaminetetraacetic acid
EGTA	Ethylene glycol tetraacetic acid
FBS	Foetal bovine serum
GAPDH	Glyceraldehyde-3-phosphate dehydrogenase
GO	Gene ontology
GST	Glutathione S-transferase
HDAC	Histone deacetylase

HEPES	4-(2-hydroxyethyl)-1-piperazineethanesulfonic acid
HGSOC	High-grade serous ovarian cancer
IgG	Immunoglobulin G
LC-MS/MS	Liquid chromatography-tandem mass spectrometry
LDS	Lithium dodecyl sulphate
MALDI-TOF	Matrix-assisted laser desorption/ionisation-time-of-flight
MARK3	MAP/microtubule affinity-regulating kinase 3
MOPS	3-(N-morpholino)propanesulfonic acid
p100α	Phosphatidylinositol 3-kinase catalytic subunit alpha
p120	Catenin delta-1, also known as p120 catenin
p85α	Phosphatidylinositol 3-kinase regulatory subunit alpha
PAGE	Polyacrylamide gel electrophoresis
PBS	Dulbecco's phosphate-buffered saline
PFA	Paraformaldehyde
PhEt-ATPγS	N^6-(2-Phenylethyl)adenosine 5'-(γ-thio)-triphosphate
PI3K	Phosphatidylinositol 3-kinase
PNBM	*p*-nitrobenzyl mesylate
SDS	Sodium dodecyl sulphate
SEM	Standard error of the mean
SIK2	Salt-inducible kinase 2, also known as QIK
SILAC	Stable isotope labelling by amino acids in cell culture
TBS-T	Tris-buffered saline-0.1% Tween 20
TCEP	Tris-(2-carboxyethyl)phosphine
TFA	Trifluoroacetic acid
ThioP	Thiophosphate ester

ACKNOWLEDGEMENTS

First and foremost, I offer my sincere thanks to my supervisor, Professor Ahmed Ashour Ahmed, for giving me the opportunity to work in his Ovarian Cancer Cell Laboratory, for being so generous with his time over the course of my DPhil, and for a great many stimulating scientific discussions. I am especially grateful for being allowed to pursue my own project with a degree of independence, which has been a valuable, if at times challenging, experience.

I would also like to thank my co-supervisor Professor Sir Andrew McMichael for his guidance in contacting potential supervisors and choosing a laboratory early in my studentship, as well as kind advice throughout my studies. I also thank the Medical Research Council for funding my studentship and research.

My screen experiments would not have been possible without the proteomics expertise of Dr Roman Fischer, to whom I am deeply grateful for his valuable advice and assistance in analysing my peptide samples.

I would like to thank Dr Clara Redondo, who taught me a great deal about protein production and kindly provided the recombinant SIK2 kinase domain which I used in many of my optimisation experiments.

I am also grateful to Professors Stefan Knapp and Fumiko Esashi, who acted as assessors for my transfer of status, and Professors Benedikt Kessler and Tudor Fulga, who were assessors for my confirmation of status, for giving up their time to familiarise themselves with my research. Their feedback was not only useful, but highly encouraging.

Additionally, I also thank all of the present and past members of our lab - friends who have been a pleasure to know both inside and outside the lab. In particular, I would like to thank Fabrizio Miranda, Shujuan Liu, Juliette Goldsmith, Karin Hellner, and Yong Zheng, for their warm welcome upon my joining the lab, and for their dedication in working with Ahmed to establish an enthusiastic and productive working environment following our relocation to the WIMM. I would also like to thank Sandra Herrero-Gonzalez, Ruoyan Xu, Yiyan Zheng, and Donatien Chedom Fotso, who have all been friendly and valued additions to the team.

I also, of course, offer my gratitude to my fellow students. I would like to thank Mohammad Karaminejadranjbar for his boundless energy and for countless lively discussions. Last, but by no means least, I would like to offer my thanks to Charlotte Taylor, for her humour, camaraderie, and mutual support over the past three years. I wish both of them, and all of my colleagues, the very best in their future endeavours.

Finally, I would like to thank all of my friends at both Keble College and Somerville College, with whom I have shared some of the most memorable and enjoyable experiences of my life so far, and my parents, for their continued support throughout my studies.

DECLARATION

I hereby declare that no part of this thesis has been accepted or submitted for any degree, diploma, certificate or other qualification in this University or elsewhere. The results presented herein are my own work, with the exception of the parts listed below:

Figure 5.6 contains data generated by Fabrizio Miranda using primary adipocytes isolated by Shujuan Liu, who also acquired the images shown in Figure 5.5.

Figure 5.7 contains data generated by Fabrizio Miranda using recombinant p85α prepared by Ruoyan Xu.

The xenograft experiments shown in Figure 5.9, Figure 5.11, and Figure 5.12 were conducted by collaborators in Takeshi Motohara's laboratory at Keio University, Tokyo, or Anil Sood's laboratory at The University of Texas MD Anderson Cancer Center, USA, using SIK2-overexpressing SKOV3 or OVCA432 cell lines, respectively, which I prepared.

CHAPTER 1: INTRODUCTION

Salt-inducible kinase 2 (SIK2) is a multi-functional AMPK-related serine-threonine protein kinase, first identified as a regulator of insulin signalling that is highly expressed in adipocytes[1]. SIK2 expression has since been studied in a number of cellular contexts, including hepatocytes[2], neurons[3], macrophages[4], and pancreatic β-cells[5], as well as ovarian cancer[6] and prostate cancer[7]. SIK2 has been implicated as a potential therapeutic target in ovarian cancer, and could be exploited to enhance the response of this disease to existing chemotherapies[6]. This introduction will provide a general overview of ovarian cancer and consider the established functions of SIK2, including its role in cancer. It will go on to introduce some fundamental themes in kinase biology, and discuss the consequent challenges of elucidating kinase signalling networks, along with a technique which seeks to address them.

1.1 Ovarian cancer

Ovarian cancer is the fifth most common cancer in women, with an estimated 239,000 new cases diagnosed globally in 2012[8]. Although survival rates have improved in the long-term due to increased access to platinum-based chemotherapies and treatment regimens combining these with taxanes[9], progress over the last 20 years has been slow[10], and five-year survival rates remain relatively low at 46%[8]. This is largely because of late diagnosis due to a lack of obvious signs or symptoms in the early stages of the disease, meaning that around 70% of cases are diagnosed at Stage III or IV[10], with widespread peritoneal metastases[11,12].

Although circulating tumour cells have been detected in the blood of ovarian cancer patients[13], metastases are usually confined to the peritoneal cavity, and ovarian cancer cells have a clear predilection for metastasis to the omentum, an adipose-rich fold of the peritoneum which hangs in front of the intestines[14]. The prevailing view is that metastatic spread within the peritoneal cavity occurs as exfoliated cancer cells from the ovarian tumour are disseminated in the peritoneal fluid[15], although it has recently been shown that ovarian cancer cells can also metastasise to the omentum haematogenously[14]. The reasons for this tropism are not fully understood, but there is evidence for the involvement of a variety of cytoskeletal[16], mechanical[17], and molecular[14] factors. Nieman *et al.* (2011) demonstrated that omental adipocytes promote migration and invasion of ovarian cancer cells via adipokine signalling, and support metastatic tumour growth by supplying them with fatty acids[18]. Peritoneal metastases are a substantial cause of morbidity in ovarian cancer as they promote abdominal adhesions which obstruct the small and large intestines, causing significant discomfort and leading to malnutrition[15,19], so understanding and intervening in these processes could have significant clinical benefits.

The single biggest risk factor for ovarian cancer is inheritance of mutations in *BRCA1* or *BRCA2*[20], which are highly penetrant and increase a woman's lifetime risk of ovarian cancer from an average of 1.8% to 39% or 17%, respectively[21]. Germline mutations in either gene account for 6 – 15% of all ovarian cancers[22]. Ovarian cancer risk also increases with menopausal hormone use[23], and increased height and body mass index (BMI)[24], whilst parity[25] and use of oral contraceptives[26] have significant protective effects.

90% of ovarian tumours are ovarian carcinomas, the rest being classified as either benign or borderline. Ovarian carcinomas can be further divided into five histologically and biologically distinct subtypes. The most common subtype is high-grade serous ovarian carcinoma (HGSOC), which includes 70% of all ovarian carcinomas, and is also the most aggressive subtype[27]. HGSOC will be the main focus of this study, as this is the subtype in which SIK2 was found to have biological significance[6], and it will be discussed in further detail below. Endometrioid carcinomas and clear cell carcinomas each account for a further 10% of ovarian carcinomas, and both can be associated with atypical endometriosis. Low-grade serous carcinomas account for <5% of the total and probably result from progression of serous borderline tumours. Finally, mucinous carcinomas account for 3 – 4% of ovarian carcinomas, and their cell of origin remains unknown[27].

The origin of HGSOC has been a matter of some debate. Since the 'incessant ovulation hypothesis' by Fathalla in 1971[28], work has been focussed on the ovarian surface epithelium (OSE) as the presumed site of origin of ovarian cancer[29]. This hypothesis was formed on the basis of comparisons with other animals, epidemiological evidence indicating a positive correlation between lifetime number of ovulations and ovarian cancer risk, and the repeated exposure of the OSE to trauma and ovulatory hormones[28]. However, HGSOCs bear little histological resemblance to the OSE, and are indistinguishable from carcinomas arising outside the ovary[30], such as fallopian tube serous carcinoma and primary peritoneal serous carcinoma[29]. An increasing body of evidence suggests that a significant proportion of HGSOCs actually originate in the distal fallopian tube. A study by Kindelberger *et al.* (2007) found that out of 42 cases diagnosed as HGSOC, 20 (48%) also had serous tubal intraepithelial carcinomas (STICs)[31]. Like HGSOC, the vast majority of STICs have mutations in *TP53*. An analysis of these mutations by Kuhn *et al.* (2012) showed that the mutations in HGSOCs were identical to those in the corresponding STICs in 93% of cases, suggesting a clonal relationship between the two[32]. Furthermore, mouse models have shown clear progression from precursor lesions in the fallopian tube epithelium to HGSOCs, and successfully recapitulate many of the molecular characteristics of human HGSOC[33–35].

As mentioned above, mutation of *TP53* is a near-universal feature of HGSOCs[36], and appears to be one of the earliest events occurring in precursor lesions. Aside from *TP53*, recurrent point mutations are relatively rare in HGSOCs, and changes in gene expression

are mediated predominantly by widespread copy number changes resulting from genomic instability[37]. A genomic analysis of a large number of HGSOCs identified dysregulation of the RB1 pathway in 67% of cases, and the PI3K/RAS pathway in 45% of cases. Around 50% of HGSOCs have defects in the homologous recombination (HR) pathway, which is responsible for high-fidelity repair of DNA double-strand breaks. The majority of these defects are caused by germline or somatic mutation of *BRCA1* or *BRCA2*, or downregulation of pathway components via epigenetic changes or copy number variations (such as *PTEN* deletion)[38].

These HR defects contribute to the high degree of sensitivity of HGSOCs to platinum-based chemotherapy (e.g. cisplatin, carboplatin)[39], which induces intra-strand DNA crosslinks, as well as inter-strand and DNA-protein crosslinks, leading to the induction of apoptosis via a number of different signalling pathways[40]. Platinum-based chemotherapy has remained a key part of ovarian cancer treatment since its introduction in the late 1970s, although cisplatin has since been replaced with carboplatin, which has less severe side effects. The current standard of care in advanced ovarian cancer consists of surgical debulking, usually involving hysterectomy, bilateral salpingo-oophorectomy, and omentectomy, and a combination of carboplatin and paclitaxel, administered intravenously every 21 days for 6 cycles[41]. More than 80% of patients respond to this first-line chemotherapy, with complete response rates of 40 – 60%. Unfortunately, 80 – 90% of patients diagnosed with advanced stage disease eventually relapse[39], with a median progression free survival time of 18 months. Upon relapse, patients can be treated again with carboplatin, but the response rate is proportional to the progression free survival time and generally decreases with each successive relapse[42]. As such, there is a pressing need for novel targeted therapies to augment the response to existing treatments, and this is an active area of research[42].

1.2 Salt-inducible kinase 2

1.2.1 SIK2 is a potential therapeutic target in HGSOC

Ahmed *et al.* (2010) identified a novel role for SIK2 in cell cycle progression in HGSOC cells, using an unbiased RNAi-based kinome screen. Depletion of SIK2 resulted in a substantial increase in the time taken for HGSOC cells to undergo mitosis, and also led to mitotic defects. Immunofluorescence microscopy showed that SIK2 localises to the centrosome, particularly during mitosis. A SIK consensus sequence was subsequently identified at S2392 of the centrosome linker protein CEP250 (also known as C-Nap1), which is required for centriole-centriole cohesion in interphase and dissociates from the centrosome during mitosis, resulting in centrosome separation[43]. Phosphorylation of CEP250 at S2392 by SIK2 was shown to promote this dissociation, whilst depletion of SIK2 blocked centrosome separation during mitosis, accounting for the observed delay in mitotic

progression and leading to an accumulation of cells arrested in prometaphase. This effect was also shown to be independent of cellular ATP levels, suggesting that it is unrelated to the previously established roles of SIK2 in cellular metabolism[6].

Crucially, depletion of SIK2 also sensitised ovarian cancer cells to paclitaxel, a microtubule-stabilising chemotherapeutic drug, both *in vitro* and in xenograft models. Furthermore, the authors found that higher *SIK2* expression correlated with increased risk of cancer progression in HGSOC patients following paclitaxel treatment, and that paclitaxel-resistant cancers had significantly higher SIK2 expression than paclitaxel-sensitive cancers. Depletion of SIK2 in ovarian cancer cell lines resulted in reduced cell proliferation and decreased activation of AKT, a major component of the PI3K/AKT oncogenic signalling pathway[44]. All of these lines of evidence suggest that inhibition of SIK2 is a plausible strategy for the treatment of HGSOC[6], and constitute the rationale for the work presented in this thesis.

There have been few other studies investigating the role of SIK2 in cancer. Genomic amplification of the *SIK2* locus was reported in a diffuse large B-cell lymphoma (DLBCL) cell line, resulting in overexpression and increased cell survival. However, elevated *SIK2* expression was not detected in primary DLBCL cases or in any other DLBCL cell lines, suggesting that this is not a frequent occurrence[45].

A recent study by Bon *et al.* (2014) found auto-antibodies against SIK2 in the plasma of patients with aggressive prostate cancer, which might constitute a novel marker for use in diagnosis. The authors also showed that SIK2 promotes cell cycle progression, cell growth, and cell survival in prostate cancer cells, suggesting that inhibition of SIK2 might also have therapeutic value in this disease. However, SIK2 inhibition resulted in enhanced CREB1 activity, which has previously been shown to promote prostate cancer progression and cell survival[7]. Nonetheless, this study is significant because it is the first strong evidence that SIK2 might have an important role in cancers other than ovarian cancer.

In addition to these three studies which have explicitly focussed on SIK2 in cancer, several other publications have identified links with pathways which are involved in cancer. SIK2 was recently shown to regulate ER-associated protein degradation (ERAD), a process by which misfolded proteins are removed from the ER, via association with and phosphorylation of p97/VCP, an ATPase also involved in the cell cycle, programmed cell death, and autophagy. Phosphorylation of p97/VCP at S770 promoted its ATPase activity, resulting in enhanced ERAD activity. It is possible that this functions to alleviate ER stress when there is a cellular energy deficit. The authors also suggested that the interaction might be relevant in cancer, citing several publications correlating p97/VCP expression with metastasis and tumour recurrence[46], although further study would be required to confirm this.

Another link to autophagy was established by Yang *et al*. (2013), who demonstrated that SIK2 is required for autophagosome maturation[47]. This can serve to maintain cancer cell viability under conditions of metabolic stress and may be contributing to the effects of SIK2 in cancer[48], but the authors did not elucidate the downstream pathway, instead focussing on upstream regulation of SIK2 through acetylation and deacetylation by p300 and HDAC6, respectively.

Finally, Wehr *et al*. (2013) showed that Sik2, the SIK2 orthologue in *Drosophila*, phosphorylates Sav, part of the conserved Hippo signalling pathway that controls organ size by promoting cell-cycle exit and apoptosis and is frequently dysregulated in human cancers. Sav is a scaffold protein which is required for formation of the Hpo/Wts signalling complex which phosphorylates the Yki transcriptional co-activator, resulting in its exclusion from the nucleus. The authors showed that phosphorylation of Sav at S413 by Sik2 disrupted formation of the Hpo/Wts complex, reducing Hippo signalling and leading to increased Yki target gene expression[49]. This is of interest as YAP, the human orthologue of Yki, has been identified as an oncogene in ovarian cancer, contributing to cell proliferation, cisplatin resistance, cell migration, and anchorage independent growth[50]. However, whilst Wehr *et al*. (2013) did show that SIK2 can promote YAP-dependent transcription in human cells, the S413 site is not conserved in the human Sav orthologue SAV1, so the underlying mechanism may differ in human cells[49].

1.2.2 SIK2 regulates energy balance and cellular metabolism

The most widely studied aspect of SIK2 is its role in the regulation of cellular metabolism. Upon the discovery of SIK2 by Horike *et al.* (2003), it was shown that SIK2 is expressed early in adipocyte differentiation and, like SIK1, represses cAMP response element (CRE)-dependent transcription. The authors also showed that SIK2 is activated in white adipose tissue in diabetic mice, and phosphorylates insulin receptor substrate 1 (IRS1) at S794, suggesting that SIK2 might be involved in disturbing insulin signalling in the development of type II diabetes[1]. Sakamaki *et al.* (2014) demonstrated that SIK2 is required for glucose-stimulated insulin secretion in pancreatic β-cells. SIK2 phosphorylates CDK5R1 (also known as p35) at S91 in response to glucose stimulation, leading to ubiquitylation and degradation. This results in increased insulin secretion, as CDK5R1 is an activator of CDK5, which in turn inhibits insulin secretion by blocking calcium influx[5].

Much of the literature concerning SIK2 focuses on its repression of CREB-dependent transcription, which is mediated by phosphorylation of the CRTC (also known as TORC) family of transcriptional coactivators[51,52]. CRTC proteins bind to the CREB transcription factor in the nucleus, resulting in increased transcription of a subset of CREB target genes[53]. Phosphorylation of CRTC2 at S171 by SIK2 strongly promotes the interaction of CRTC2 with 14-3-3 proteins, inhibiting its nuclear translocation, resulting in its

sequestration in the cytoplasm and decreased CREB-mediated gluconeogenic gene expression[51].

This interaction is regulated by the cAMP and calcium second messenger pathways in response to hormonal signalling (e.g. glucagon). cAMP activates PKA, which inhibits SIK2 through direct phosphorylation of S587, whilst calcium activates the calcineurin phosphatase which dephosphorylates CRTC2 S171. Both of these signals disrupt the phosphorylation-dependent binding of 14-3-3, resulting in nuclear translocation, CREB-mediated transcription and up-regulation of gluconeogenesis in adipocytes[51].

Conversely, insulin leads to activation of AKT signalling, which reportedly activates SIK2 via phosphorylation of S358 by AKT2, leading to CRTC2 phosphorylation, sequestration, and degradation, and repression of hepatic gluconeogenesis during re-feeding following fasting[52]. However, the methods used in this study did not provide direct evidence that AKT2 directly phosphorylates SIK2 in cells. A recent study by Patel *et al.* (2014) found no evidence of SIK2 phosphorylation in response to insulin, consistent with the findings of an earlier study by Henriksson *et al.* (2012)[54], and disputed the effect of S358 or S587 phosphorylation on SIK2 activity. The authors argued that phosphorylation of the SIK2 activation loop at T175 by LKB1, the canonical 'master regulator' of the AMPK family kinases[55] (Figure 1.2), is the primary determinant of SIK2 activity in hepatocytes. They did, however, also show that treatment of hepatocytes with the HG-9-91-01 SIK inhibitor resulted in dephosphorylation of CRTC2 and increased gluconeogenic gene expression[56], which is broadly consistent with the original model proposed by Horike *et al.* (2003). Taken together, the available evidence supports a role for SIK2 in repressing gluconeogenesis via CTRC2 phosphorylation, which is disrupted by glucagon/cAMP signalling.

Phosphorylation of CRTC2 by SIK2 has also been shown to repress lipogenesis in white adipocytes by reducing CREB-mediated transcription of lipogenic genes including *SREBP1*, *FAS*, and *ACC*[57,58]. Inhibition or knockout of SIK2 led to increased expression of the ATF3 transcription factor, resulting in a concomitant decrease in *GLUT4* and adiponectin expression, which reduced glucose uptake and insulin sensitivity[57].

In the liver, direct phosphorylation of the p300 histone acetyltransferase (HAT) at S89 by SIK2 inhibits its HAT activity, reducing acetylation and activity of the pro-lipogenic ChREBP transcription factor, as well as reducing pro-inflammatory cytokine production downstream of the NF-κB pathway. This inhibition of lipogenesis and inflammation has a protective effect on the liver in the context of obesity or insulin resistance[2]. It is also likely that inhibition of p300 HAT activity by SIK2 contributes to regulation of CRTC2, as acetylation of L628 by p300 protects CRTC2 from ubiquitylation and degradation[53].

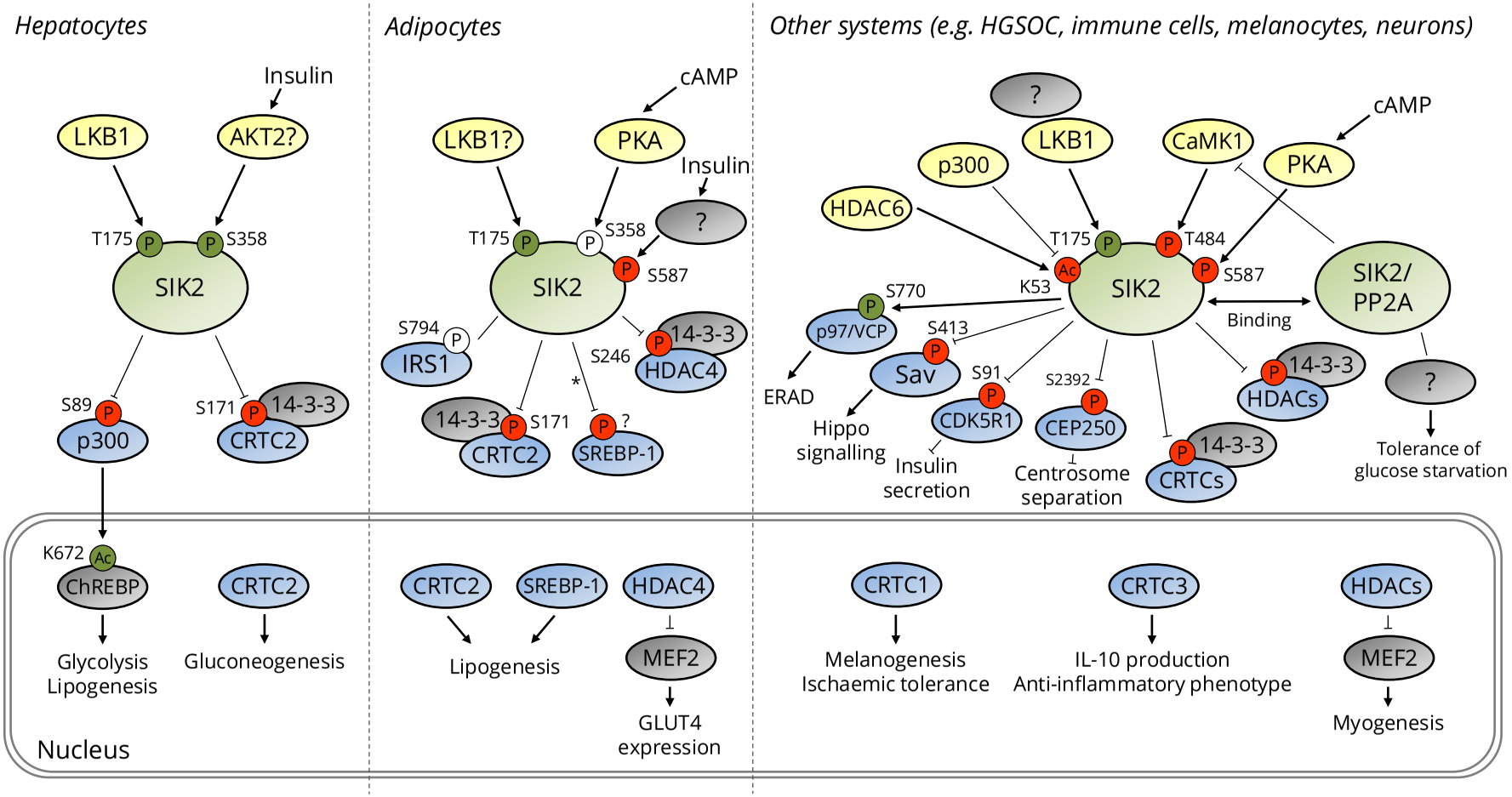

Figure 1.1. SIK2 signalling pathways

Schematic depicting signalling pathways both upstream and downstream of SIK2, based on the existing literature. Pathways studied in adipocyte or hepatocyte systems are shown in in separate panels as the literature suggests that regulation of SIK2 is distinct in different insulin-responsive tissues. Pathway components which are uncertain or as yet unidentified are marked with question marks (?).*The interaction between SIK2 and SREBP-1 may not be direct.

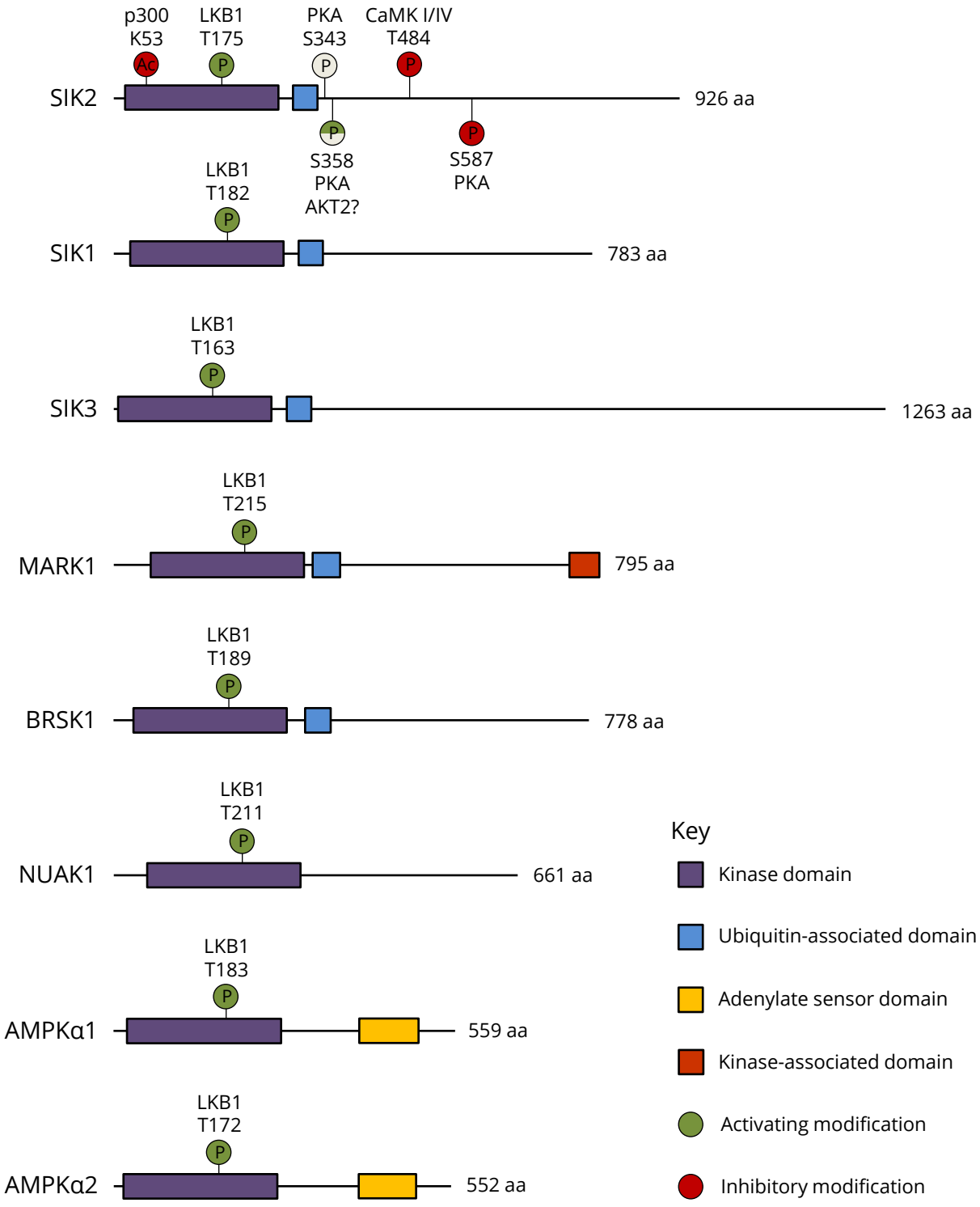

Figure 1.2. Domain structure of AMPK-related kinases

Schematic representations of selected AMPK-related kinases. Only one kinase is shown from each of the MARK, BRSK and NUAK sub-families. Major sites of post-translational are depicted on the SIK2 schematic, including the activation loop LKB1 phosphorylation site which is conserved throughout the AMPK family. The effects of SIK2 S358 phosphorylation on kinase activity are subject to contradictory reports in the literature. This site has also been reported to mediate binding of 14-3-3 proteins.

1.2.3 SIK2 regulates a variety of other processes

SIK2 has also been shown to phosphorylate CRTC1, repressing melanogenesis in melanocytes by excluding CRTC1 from the nucleus[59]. Chemical inhibition of SIK2 results in increased melanogenesis (and markedly darker hair colour) in mice, and also in B16F10 melanoma cells[60].

Sasaki *et al.* (2011) showed that in neurons, degradation of SIK2 is triggered in response to oxygen-glucose deprivation by phosphorylation of T484 by CaMK I/IV, resulting in dephosphorylation of CRTC1 and activation of CREB-mediated transcription. This promotes neuronal survival; mice lacking SIK2 had significantly smaller brain lesions following focal ischemia (restriction of blood flow) than controls[3].

Phosphorylation of CRTC3 by SIK2 has been implicated in regulation of inflammation. Clark *et al.* (2012) demonstrated that inhibition of SIK2 in macrophages using HG-9-91-01 results in dephosphorylation and nuclear translocation of CRTC3, activating CREB-mediated transcription, including expression of the anti-inflammatory cytokine IL-10. Production of pro-inflammatory IL-12 was also decreased, suggesting that the macrophages had been reprogrammed into anti-inflammatory regulatory macrophages, although the endogenous stimuli which might ordinarily regulate this conversion were not identified. The authors suggested that SIK2 inhibition might have therapeutic potential in chronic inflammatory diseases[4]. The same group later showed that the clinically approved Src inhibitors dasatinib and bosutinib also inhibit SIKs and can promote conversion of macrophages into this 'regulatory-like' phenotype[61].

SIK2 also regulates class IIa histone deacetylases (i.e. HDAC4, 5, 7 & 9) in a similar manner to CRTCs, with phosphorylation leading to 14-3-3 binding and nuclear export. Acetylation of the MEF2 transcription factor by class IIa HDACs reduces MEF2-mediated transcription, repressing myogenesis, so activation of SIK2 by LKB1 leads to de-repression of myogenesis. Inhibition of SIK2 by PKA signalling has the opposite effect[62]. MEF2 also promotes expression of *GLUT4* in adipocytes[63], so regulation of HDAC4 by SIK2 promotes *GLUT4* expression and glucose uptake in this context[64], in parallel to the effect of CRTC2 regulation mentioned above[57].

Substrate protein	Phosphorylation site(s)	Reported function(s) of site phosphorylation	Reference(s)
IRS1	S794	Modulation of insulin signalling	Horike *et al.* (2003)
CRTC2	S171 S275	14-3-3 binding, nuclear export, repression of CREB-mediated transcription	Screaton *et al.* (2004) Dentin *et al.* (2007) Muraoka *et al.* (2009) Henriksson *et al.* (2015)
CEP250	S2392	Promotes centrosome separation during mitosis	Ahmed *et al.* (2010)
p300	S89	Inhibits p300 histone acetyltransferase activity	Bricambert *et al.* (2010)
CRTC1	S167	14-3-3 binding, nuclear export, repression of CREB-mediated transcription	Horike *et al.* (2010) Sasaki *et al.* (2011) Kumagai *et al.* (2011)
CRTC3	S162	14-3-3 binding, nuclear export, downstream repression of CREB	Clark *et al.* (2012) Sundberg *et al.* (2014)
Class IIa HDACs	S246 (HDAC4)	14-3-3 binding, nuclear export, de-repression of MEF2	Walkinshaw *et al.* (2013) Henriksson *et al.* (2015)
Sav (*Drosophila*)	S413	Dissociation of Hpo/Wts complex, decreased Hippo signalling	Wehr *et al.* (2013)
p97/VCP	S770	Increased ATPase activity, degradation of ERAD substrates	Yang *et al.* (2013)
CDK5R1	S91	Ubiquitylation/degradation, increased insulin secretion	Sakamaki *et al.* (2014)

Table 1.1. Previously identified SIK2 substrates

Previously identified substrates are shown in chronological order, along with the corresponding phosphorylation site(s) and a brief functional summary.

1.3 Protein kinases and kinase inhibitors

For several decades, it has been clear that protein kinases play a critical role in cellular signal transduction[65,66]. Following the sequencing of the human genome in the early 2000s[67,68], it was established that there are as many as 518 different protein kinases in humans[69]. Kinases are an attractive class of therapeutic target because the majority of signal transduction processes involve protein kinase cascades, and aberrant kinase signalling has been implicated in a wide range of diseases, particularly in cancer[70].

1.3.1 Structure and function

Protein kinases catalyse the transfer of the γ-phosphate group from a nucleoside triphosphate (usually ATP) to the hydroxyl group of a specific amino acid residue in a substrate protein, a process referred to as protein phosphorylation. Serine-threonine kinases phosphorylate serine and threonine residues, whilst tyrosine kinases phosphorylate tyrosine residues, although there are a small number of dual-specificity kinases which share both functions[71].

All protein kinases contain a conserved catalytic core of 200-250 amino acids in length which folds into a smaller N-terminal lobe and a larger C-terminal lobe[72]. The cavity between these two lobes forms the ATP binding pocket, which is lined with hydrophilic residues that interact with the ribose and phosphate moieties of ATP. The 'hinge region' which connects the two lobes forms hydrogen bonds with the adenine ring of ATP, orienting the phosphates towards the solution[70].

Protein kinases also contain a disordered activation loop which plays an important role in regulating kinase activity, and can sometimes influence ATP and substrate binding. The N-terminal end of the activation loop is marked by a universally conserved DFG (Asp-Phe-Gly) motif. The DFG aspartate (D160 in SIK2) interacts with the phosphate groups of ATP either directly or by coordinating one or two magnesium ions, which must be correctly positioned for efficient catalysis. Many kinases require the activation loop to be phosphorylated, which induces a conformational change leading to activation. In addition to the DFG motif, there is also a conserved lysine residue (K49 in SIK2) in the N-terminal lobe which interacts with the α- and β-phosphates of ATP[72].

To successfully catalyse phosphorylation, a protein kinase must also specifically recruit its substrates. There are a number of different mechanisms which contribute to the ability of a protein kinase to recognise substrate proteins amongst the thousands of proteins present in a cell. The residues surrounding the active site may be complementary to a particular consensus sequence of around four residues either side of the target phosphorylation sites, establishing interactions based on charge, hydrogen bonding, or hydrophobicity. Although kinases' target consensus sequences can be used to identify putative substrates *in silico*, the presence of a consensus sequence does not guarantee

phosphorylation by the corresponding kinase. Furthermore, physiological substrates may not contain a consensus sequence[73].

This is because substrates may also be recruited by interactions which occur distally to the active site. Docking domains elsewhere in the kinase bind to corresponding sites on substrate proteins, increasing the local substrate concentration and potentially favouring the correct orientation. These sites may also be phosphorylation-dependent, enabling more complex regulation and signal integration. Docking can also occur indirectly via a dedicated targeting subunit which transiently interacts with substrates (e.g. CDKs/cyclins), or via scaffolding proteins which recruit both kinase and substrate into a complex[73].

Once both ATP and the substrate have been recruited to the active site (not necessarily in this order), the γ-phosphate of ATP should be in close proximity with the hydroxyl group of the residue to be phosphorylated. A conserved aspartate in the activation loop interacts with the acceptor hydroxyl group and orients it for optimal attack geometry with respect to the γ-phosphate. The hydroxyl group then displaces the γ-phosphate in a single step, yielding a phosphorylated substrate, ADP, and a proton[74]. This phosphorylation can have diverse effects on the substrate, including conformational changes, activation or inhibition of enzyme activity, and modulation of protein-protein interactions[75].

1.3.2 Kinases as therapeutic targets in cancer

Protein kinase signalling is frequently dysregulated in cancer, and plays a key role in oncogenesis. Protein kinases are the most abundant class of known cancer gene[76], and are frequently mutated in a range of different tumour types[77]. These mutations can promote transformation by activating oncogenic kinases (e.g. BRAF[78]), or by inactivating tumour suppressor kinases (e.g. ATM[79]). Kinases may also be overexpressed due to copy number changes, and this is a particularly important mechanism in ovarian cancer, leading to increased expression of *EGFR* in 70% of cases, for example[42]. Alternatively, protein kinases may be essential to tumour survival due to the inactivation of functionally overlapping pathways, a phenomenon known as synthetic lethality. They may also influence cell survival and proliferation without being essential for transformation, or promote particular stages of tumour progression such as metastasis[70].

Some cancers are reliant on constitutive activation of particular kinases for transformation, making such kinases appealing targets for therapeutic intervention[70]. The conserved ATP binding site in protein kinases makes them particularly amenable to inhibition using ATP-mimetic small-molecular inhibitors, although producing inhibitors to target specific kinases can be challenging[80], and most approved kinase inhibitors have limited selectivity[81].

The first kinase inhibitor to receive clinical approval was imatinib, which selectively inhibits the constitutively active BCR-ABL kinase, a key driver of cell proliferation and

survival in chronic myelogenous leukaemia (CML)[82]. A study of a large cohort of CML patients treated with imatinib over five years found that it resulted in a complete cytogenetic response in up to 87% of cases, greatly superior to previous CML treatments[83]. The success of imatinib in clinical trials demonstrated the value of kinase inhibition as a therapeutic strategy and has led to intensive drug discovery efforts in this area[81].

Imatinib is an example of a type II inhibitor, meaning that it targets the kinase ATP binding pocket and an adjacent pocket exposed in the inactive kinase conformation (referred to as 'DFG-out'), preventing ATP binding and activation. Conversely, type I inhibitors bind to the ATP binding pocket in the active conformation and inhibit kinase activity by competing with ATP[80]. The majority of existing kinase inhibitors are ATP competitive and fall into this category, possibly because they have been identified in assays using kinases in their active conformation, or because they are based on existing ATP-mimetic compounds[84]. Type III inhibitors modulate kinase activity by binding at allosteric sites (i.e. outside the active site). These can be highly specific as they can target unique features of particular kinases[70], but development is challenging as potent binding does not necessarily result in kinase inhibition[80].

The ability to discover potent, highly selective small molecule inhibitors using compound screens or structure-guided design provides opportunities for targeted cancer therapies, but to date, drug discovery efforts have focussed on a small set of protein kinases which have well-established roles in cellular signalling. Around 50% of protein kinases remain largely uncharacterised and a further 25% have totally unknown functions, although unbiased screens using RNAi have identified some of these as being important in cancer in particular genetic or therapeutic contexts[81]. SIK2 is a good example of this class of target, its potential role in paclitaxel resistance having been identified in one such screen[6]. However, the functions of SIK2 in ovarian cancer are not fully understood, and a deeper mechanistic understanding will be required to facilitate its development as a potential therapeutic target.

1.4 Investigating protein phosphorylation

A range of different techniques have been used in the study of protein kinase signalling[85]. In the pre-molecular era, kinase substrates were often discovered by co-immunoprecipitation with the kinase of interest. Downstream substrate phosphorylation at specific known sites is routinely investigated using phosphorylation-specific antibodies. The function of these sites can be determined by expressing mutants in which the target site has been mutated to alanine, preventing phosphorylation, whilst mutation to aspartic acid or glutamic acid may mimic the effects of phosphorylation. These approaches have a great deal of utility, but they are low-throughput and can only be applied to previously identified substrates.

For some kinases, antibodies are available which recognise the phosphorylation site consensus sequence. Alternatively, the consensus sequence can be used to identify potential substrates *in silico*, but as mentioned earlier in this chapter, the utility of these approaches is limited as not all physiological kinase substrates contain the corresponding consensus sequence, and the presence of a consensus sequence neither guarantees phosphorylation, nor rules out the involvement of alternative kinases.

Phosphorylation can be studied at a whole-proteome level using powerful mass-spectrometry based approaches, which have enabled quantitative analysis of thousands of individual phosphorylation sites at once[86,87], as well as individual sites in isolation[88]. Advances in instrumentation, sample fractionation, and phosphopeptide enrichment techniques mean that it is now possible to identify 20,000 – 30,000 unique phosphorylation sites in a single experiment[89]. These approaches are ideal for dissecting changes in kinase signalling at a systems level in response to particular stimuli[87,90,91], or during significant biological events such as mitosis[92,93], but alone they do not establish a direct link between phosphorylation sites and their upstream kinase(s). Global phosphoproteomics could be used in conjunction with inhibitors or RNAi against a kinase of interest to attempt to identify substrates, but these approaches often have off-targets and even the specific inactivation of a kinase will cause wider perturbations in the signalling network.

Demonstrating a direct interaction between a kinase of interest and a particular phosphorylation site is inherently challenging. Any given cell might express hundreds of different protein kinases, and as has been discussed earlier in this chapter, the catalytic function of these is highly conserved. Beyond the simple distinction between serine/threonine and tyrosine kinases, it is not possible to attribute specific phosphorylation events to individual kinases as all of these post-translational modifications (PTMs) are indistinguishable from one another[94]. Furthermore, phosphorylation is the most abundant PTM in the proteome, with at least 70% of cellular proteins subject to phosphorylation[93] and over 240,000 non-redundant phosphorylation sites listed in the PhosphoSitePlus database[95], so the scale of the challenge is considerable.

1.4.1 Kinase-substrate mapping

To identify the direct substrates of a particular kinase of interest, one approach is to use a transferrable tag which can be distinguished from a normal phosphate group. However, widespread use of ATP as a phosphodonor amongst the protein kinases makes it impossible to experimentally manipulate the supply of phosphodonors for an individual wild-type kinase in a complex system in this manner. In order to overcome this limitation, a technique has been developed which allows kinases to be engineered with artificial nucleotide specificity[96,97].

In 1997, Kevan Shokat and colleagues mutated the v-Src tyrosine kinase to utilise a 'bulky' ATP analogue (N^6-cyclopentyl-ATP)[96], and they later showed that this approach was applicable to protein kinases more broadly[98–100]. The technique involves mutating a conserved hydrophobic residue which is located in the hinge region at the back of the ATP binding pocket, known as the 'gatekeeper' residue (Figure 1.3a). Mutating this to a smaller residue such as alanine or glycine creates an enlarged ATP binding pocket that is uniquely capable of accepting 'bulky' ATP analogues, which carry chemical modifications at the N^6 position of the adenine ring[100] (Figure 1.3b). Crucially, the additional group prevents utilisation of the analogue by other cellular kinases due to a steric clash with the wild-type gatekeeper residue.

Because the gatekeeper residue is located deep inside the ATP binding pocket, mutated kinases retain their natural substrate specificity[101], which is crucial for physiological substrate identification. Mutation of the gatekeeper residue can affect kinase activity, as it forms part of the 'hydrophobic spine' which is characteristic of the active kinase conformation[102]. This means that around 30% of protein kinases do not tolerate alanine or glycine gatekeeper mutations, but it is possible to restore kinase activity by mutating one of several conserved positions in the N-terminal lobe of the kinase domain[100].

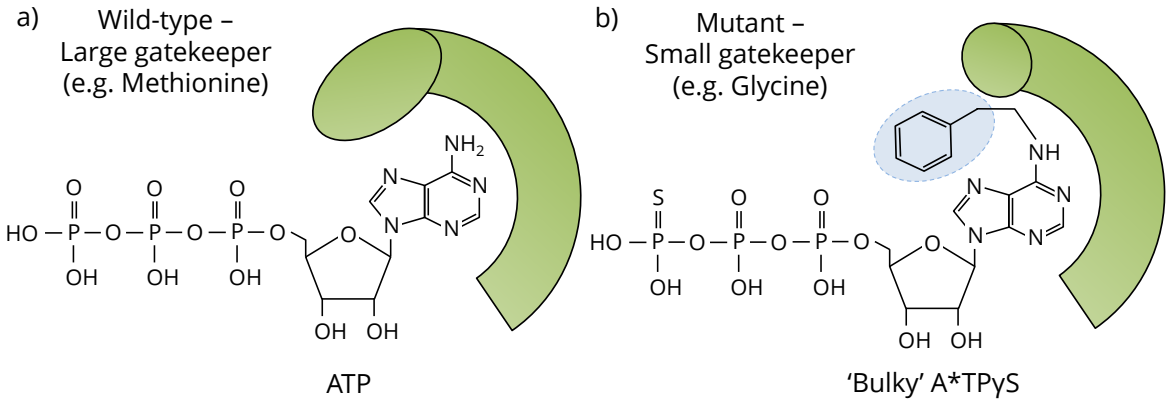

Figure 1.3. Schematic representation of the ATP binding pocket

a) In a wild-type kinase, the gatekeeper residue comes into close contact with the adenine ring of ATP. 'Bulky' analogues are prevented from binding due to a steric clash between the gatekeeper residue and the additional chemical group. **b)** Mutation of the gatekeeper to a smaller residue creates additional space (shown in blue), allowing the ATP binding pocket to accommodate 'bulky' analogues. The analogue also carries a γ-thiophosphate group which contains a reactive sulphur nucleophile.

Supplying a kinase gatekeeper mutant with a 'bulky' ATP analogue which also carries a chemically distinct transferable tag allows specific identification of direct substrates. This is referred to as a chemical genetic screen, or kinase-substrate mapping. Early screens for

CDK1 and ERK2 substrates used radiolabelled [γ-^{32}P]ATP analogues to detect novel substrates. However, the screen for CDK1 substrates relied on immunoprecipitation of exogenously expressed GST-tagged substrate proteins[98], whilst the ERK2 screen was restricted to substrates which co-immunoprecipitate with ERK2[99]. These approaches were necessary because ^{32}P allows detection of target substrates, but cannot be used to chemically isolate them.

A variety of ATP analogues featuring chemical tags on their γ-phosphate groups have been reported, for example ATP-biotin[103], but the best documented analogue in this context is ATPγS, which carries a γ-thiophosphate group (Figure 1.3b). Allen *et al.* (2007) demonstrated that this tag can be transferred by a majority of kinases, and that the reactivity of the sulphur nucleophile can be exploited for affinity purification of tagged endogenous substrates. Specifically, alkylation of the thiophosphate forms a thiophosphate ester which can be used as a handle to immunoprecipitate substrates using a specific antibody. These substrates can then be subjected to proteolytic digestion and identified using tandem mass spectrometry. Importantly, the antibody is selective for the thiophosphate ester over the thioethers which are formed upon alkylation of other cellular thiols, such as cysteine[104].

This technique enables the identification of large numbers of direct substrates of a kinase of interest, and is compatible with the majority of protein kinases. It has been used elsewhere to identify 28 previously unidentified substrates of AMPKα2[105], suggesting that SIK2 might also be amenable to this approach. Given that relatively few substrates have been identified downstream of SIK2, and only one of these in the context of ovarian cancer, kinase-substrate mapping is ideal for the discovery of novel substrates to elucidate the role of SIK2 in ovarian cancer.

1.5 Aims & Objectives

The main aim of this project was to optimise and conduct a screen to discover previously unidentified SIK2 substrates in ovarian cancer. The secondary aims were to use the results of the screen to develop novel insights into the role of SIK2 in ovarian cancer biology, and to identify potential biomarkers of SIK2 activity to support ongoing preclinical drug discovery efforts. Meeting these aims required the completion of a series of objectives, which are detailed below.

- Conducting a chemical genetic screen for novel SIK2 substrates
    - Determining the ability of SIK2 to utilise ATPγS *in vitro* using recombinant SIK2 and substrate peptides or proteins
    - Generating SIK2 gatekeeper mutants using site-directed mutagenesis
    - Expressing these mutants and verifying their ability to utilise 'bulky' ATPγS analogues *in vitro*

    - Optimising and testing different methods of using SIK2 gatekeeper mutants to label substrate proteins (e.g. live cells vs cell lysates)
    - Establishing a protocol for covalent capture of thiophosphorylated substrate peptides and testing the recovery of a synthetic peptide thiophosphorylated *in vitro*
    - Using a lentiviral system to generate an ovarian cancer cell line with stable expression of a SIK2 gatekeeper mutant for use in screen experiments and subsequent functional work
    - Combining the protocols established in the previous objectives to conduct preliminary screen experiments
    - Further optimising the screen protocol as necessary to yield a list of putative SIK2 substrates
- Identifying novel biomarkers of SIK2 activity
    - Generating phosphorylation-specific antibodies for sites of SIK2 autophosphorylation identified in the screen
    - Testing the SIK2 pS358 antibody for use in western blots of recombinant protein or SIK2 immunoprecipitates
- Using the screen results to gain new insights into SIK2 biology
    - Conducting a gene ontology analysis using the list of putative substrates to infer potential functions of SIK2
    - Confirming the ability of SIK2 to phosphorylate p85α *in vitro* and in cell lines using a custom phosphorylation-specific antibody
    - Investigating the effect of p85α phosphorylation by SIK2 on PI3K activity *in vitro* and in ovarian cancer cells
    - Using the SIK2 pS358 antibody to investigate activation of SIK2 in ovarian cancer cells in response to external stimuli (e.g. co-culture with adipocytes)
    - Using ovarian cancer cell lines overexpressing SIK2 in xenograft models to determine the effect on metastasis
    - Conducting preliminary investigations into additional screen hits, including CLASP1 and p120 catenin

CHAPTER 2: MATERIALS & METHODS

2.1.1 *In vitro* kinase assays

Assays were carried out using recombinant GST-tagged SIK2 kinase domain (either wild-type, T96A or T96G) or GST-tagged full-length SIK2 (SignalChem), along with PI3K p85α (His tag; Abcam) as a substrate. Proteins were incubated with ATP (Sigma Aldrich), ATPγS (Tocris), N^6-Phenylethyl-ATPγS, or N^6-Benzyl-ATPγS (BioLog) at a final concentration of 100 μM in Kinase Assay Buffer I (25 mM MOPS, pH7.2, 12.5 mM β-glycerophosphate, 25 mM $MgCl_2$, 5 mM EGTA, 2 mM EDTA, 0.25 mM DTT; SignalChem) for 20 min at 30 °C. Reactions were terminated by incubation at 95 °C for 5 min. Samples intended for anti-thiophosphate ester western blotting were allowed to cool to room temperature before addition of 50 mM PNBM in DMSO to a final concentration of 2.5 mM. Alkylation was allowed to proceed for 1 h at room temperature before sample preparation for SDS-PAGE as described below.

2.1.2 MALDI-TOF/TOF

Model peptide data were acquired using a Bruker UltraflexTOF/TOF mass spectrometer. Sample clean-up was performed using C_{18} ZipTips (Millipore) and peptides were eluted in α-Cyano-4-hydroxycinnamic acid matrix solution onto a steel MALDI target. Data were analysed using the FlexAnalysis software package (Bruker).

2.1.3 SDS-PAGE and western blotting

Protein samples were prepared by addition of 4x LDS Sample Buffer and incubated at 95 °C for 5 min prior to loading onto NuPAGE 4-12% Bis-Tris 1.5 mm gels (Life Technologies) alongside SeeBlue Plus 2 Pre-stained Protein Standard (Life Technologies). SDS-PAGE was conducted in 1x MOPS buffer at 160V. Proteins were transferred onto nitrocellulose membranes using an iBlot machine (Program 0, 9 min; Invitrogen) and blocked in 5% milk in 1x TBS, 0.1% Tween 20 for 30 min. Primary antibodies used in western blotting were anti-thiophosphate ester (Abcam, ab133473, 1:2000), anti-V5 tag (Abcam, ab27671, 1:1000), anti-PI3K p85α (Abcam, ab22653, 1:1000), anti-myc-tag (Cell Signaling, #2276, 1:1000), anti-GAPDH (Proteintech, #60004-1-Ig, 1:10,000), anti-SIK2 pS358 (Biogenes, custom rabbit polyclonal, 1 μg/ml), anti-p85α pS154 (Biogenes, custom rabbit polyclonal, 1 μg/ml), anti-phospho-AKT (Ser473) (Cell Signaling, #4060, 1:1000), anti-delta 1 catenin (Abcam, ab11508, 1:1000), anti-delta 1 catenin (phospho S268) (Abcam, ab79545, 1:1000), and anti-V5 tag (Abcam, ab9116, 1:1000). Secondary antibodies were Goat anti-Rabbit IRDye 800CW (LI-COR Biosciences, 926-32230, 1:10,000) and Goat anti-Mouse IRDye 680RD (LI-COR Biosciences, 926-68070, 1:15,000). Fluorescent blot images were acquired using a LI-COR Odyssey infrared imaging system[106] (LI-COR Biosciences).

2.1.4 Plasmid preparations

Transformed bacteria were cultured in LB broth at 37 °C overnight (for TOP10 cells) or for 24 h (for Stbl3 cells). LB broth was supplemented with either ampicillin (Sigma Aldrich) at a concentration of 100 µg/ml, chloramphenicol (Sigma Aldrich) at a concentration of 25 µg/ml or kanamycin (Sigma Aldrich) at a concentration of 50 µg/ml, as appropriate. For small scale preparations, plasmid DNA was purified from 5 ml cultures using a QIAprep Spin Miniprep Kit (Qiagen) in accordance with the manufacturer's protocol. For larger preparations, plasmid DNA was purified from 400 ml cultures using a QIAfilter Plasmid Maxi Kit (Qiagen) in accordance with the manufacturer's protocol.

2.1.5 Site-directed mutagenesis

SIK2 human cDNA (also encoding a C-terminal myc-FLAG tag) was obtained from Origene and transformed into One Shot TOP10 Chemically Competent *E.coli* (Life Technologies) using the manufacturer's protocol. Methylated template DNA was obtained from 5 ml bacterial cultures as described in section 2.1.4.

PCR reactions were conducted using Phusion High-Fidelity DNA Polymerase (New England Biolabs) in the reaction buffer supplied, along with 50 ng template DNA and 125 ng of each primer. Table 2.1 contains sequences of primers designed to introduce mutations in the indicated cDNAs. All primers were synthesised by Sigma Aldrich.

Primer	Sequence (5' to 3')
SIK2 T96A +	GTATGTTGTACCTTGTGGCAGAATATGCCAAAAATGGAG
SIK2 T96A -	CTCCATTTTTGGCATATTCTGCCACAAGGTACAACATAC
SIK2 T96G +	GTATGTTGTACCTTGTGGGAGAATATGCCAAAAATGGAG
SIK2 T96G -	CTCCATTTTTGGCATATTCTCCCACAAGGTACAACATAC
SIK2 T96M +	GTATGTTGTACCTTGTGATGGAATATGCCAAAAATGGAG
SIK2 T96M -	CTCCATTTTTGGCATATTCCATCACAAGGTACAACATAC
SIK2 T175A +	GGTGAACTGCTGGCAGCATGGTGTGGCAGCCCC
SIK2 T175A -	GGGGCTGCCACACCATGCTGCCAGCAGTTCACC
SIK2 S358A +	CAGCGTCGGCCTGCAACCATTGCTGAGC
SIK2 S358A -	GCTCAGCAATGGTTGCAGGCCGACGCTG
CLASP1 S600A +	GGGTCCCTCCAGCGATCTCGAGCAGATATTGATGTGAACGCAGCA
CLASP1 S600A -	TGCTGCGTTCACATCAATATCTGCTCGAGATCGCTGGAGGGACCC
CLASP1 S600E +	GGGTCCCTCCAGCGATCTCGAGAAGATATTGATGTGAACGCAGCA
CLASP1 S600E -	TGCTGCGTTCACATCAATATCTTCTCGAGATCGCTGGAGGGACCC
CLASP2 S370A +	GGAAGCCTGCAGCGTTCACGAGCAGACATTGATGTGAATGCTGCT
CLASP2 S370A -	AGCAGCATTCACATCAATGTCTGCTCGTGAACGCTGCAGGCTTCC
CLASP2 S370E +	GGAAGCCTGCAGCGTTCACGAGAAGACATTGATGTGAATGCTGCT
CLASP2 S370E -	AGCAGCATTCACATCAATGTCTTCTCGTGAACGCTGCAGGCTTCC

Table 2.1. Site directed mutagenesis primers

After 18 cycles of amplification, template DNA was digested by addition of DpnI (New England Biolabs) followed by a 1 h incubation at 37 °C. Products were then transformed into One Shot TOP10 cells as above and, following plating on agar containing an appropriate antibiotic, colonies were picked for subsequent DNA preparation and verification by Sanger sequencing (carried out by the WIMM Sequencing Facility). Table 2.2 contains sequences of primers used for Sanger sequencing.

Primer	Sequence (5' to 3')
M13 Forward (−20)	GTAAAACGACGGCCAG
M13 Reverse	CAGGAAACAGCTATGAC
CMV-F	CGCAAATGGGCGGTAGGCGTG
WPRE-R	CATAGCGTAAAAGGAGCAACA
SIK2 753_forward	GTTGGTCCTAGACCCATCCA
CLASP1 1459_forward	TTAGCTGAAACAATAAAGAAGGGAA
CLASP2 1441_forward	TCATTGGAAAGACATGCAGC

Table 2.2. Sequencing primers

2.1.6 Agarose gel electrophoresis

DNA samples were resolved by agarose gel electrophoresis on gels consisting of 0.7% UltraPure Agarose (Life Technologies) in 1x Tris-acetate-EDTA (TAE) buffer (Life Technologies) with 1x GelRed Nucleic Acid Gel Stain (Biotium). Samples were mixed with Gel Loading Dye (NEB) prior to loading alongside an appropriate DNA ladder. Samples were then electrophoresed at 100V for 15 – 45 min. DNA bands were visualised using a UV light box. When necessary, bands were excised using sterile disposable scalpels (Swann Morton) and stored at 4 °C prior to DNA extraction using a QIAquick gel extraction kit (QIAGEN).

2.1.7 Cell culture

293T and OVCA432 cells were maintained in DMEM, High Glucose (Gibco) supplemented with 10% FBS and 1% Penicillin-Streptomycin solution. SK-OV-3 cells were maintained in McCoy's 5A (Gibco) supplemented with 10% FBS and 1% Penicillin-Streptomycin solution. Media for pLX302 stable lines also contained 0.5 µg/ml puromycin. Cell lines for kinase-substrate mapping were maintained in DMEM-R0K0 or -R10K8 SILAC media (Dundee Cell Products), supplemented with 10% dialysed FBS (Gibco), 1% Penicillin-Streptomycin solution, and 0.5 µg/ml puromycin. All cell lines were incubated at 37 °C and 5% CO_2.

2.1.8 Plasmid transfection

293T cells were transiently transfected using FuGENE HD (Promega) in accordance with the manufacturer's protocol (FuGENE HD Protocol Database).

2.1.9 Immunoprecipitation

Cells were collected and washed in ice-cold PBS, and pelleted by centrifugation at 1,500 rpm for 5 min. Cell pellets were lysed in an appropriate volume of TGN buffer (50 mM Tris, pH 7.5, 50 mM Glycerophosphate, 150 mM NaCl, 10% Glycerol, 1% Tween-20, 1 mM NaF, 1 mM $NaVO_4$ and 1 mM DTT, with 1:100 Halt Protease Inhibitor Cocktail (Thermo Scientific) and 1:100 Phosphatase Inhibitor Cocktail 3 (Sigma) freshly added) for 30 min on ice. Lysates were clarified by centrifugation at 13k rpm and 4 °C for 10 min, and protein concentrations were determined using a Pierce BCA Protein Assay Kit (Thermo Scientific) in accordance with the manufacturer's protocol. 30 µl Dynabeads Protein A (Life Technologies) per sample were pelleted using a DynaMag-2 (Life Technologies) magnetic rack, washed, and re-suspended in 50 µl PBS. 3 µg of anti-V5 tag antibody (Abcam) or rabbit control IgG were added and pre-incubated for 30 min. Dynabeads were then washed in 200 µl TGN buffer and added to 0.5 mg lysate. Samples were incubated overnight at 4 °C with end-over-end rotation. Dynabeads were pelleted and washed three times with 0.5 ml TGN buffer, and a further two times in 200 µl 1x Kinase Assay Buffer I (SignalChem, described in section 2.1.1). Dynabeads were then either heated in 1x LDS Sample Buffer at 95 °C for 10 min for SDS-PAGE, or re-suspended in an appropriate volume of 1x Kinase Assay Buffer I for use in *in vitro* kinase assays.

2.1.10 Substrate labelling in live cells

Intact cells were permeabilised and labelled as described by Allen *et al.* (2007). Briefly, transfected 293T cells were collected in ice-cold PBS, pelleted, re-suspended in 0.5 ml permeabilisation buffer (1x PBS, 1x Kinase buffer (Cell Signalling), 1x Halt protease inhibitor cocktail (Thermo Scientific), 1x Phosphatase inhibitor cocktail 3 (Sigma Aldrich) and 50 µg/ml digitonin (Calbiochem)), and incubated on ice for 5 min. Cells were then pelleted and re-suspended in 0.5 ml of the same buffer without digitonin containing 100 µM ATPγS, PhEt-ATPγS or Bn-ATPγS, and 1 mM GTP (Sigma Aldrich). Reactions were incubated for 30 min at 30 °C with orbital shaking at 300 rpm. Cells were then pelleted and lysed in NP-40 buffer (150 mM NaCl, 50 mM Tris and 1% NP-40, pH 8.0, with 1x Halt protease inhibitor cocktail (Thermo Scientific), 1x Phosphatase inhibitor cocktail 3 (Sigma Aldrich)) for 30 min on ice. Lysates were clarified by centrifugation at 13k rpm and 4 °C for 10 min and stored at -80 °C. Aliquots for western blot analysis were alkylated using PNBM as described in section 2.1.1.

2.1.11 Substrate labelling in cell lysates

Cell lysates were labelled using a modified version of the protocol described by Hertz *et al.* (2010). 293T cells transfected with SIK2 wild-type, T96A or T96G, or non-transfected SK-OV-3 cells were collected and lysed in NP-40 buffer as described in section 2.1.10 above. Lysate protein concentrations were determined using a Pierce BCA Protein Assay Kit

(Thermo Scientific) in accordance with the manufacturer's protocol. Protein extracts were labelled in 100 µl reactions containing 100 µg lysate, 1x Kinase buffer (Cell Signalling), 100 µM ATP, 2 mM GTP and 250 µM ATPγS, PhEt-ATPγS or Bn-ATPγS for 30 min at 37 °C. Reactions using protein extracted from non-transfected cells (i.e. not already containing gatekeeper-mutant SIK2) were supplemented with recombinant SIK2 kinase domain to 1% of the total protein mass. Aliquots for western blot analysis were alkylated using PNBM as described in section 2.1.1.

2.1.12 Covalent capture of model thiophosphorylated peptide

Labelled peptides were isolated as described by Hertz *et al.* (2010). Briefly, *in vitro* labelled peptide or digested labelled peptide mixtures were incubated with 50 µl SulfoLink iodoacetyl resin (Thermo Scientific) suspended in 150 µl 50% acetonitrile, 20 mM HEPES, pH 7.0 overnight at room temperature in darkness with end-over-end rotation. Disposable 1 ml columns (Biotage) were equilibrated with 1 ml 50% acetonitrile followed by 1 ml HPLC-grade water (Sigma Aldrich). The reactions were subsequently added to the columns and the flow-through was kept for analysis. 15 ml column reservoirs were attached to the columns and resin was washed with 10 ml HPLC-grade water, 10 ml 5 M NaCl, 10 ml 50% acetonitrile and 10 ml 5% formic acid. The resin was then chemically inactivated by incubation with 1 ml 10 mM DTT for 10 min and thiophosphate-ester linked peptides were eluted with 100 µl 1 mg/ml Oxone (Sigma Aldrich).

2.1.13 Gateway cloning

Following mutagenesis in pDONR221 (Life Technologies), cDNAs were transferred into the pLX302 lentiviral expression vector[107] (a gift from David Root, Addgene plasmid #25896) using Gateway LR Clonase II Enzyme Mix (Life Technologies).

CLASP1 isoform 2 and CLASP2 isoform 3 were amplified from pCMV-SPORT6-CLASP1 (Dharmacon, MGC clone 5501463) and pCR-XL-TOPO-CLASP2 (Dharmacon, MGC clone 9021646) respectively, using the *att*B-containing primers listed below, and PCR products were transferred into the pDONR221 vector using Gateway BP Clonase II Enzyme Mix (Life Technologies).

Primer	Sequence (5' to 3')
CLASP1-*att*B1	GGGGACAAGTTTGTACAAAAAAGCAGGCTTCGAAGGAGATAGAACCATGGAGCCTCGCATGGAGTCC
CLASP1-*att*B2	GGGGACCACTTTGTACAAGAAAGCTGGGTCGCTGTGCGTGGAGACATCGGA
CLASP2-*att*B1	GGGGACAAGTTTGTACAAAAAAGCAGGCTTCGAAGGAGATAGAACCATGGAGCCCCGCAGCATGGAG
CLASP2-*att*B2	GGGGACCACTTTGTACAAGAAAGCTGGGTCACTTTGTCCAGAAACATCAGT

Table 2.3. *att*B primers

2.1.14 Lentiviral transduction

293T cells were transfected (as described in section 2.1.8) with pLX302 plasmids containing the cDNAs of interest along with pMD2.G and pCMV delta R8.2 packaging plasmids (gifts from Didier Trono, Addgene plasmids #12259 and #12263) to produce lentivirus. 24 h after transfection, culture media were replaced with fresh media. A further 24-48 h later media containing lentiviruses were collected, filtered through 0.2 µm syringe filters (Corning) and transferred onto SK-OV-3 or OVCA432 cells in T25 flasks (Corning). The next day, culture media were replaced with fresh media, and 24-48 h later replaced again with media containing 0.5 µg/ml puromycin for selection. Surviving cells were then expanded and protein expression was determined by western blotting.

2.1.15 Kinase-substrate mapping

SKOV3-SIK2 wild-type or T96G cells were cultured in T175 flasks (Corning) as described in section 2.1.7. Two confluent flasks of each cell line were washed once with PBS and disaggregated using trypsin-EDTA for 5 min at 37 °C. Media containing FBS was added to antagonise trypsin activity. Cells were collected and pelleted by centrifugation at 1,500 rpm and 4 °C. Supernatant was removed and cell pellets were re-suspended in 1 ml PBS, transferred to microcentrifuge tubes and pelleted again at 1,500 rpm and 4 °C. Supernatant was removed and lysates were prepared and labelled as described in section 2.1.11. After aliquots were taken for western blotting, 1 M DTT was added to samples to a final concentration of 10 mM and samples were incubated for 30 min at room temperature.

Samples were split into 200 µl aliquots and contaminants were removed using methanol-chloroform extraction. Briefly, 600 µl methanol was added to each aliquot, followed by 150 µl chloroform. Samples were then mixed by vortexing, and 450 µl HPLC-grade water was added to each. Samples were vortexed again prior to centrifugation at 13k rpm for 1 min. The aqueous phase was then removed by pipetting and discarded. 450 µl HPLC-grade water was then added to each sample prior to vortexing. Protein was then pelleted by centrifugation at 13k rpm for 2 min, after which supernatant was removed by pipetting and discarded.

Protein from both sets of samples was then re-dissolved in one volume of 6 M Urea buffer (6 M Urea, 0.1 M Tris, pH 7.8, and 30 mM TCEP). After 30 min, the sample was diluted to 1 M Urea by adding 5 volumes of HPLC-grade water (Sigma Aldrich), and pH was adjusted to ≈ 8.0. Sequencing-grade modified trypsin was dissolved in 0.1 M Tris, pH 7.8 on ice, and added to the sample at a ratio of 1:20 (w/w). pH was checked again, and digestion proceeded overnight at 37 °C.

Tryptic peptides were prepared for covalent capture as described by Hertz *et al.* (2010). Briefly, peptides were desalted using a C18 Sep-Pak cartridge (Waters) and concentrated

to a volume of 50 – 100 µl in a vacuum centrifuge. The sample was then made up to a final concentration of 20 mM HEPES, 50% acetonitrile by adding appropriate volumes of 200 mM HEPES, HPLC-grade water, and acetonitrile (Sigma Aldrich). In an addition to the Hertz *et al*. (2010) protocol, based on a later protocol by Carlson & White (2012), TCEP was added to a final concentration of 5 mM.

Iodoacetyl resin was prepared as described by Carlson & White (2012). Peptides were added to the resin and incubated overnight with end-over-end rotation at room temperature in darkness. Resin was washed and peptides eluted using the gravity-flow protocol described by Carlson & White (2012). The eluate was immediately desalted using C18 SOLA columns (Thermo Scientific) and dried in a vacuum centrifuge. Dried peptide samples were stored at -80 °C prior to LC-MS/MS analysis.

2.1.16 LC-MS/MS

Mass spectrometry data were acquired as described by Fischer & Kessler (2015)[108], using a Q Exactive mass spectrometer (Thermo Scientific) coupled to a Dionex Ultimate 3000 UPLC system (Thermo Scientific). Briefly, samples were separated on an nEASY column (PepMap C18, 75 µm x 500 mm, 2 µm particle, Thermo Scientific) over 60 min using a gradient of 2%-35% acetonitrile in 5% DMSO/0.1% formic acid at 250 nl/min. Survey scans were acquired at a resolution of 70,000 @ 200 m/z and the 15 most abundant precursors were selected for HCD fragmentation[108].

2.1.17 LC-MS/MS data analysis

Peptides were identified using MASCOT (v2.4.1, Matrix Science, USA) with a peptide mass tolerance of 10 ppm, a fragment mass tolerance of 0.07 Da, and a false discovery rate adjusted to 1%. Variable modifications included in the database search were: Deamidated (N), Deamidated (Q), Oxidation (M), Label:13C(6)15N(4)(R), Label:13C(6)15N(2)(K), and Phospho (ST).

2.1.18 Gene ontology analysis

Gene ontology analyses were conducted using PANTHER[109–111] (University of Southern California, USA). The PANTHER Overrepresentation Test (release 20150430) was used to compare lists of proteins to a reference database (GO Ontology database release 20150806). SIK2 was not included in the lists analysed to avoid biasing the results towards previously identified SIK2 functions. Ontologies with Bonferroni corrected *p*-values <0.05 were considered to be significantly enriched.

2.1.19 PI3K Activity Assay

Recombinant PI3K was incubated with SIK2 *in vitro* as described in section 2.1.1 above. PI3K activity was assayed using a PI3 Kinase Activity/Inhibitor ELISA kit (Millipore) in accordance with the manufacturer's protocol.

2.1.20 Xenograft model

Cell lines with stable overexpression of SIK2 were generated as described in section **Error! Reference source not found.** above. Xenograft experiments were carried out as described by Motohara *et al*. (2011). Briefly, cells were injected orthotopically into the left ovarian bursa of 7-week-old C57BL/6 mice (CLEA Japan). Mice were maintained in accordance with institutional guidelines for 6 weeks or until moribund. All experiments were conducted using protocols approved by the animal ethics committees of Keio University, Japan, or The University of Texas MD Anderson Cancer Center, USA.

2.1.21 RNAi

Cells were transfected with siRNA at a concentration of 40 nM using DharmaFECT 4 Transfection Reagent (Dharmacon) in accordance with the manufacturer's protocol at a ratio of 1:200. Cells were incubated for 72 h following transfection. All siRNAs were obtained from the Dharmacon siGENOME collection. siRNA sequences are listed in Table 2.4 below.

siRNA	Sequence (5' to 3')
Non-targeting #4	AUGAACGUGAAUUGCUCAA
SIK2 #10	GGACCGACUCUUCCAAUUU
SIK2 #23	GGUGUGUGCUAUUGCAUAU

Table 2.4. siRNA sequences

2.1.22 Immunofluorescence microscopy

Cells were cultured on glass cover slips in 12-well plates (Corning). Scratch assays were conducted using a 10 µl pipette tip 4 h before fixation. After aspiration of culture media, cells were fixed in 0.5 ml 4% paraformaldehyde in PBS per well for 3 min. 4% PFA was aspirated and 1 ml 100% ethanol (pre-cooled to -20 °C) was added to each well. Plates were stored at -20 °C overnight prior to staining. Ethanol was removed and cover slips were rehydrated for 5 min in 0.5 ml IF wash buffer (1xTBS, 0.2% Triton X-100, and 0.04% SDS), then incubated in blocking buffer (1.5% BSA in 1xTBS) for 1 h. Primary antibodies were added in fresh blocking buffer at an appropriate concentration and incubated for 1 h at room temperature. Cover slips were subjected to three 3 min washes with 0.5 ml wash buffer, before adding secondary antibodies at a concentration of 1:250 in fresh blocking buffer. Secondary antibodies were incubated for 1 h at room temperature in the

dark before a further three washes as above, and cover slips were mounted on glass microscope slides (Fisher Scientific) using VECTASHIELD Antifade Mounting Medium with DAPI (Vector Laboratories). Primary antibodies used for immunofluorescence were anti-V5 tag (Abcam, ab9116, 1:1000) and anti-α-tubulin (Sigma Aldrich, T5168, 1:100). Secondary antibodies were Alexa Fluor 546 Donkey anti-Mouse and Alexa Fluor 488 Donkey anti-Rabbit (Life Technologies, both 1:250). Images were acquired using a Zeiss Axio Observer Z1 inverted microscope with a 100x oil immersion objective lens.

2.1.23 Time-lapse microscopy

SK-OV-3-pLX302 cells were seeded into 12 well plates at a density of 50,000 cells/well. Images were acquired using a Leica DM IRE2 inverted microscope equipped with a Hamamatsu ORCA-ER CCD camera at 5 min intervals over a period of 3 h. Cells were incubated at 37 °C, 5% CO_2 for the duration.

2.1.24 Software

Protein sequence alignments were carried out using COBALT (NCBI, USA)[112]. Protein structures were rendered in QuteMol (ISTI, Italy)[113]. Primers were designed using either the QuikChange Primer Design Tool (Agilent Technologies, USA), or SnapGene (v2.5 – v2.7, GSL Biotech, USA). Statistical tests were conducted using GraphPad Prism (v6.07, GraphPad Software, USA). Quantification of western blot bands was conducted using the LI-COR Odyssey Application (v3.0.16, LI-COR Biosciences, USA). Canonical SIK substrate motifs were identified using ScanProsite[114] (Swiss Institute of Bioinformatics, Switzerland). Sequence logo analysis was conducted using the PSP Production algorithm in PSPlogo[115] (Cell Signaling Technology, USA). Fluorescence microscope images were acquired using the Zeiss Zen Software (v2012, ZEISS, Germany). Scale bars were added to microscope images using Fiji (ImageJ v1.50b, National Institutes of Health, USA).

CHAPTER 3: OPTIMISING A SCREEN FOR NOVEL SIK2 SUBSTRATES

3.1 Introduction

In order to conduct a screen to identify novel substrate proteins downstream of SIK2, it was first necessary to determine whether SIK2 would be tractable to such an approach. The first portion of this chapter addresses the ability of SIK2 to utilise ATPγS or 'bulky' analogues, whilst the remainder deals with the optimisation of several discrete components of the screen experiment.

Once a modified kinase has labelled its substrate proteins using an ATPγS analogue, there are two distinct protocols which can be used to isolate thiophosphorylated products for analysis. The first of these is based on immunoprecipitation (Figure 3.1a) and utilises an electrophilic tag, *p*-nitrobenzyl mesylate (PNBM), to alkylate the thiophosphate, constructing a thiophosphate ester which serves as a 'semi-synthetic' epitope for recognition by a monoclonal antibody. Critically, although PNBM also alkylates other cellular thiols (e.g. cysteine), these form chemically distinct thioethers, which are not recognised by the antibody[104]. Thus the antibody allows specific immunoprecipitation of the substrates of the kinase of interest, which can then be subjected to proteolytic digestion and identification by tandem mass spectrometry.

Alternatively, labelled proteins can be digested and labelled peptides can be covalently captured by an iodoacetyl resin (Figure 3.1b). Similar to the previous method, cysteine-containing peptides are also captured but form a distinct thioether linkage. Upon treatment with an oxidising agent, the thiophosphate ester linkages undergo spontaneous hydrolysis, whereas the thioether linkages remain stable, resulting in specific elution of phosphorylated peptides for analysis by mass spectrometry[116] (Figure 3.2).

An obvious drawback of the covalent capture approach is that any thiophosphorylated peptides which also contain cysteine will remain bound to the resin and will therefore not be detected, although this can theoretically be alleviated by conducting two screen experiments in parallel using two distinct proteases[116]. On the other hand, because labelled peptides are specifically isolated (as opposed to whole proteins digested following immunoprecipitation), target phosphorylation sites are directly identified by mass spectrometry, facilitating subsequent functional experiments. For this reason, the covalent capture method was selected for the screen described herein.

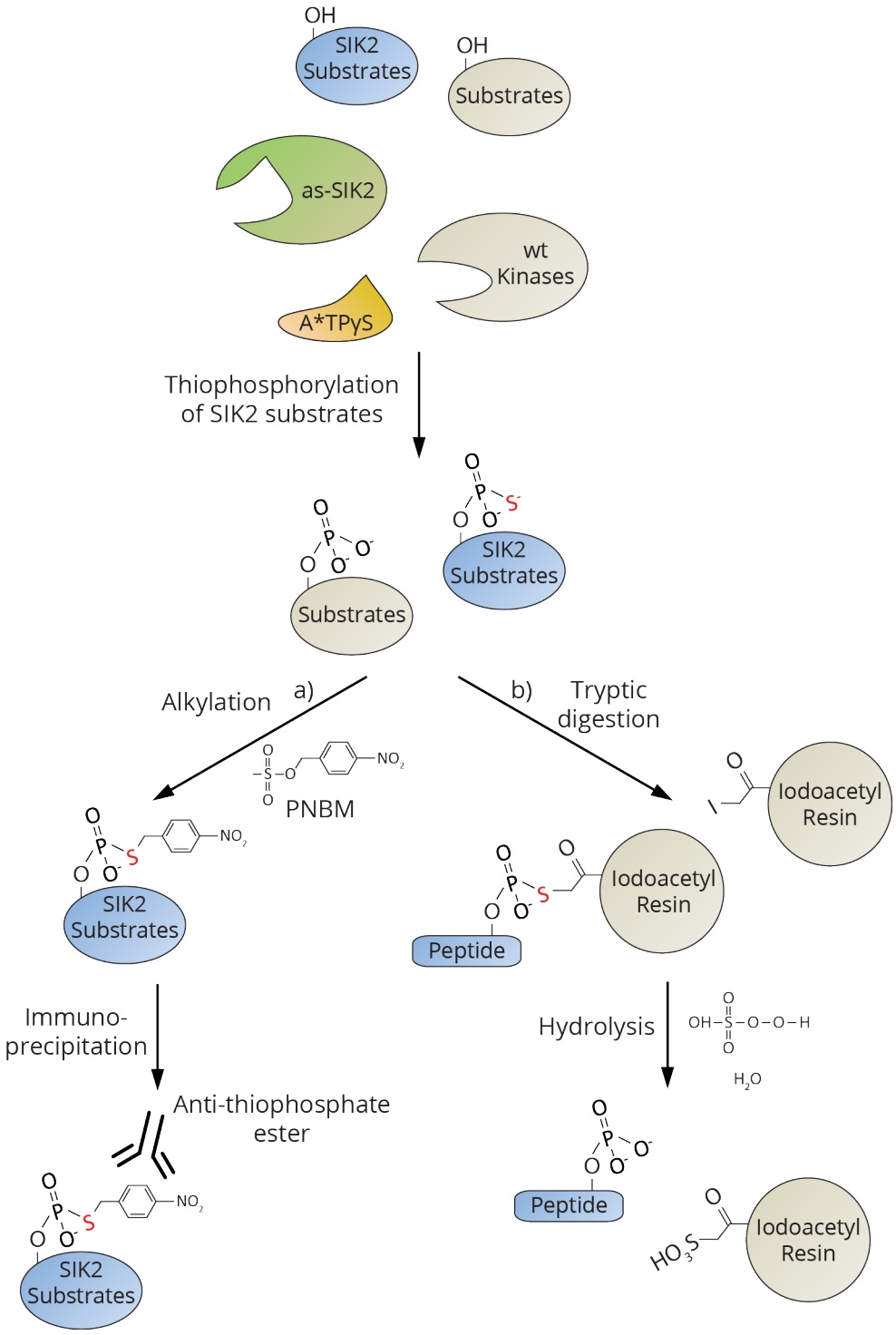

Figure 3.1. Chemical genetic screening techniques

In a chemical genetic screen, a 'bulky' A*TPyS analogue is supplied to an engineered kinase resulting in specific labelling of its substrates with thiophosphate groups. These may be: **a)** alkylated to construct an epitope for immunoprecipitation, or **b)** captured on an iodoacetyl resin, allowing specific recovery of substrate peptides for identification.

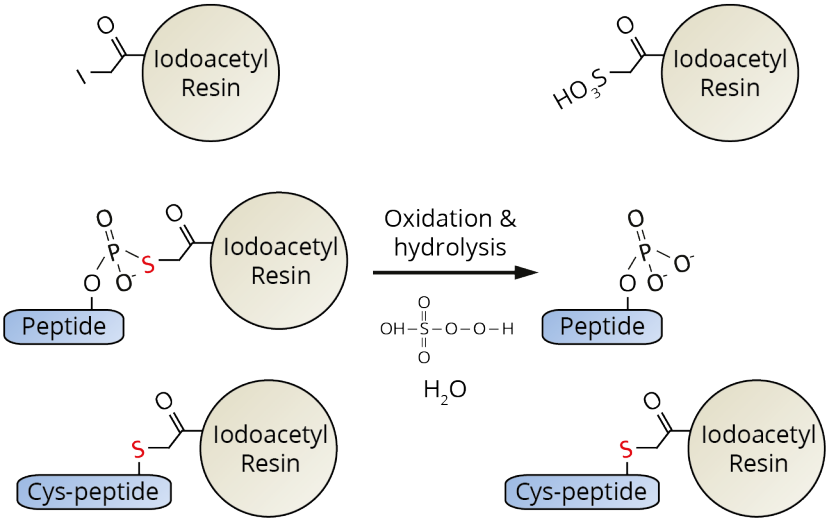

Figure 3.2. Retention of cysteine-containing peptides

Peptides containing cysteine are also captured by the iodoacetyl resin, forming a thioether linkage. Whilst thiophosphate ester linkages undergo spontaneous hydrolysis in the presence of an oxidising elution buffer, the thioether linkages remain stable, leaving cysteine-containing peptides bound to the resin.

3.2 Results

3.2.1 Wild-type SIK2 can utilise ATPγS

Although a majority of protein kinases are capable of catalysing the transfer of a γ-thiophosphate group from ATPγS, an essential requirement for the intended method of screening, this is not a universal trait[104]. In order to verify the ability of SIK2 to utilise ATPγS, recombinant His/GST-tagged SIK2 kinase domain was produced in Sf9 insect cells using a baculovirus expression system, and purified with a Ni^{2+}-affinity resin. Recombinant SIK2 was incubated with substrate peptides in the presence of ATP or ATPγS.

The first of these peptides (LAGLHHSLSHSLLAV) corresponds to the SIK2 phosphorylation site on CEP250 identified by Ahmed *et al*. (2010). MALDI-TOF analysis of the peptides following incubation with SIK2 kinase domain *in vitro* showed clear utilisation of both ATP and ATPγS, as indicated by respective peaks at m+80 and m+96 relative to the untreated peptide (Figure 3.3).

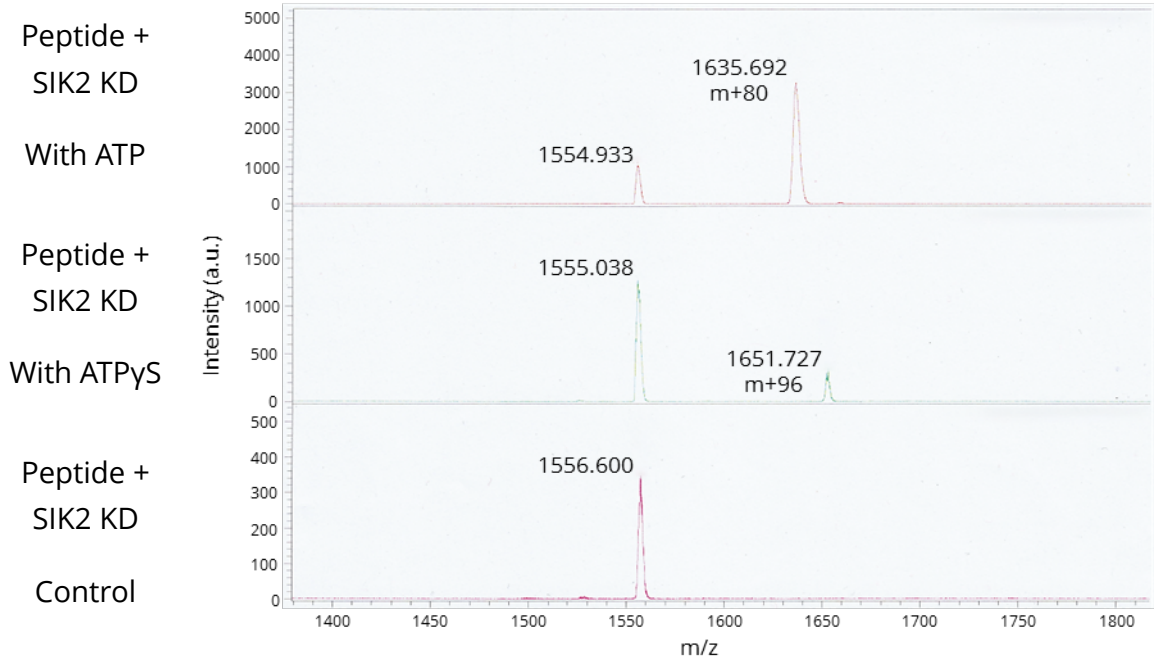

Figure 3.3. Mass spectra following *in vitro* kinase reactions (CEP250)

Peptides corresponding to the previously identified SIK2 phosphorylation site on CEP250 (S2392) were analysed by MALDI-TOF mass spectrometry following incubation with SIK2 and ATP or ATPγS. Spectra are representative results from triplicate experiments. Peak intensity is shown in arbitrary units (a.u.). m/z denotes mass/charge ratio.

Similar results were also obtained using a second peptide (TQSSSNLAESTLYR, Figure 3.4), which corresponds to a consensus phosphorylation site (S154) in the p85α regulatory subunit of PI3K, which we identified in an *in silico* screen for instances of the published SIK substrate motif LX[H/K/R][S/T]XpSXXXL[51] in the Swiss-Prot database using ScanProsite[114] (for full results see Appendix I). The presence of a potential site of SIK2 phosphorylation in p85α is of significant interest as the PI3K/AKT pathway is a key oncogenic signalling pathway[44,117], and depletion of SIK2 has been associated with decreased activation of AKT in ovarian cancer cells[6]. Since CEP250 recombinant protein is not readily available, p85α recombinant protein was used for subsequent *in vitro* experiments.

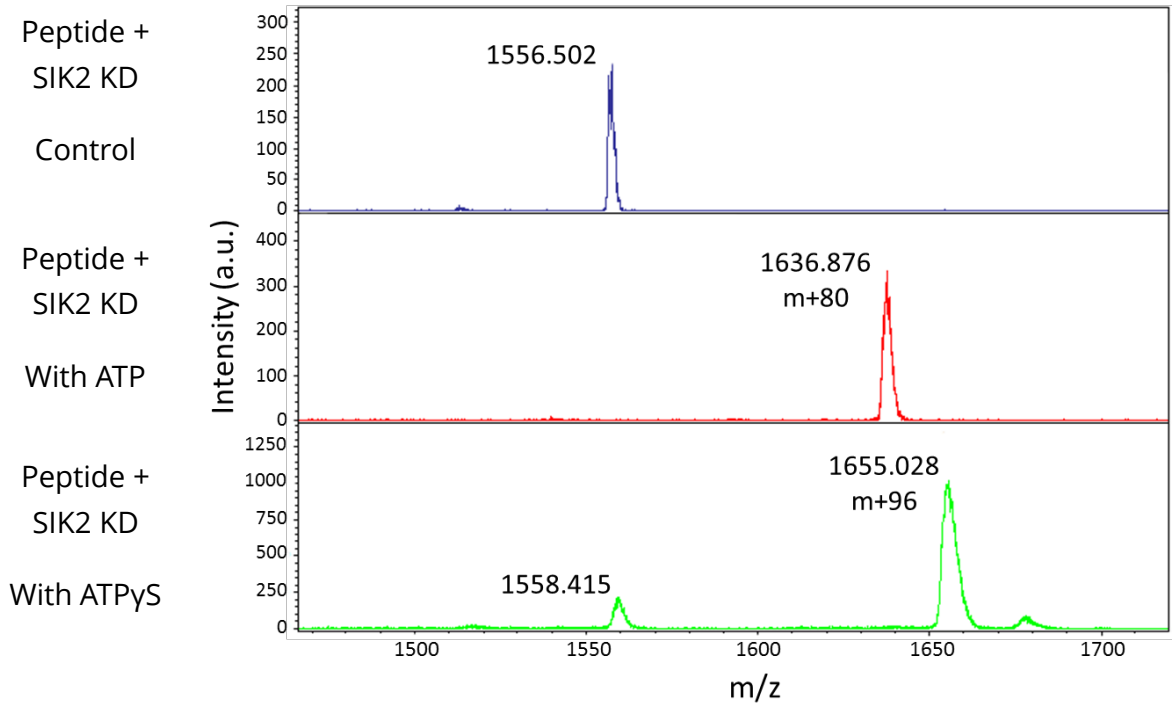

Figure 3.4. Mass spectra following *in vitro* kinase reactions (p85α)

Peptides corresponding to a newly identified SIK consensus sequence at S154 of p85α were analysed by MALDI-TOF mass spectrometry following incubation with SIK2 and ATP or ATPγS. Spectra are representative results from triplicate experiments. Peak intensity is shown in arbitrary units (a.u.). m/z denotes mass/charge ratio.

3.2.2 The SIK2 gatekeeper residue is threonine 96

In order to identify the gatekeeper residue in SIK2, the amino acid sequence was aligned with a number of kinases which have previously been used in chemical genetic approaches, in addition to several closely related kinases (Figure 3.5a). This revealed that threonine 96 is the gatekeeper residue in human SIK2, and is consistent with the result of another analysis which has since been published by Clark *et al*. (2012).

Since no crystal structure is available for SIK2, confirmation of this result using structural data was not possible. However, in the crystal structure of the closely-related MARK3 kinase[118] (PDB: 3FE3) the equivalent methionine 132 residue occupies the expected position at the hinge region of the ATP binding pocket (Figure 3.5b), suggesting that this is indeed the gatekeeper residue.

a)

Kinase	Sequence
SIK2	^{88}T K S M L Y L V **T** E Y A K N G E I
SIK1	^{95}T K D M L Y I V **T** E F A K N G E M
SIK3	^{76}T E R M I Y L V **T** E Y A S G G E I
AMPKα1	^{87}T P S D I F M V **M** E Y V S G G E L
AMPKα2[10]	^{85}T P T D F F M V **M** E Y V S G G E L
MARK3	^{124}T E K T L Y L I **M** E Y A S G G E V
CDK1[116]	^{72}Q D S R L Y L I **F** E F L - S M D L
CDK2[100]	^{72}T E N K L Y L V **F** E F L - H Q D L
ERK2[99]	^{95}Q M K D V Y I V **Q** D L M - E T D L

b)

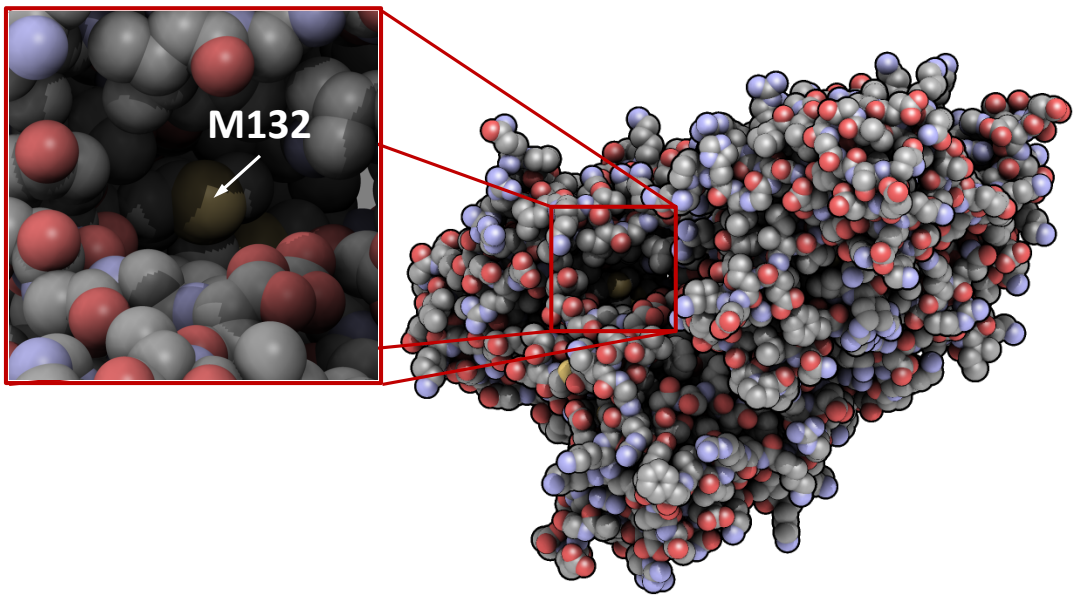

Figure 3.5. Gatekeeper sequence alignment and MARK3 structure

a) Sequence alignment of nine protein kinases. The amino acid sequences of SIK2 and five other members of the AMPK-related family were aligned with those of kinases which have previously been used in chemical genetic screens using the COBALT Multiple Alignment Tool (NCBI). The gatekeeper residue is marked in red. **b)** Representative structure of the MARK3 homodimer (PDB: 3FE3)[118]. M132 corresponds to SIK2 T96 and is clearly located within the ATP binding pocket. Structures were rendered in QuteMol.

3.2.3 Wild-type SIK2 cannot utilise ‘bulky’ ATPγS analogues

To confirm that wild-type SIK2 is a suitable negative control for use in screen experiments despite having a relatively small threonine gatekeeper, recombinant SIK2 kinase domain was incubated with p85α protein along with ATPγS or one of several N^6-substituted analogues. Quantification of western blot bands demonstrated that wild-type SIK2 is not able to utilise any of the analogues tested to thiophosphorylate p85α (Figure 3.6a & b). Similar results were also obtained using a commercially available full-length SIK2 protein (data not shown).

In order to detect ATPγS utilisation by western blot, an alkylating agent (PNBM) was used to tag transferred thiophosphate groups, constructing a ‘semi-synthetic’ epitope for recognition by a monoclonal antibody. The antibody is highly specific to the resulting thiophosphate ester, resulting in a signal only in samples treated with both ATPγS and PNBM (Figure 3.6c).

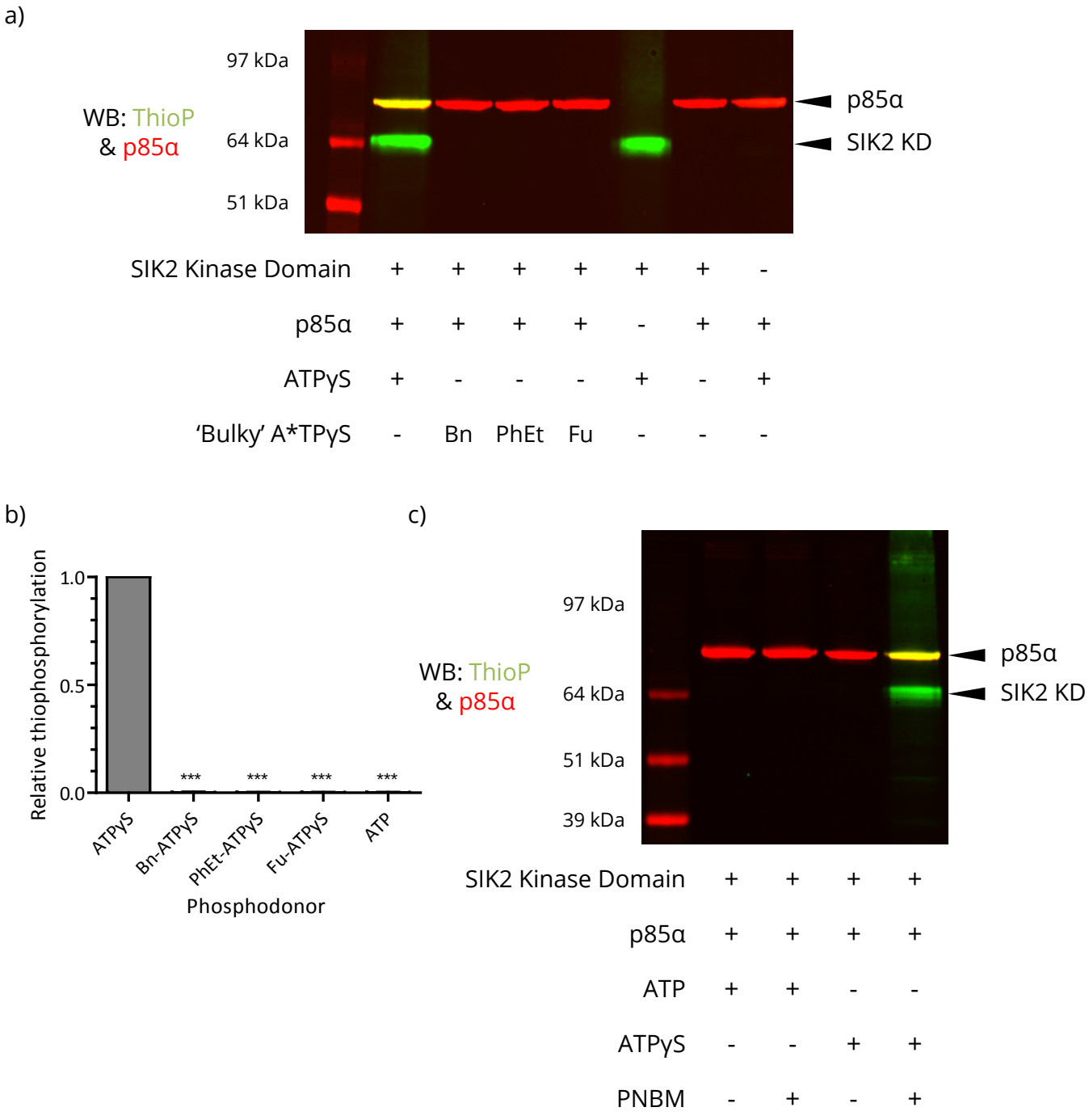

Figure 3.6. Western blot detection of thiophosphorylated proteins

a) SIK2 kinase domain was incubated with p85α and a variety of different phosphodonors. All samples were treated with PNBM prior to western blotting. **b)** Graph of relative p85α thiophosphorylation by SIK2 kinase domain with different phosphodonors. Bands from triplicate experiments were quantified using the LI-COR Odyssey Application (LI-COR Biosciences, v3.0.16). All values were normalised to the ATPγS positive control. ANOVA with Dunnett's Multiple Comparison Test was used to test for significant differences between the means for each treatment and the positive control (*** denotes p≤0.001). **c)** p85α was phosphorylated or thiophosphorylated by SIK2 *in vitro*. Half of the samples were treated with PNBM prior to western blotting. All experiments were conducted in triplicate.

3.2.4 SIK2 T96G can utilise 'bulky' ATPγS analogues *in vitro*

Purified SIK2 T96A or T96G mutant protein was incubated with ATPγS or 'bulky' analogues *in vitro* in order to determine the most suitable mutant/analogue combination for screening. Although kinase activity of both mutants appeared to be compromised compared to the wild-type with regular ATPγS, activity of the T96G mutant was recovered in the presence of PhEt-ATPγS (Figure 3.7a). To confirm this finding, SIK2 containing a C-terminal V5 tag was transiently expressed in 293T cells and immunoprecipitated using an anti-V5 tag antibody. The immunoprecipitate was then incubated with ATPγS analogues *in vitro*. In contrast to the previous experiment, both wild-type and T96G appear to be active and able to utilise ATPγS, as evidenced by clear autothiophosphorylation (Figure 3.7b). When supplied with Bn- or PhEt-ATPγS, autothiophosphorylation was observed only in the T96G mutant, demonstrating specific analogue utilisation.

a)

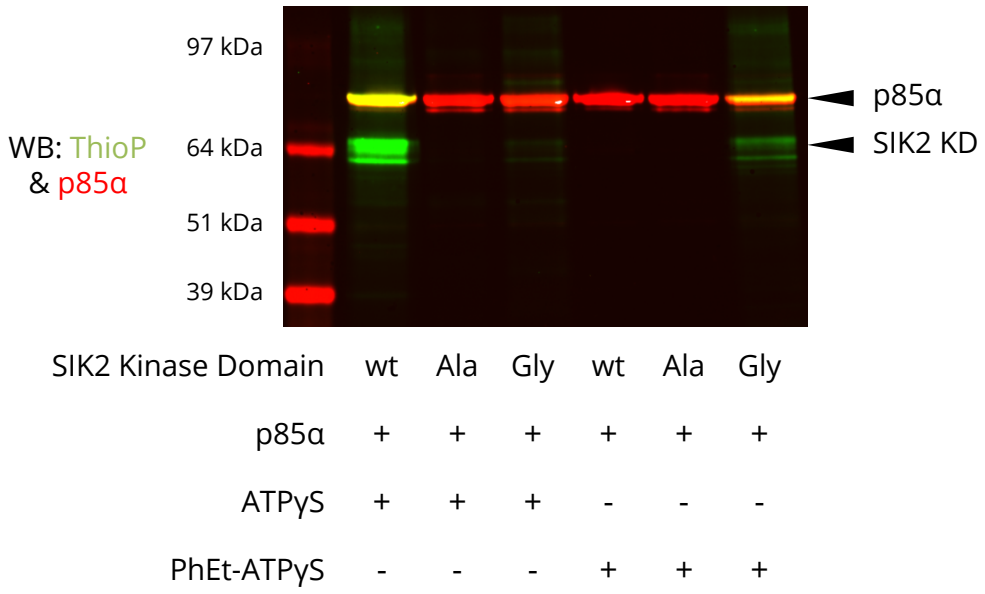

SIK2 Kinase Domain	wt	Ala	Gly	wt	Ala	Gly
p85α	+	+	+	+	+	+
ATPγS	+	+	+	-	-	-
PhEt-ATPγS	-	-	-	+	+	+

b)

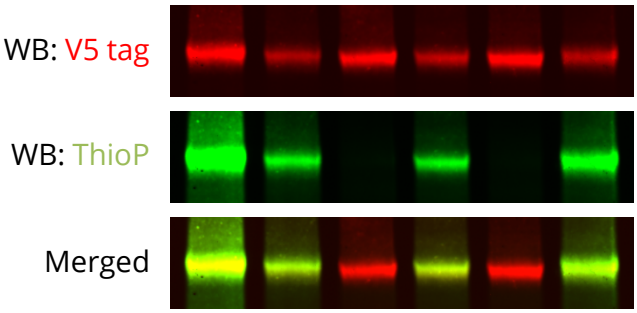

IP:SIK2-V5	wt	Gly	wt	Gly	wt	Gly
ATPγS	+	+	-	-	-	-
Bn-ATPγS	-	-	+	+	-	-
PhEt-ATPγS	-	-	-	-	+	+

Figure 3.7. Western blots following incubation with 'bulky' analogues

a) Wild-type, T96A or T96G SIK2 kinase domains were incubated with p85α and ATPγS or PhEt-ATPγS. **b)** Wild-type or T96G SIK2-V5 was immunoprecipitated and incubated with ATPγS, Bn-ATPγS or PhEt-ATPγS. All samples were treated with PNBM prior to western blotting. Blots are representative of duplicate experiments.

3.2.5 SIK2 T96G can utilise 'bulky' ATPγS analogues in live cells and cell lysates

Having established the ability of the T96G mutant to utilise PhEt-ATPγS, three different strategies to label SIK2 substrates were trialled: 1) transient expression of SIK2 T96G in 293T cells followed by permeabilisation and labelling; 2) transient expression of SIK2 T96G in 293T cells followed by lysis and labelling in lysates; and 3) addition of recombinant SIK2 kinase domain to non-transfected cell lysates for labelling.

The first of these approaches yielded a 2.25-fold difference in labelling intensity between the wild-type and T96G mutant when treated with PhEt-ATPγS, however there was clear background utilisation of the analogue in the wild-type control (Figure 3.8). This is likely to be attributable to other kinases, since wild-type SIK2 was not able to utilise 'bulky' analogues *in vitro*. Autothiophosphorylation with PhEt-ATPγS is visible in the T96G mutant, but not in wild-type SIK2, providing further evidence for specific analogue utilisation by this gatekeeper mutant.

For the remaining approaches, 293T cells were lysed using a mild NP-40 buffer prior to labelling. This buffer was selected as it is non-denaturing, and similar buffers have been successfully used in other such experiments[104].

Similar to the first approach, incubation of lysates of transfected 293T cells with PhEt-ATPγS also yielded a clear quantitative difference in substrate labelling between wild-type SIK2 and the T96G mutant, with 5-fold more labelling in the mutant and clear autothiophosphorylation (Figure 3.9). In addition to a greater signal-to-background ratio, the fluorescence intensity was also higher in absolute terms when compared to labelling in permeabilised cells (although it is difficult to draw robust comparisons between separate western blots, this held true across multiple replicates). Whilst some autothiophosphorylation using Bn-ATPγS is visible in the T96G mutant, quantification of fluorescence from the whole lane shows little difference from the wild-type.

For the final approach, in which lysates were supplemented with recombinant kinase, no clear utilisation of PhEt-ATPγS was observed using either the T96G or T96A gatekeeper mutants compared to the wild-type (Figure 3.10), suggesting that this approach is not ideal for identifying SIK2 substrates.

a)

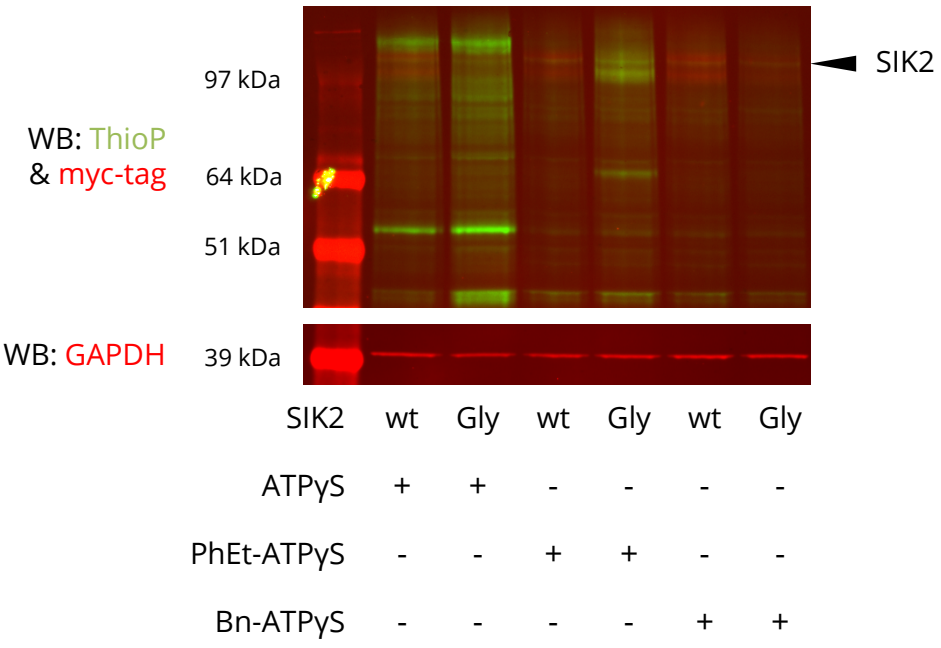

b)

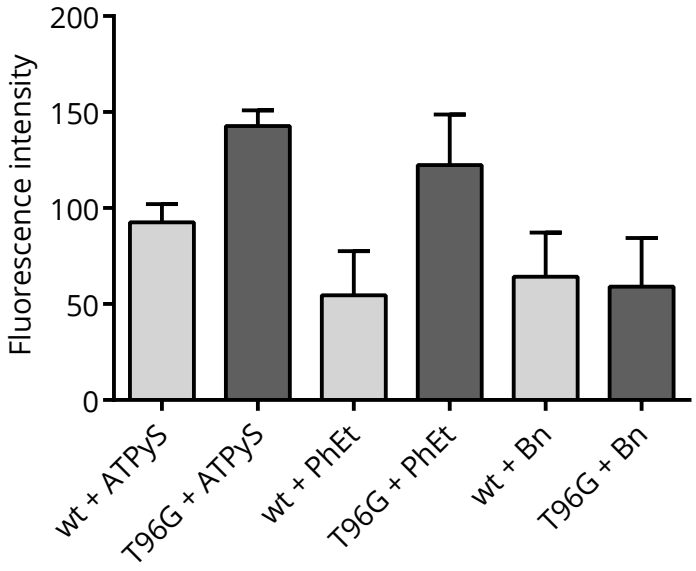

Figure 3.8. Western blot following labelling in intact cells

a) 293T cells were transfected with SIK2-myc-FLAG constructs, permeabilised using digitonin, and incubated with ATPγS or PhEt-ATPγS. Thiophosphorylation and SIK2 expression were detected by western blotting. **b)** Signal from the anti-thiophosphate ester antibody was quantified for each lane using the LI-COR Odyssey Application (LI-COR Biosciences, v3.0.16). Data shown are mean fluorescence intensities (±SEM) from two independent experiments, in arbitrary units.

a)

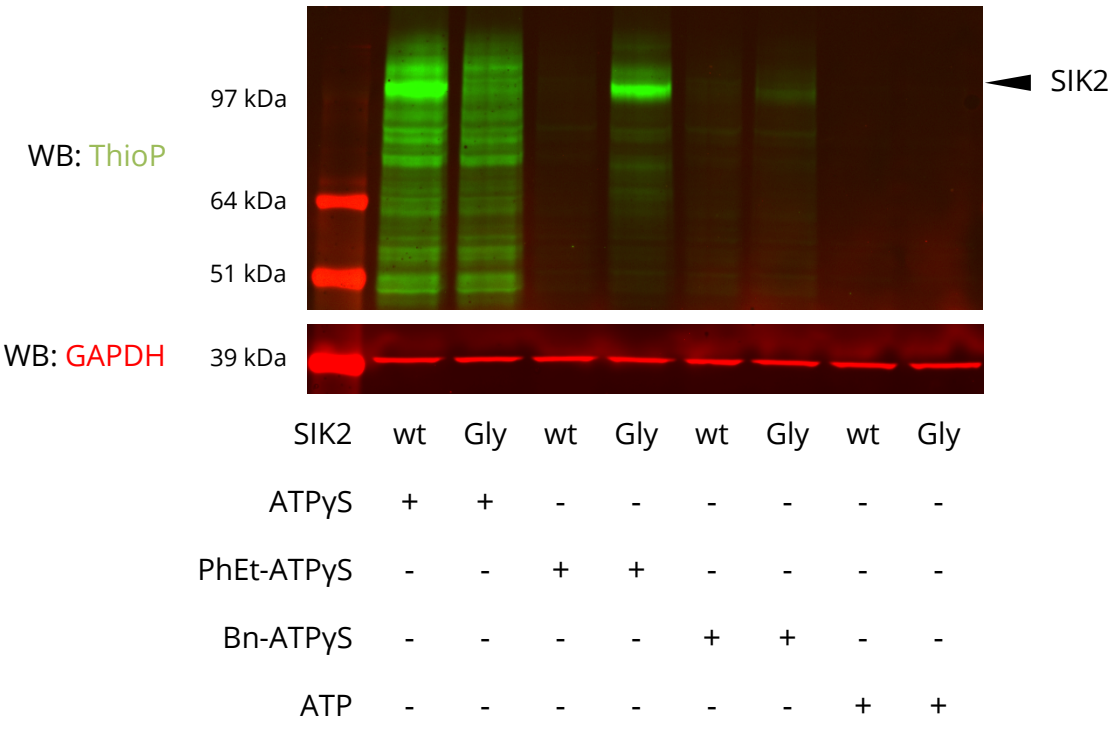

b)

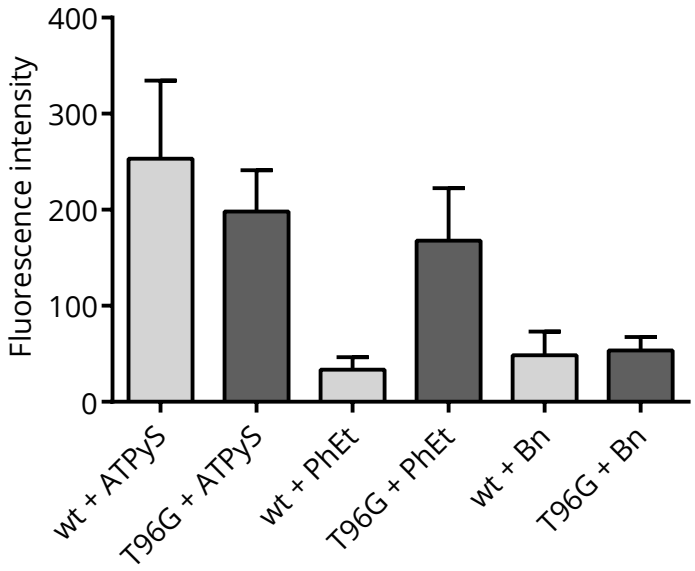

Figure 3.9. Western blots following labelling in 293T lysates

a) 293T cells overexpressing SIK2-V5 were lysed and incubated with ATPγS or 'bulky' analogues. Thiophosphorylation was detected by western blotting. **b)** Signal from the anti-thiophosphate ester antibody was quantified for each lane using the LI-COR Odyssey Application (LI-COR Biosciences, v3.0.16). Data shown are mean fluorescence intensities (±SEM) from two independent experiments, in arbitrary units.

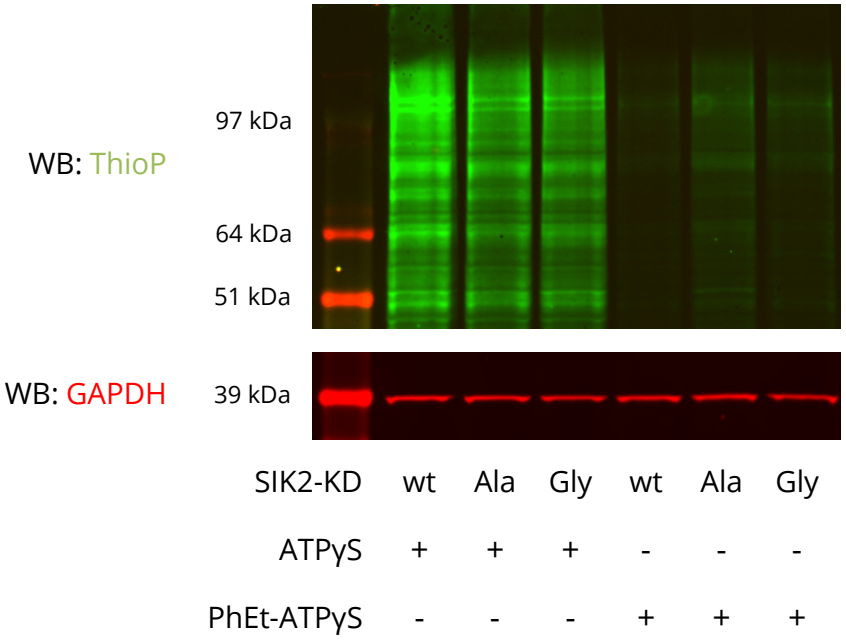

Figure 3.10. Western blots following labelling using recombinant SIK2

SK-OV-3 lysates were supplemented with recombinant SIK2 to 1% of total protein mass and incubated with ATPγS or PhEt-ATPγS. GAPDH confirms equal loading.

3.2.6 Thiophosphorylated peptides can be specifically captured

In order to test a protocol for specific recovery of labelled peptides[119] (see section 2.1.12), thiophosphorylated peptides were generated *in vitro* (as in Figure 3.3 and Figure 3.4) and captured covalently using an iodoacetyl resin. Following multiple washes, elution in an oxidising buffer, and sample desalting, eluted peptides were analysed using MALDI-TOF mass spectrometry and compared with an identical sample not subjected to purification (Figure 3.11). In the non-purified sample, unmodified peptide was the dominant constituent whilst thiophosphorylated peptide was visible as a much smaller peak (m+96). However, following enrichment, unmodified peptide was almost entirely removed from the sample and phosphopeptides were recovered (m+80). This change in mass is due to replacement of the sulphur by an oxygen atom during hydrolysis of the thiophosphate ester linkage.

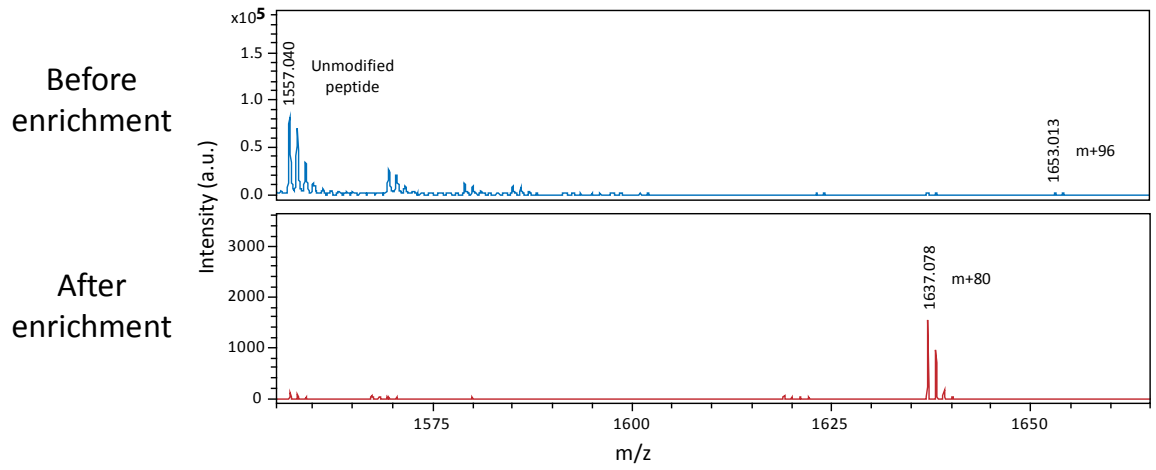

Figure 3.11. Mass spectra showing peptide enrichment following covalent capture

Peptides were subjected to MALDI-TOF before and after enrichment and data were analysed using FlexAnalysis (Bruker). Note that y-axes are scaled differently due to a large excess of unmodified peptide in the non-purified sample. Results represent the culmination of a series of optimisation experiments.

3.2.7 Generation of SK-OV-3-SIK2 cell lines

To allow screening for substrates in an ovarian cancer system, a lentiviral expression vector[107] (see section 2.1.14) was used to overexpress SIK2 in the SK-OV-3 ovarian cancer cell line. Puromycin selection was used to generate pools of SK-OV-3 cells stably overexpressing either SIK2 wild-type or T96G. Following selection, these SK-OV-3-SIK2 lines had high expression of SIK2 and exhibited highly specific substrate labelling when lysates were incubated with PhEt-ATPγS (Figure 3.12), with 24.1-fold more labelling in the T96G mutant compared to the wild-type.

a)

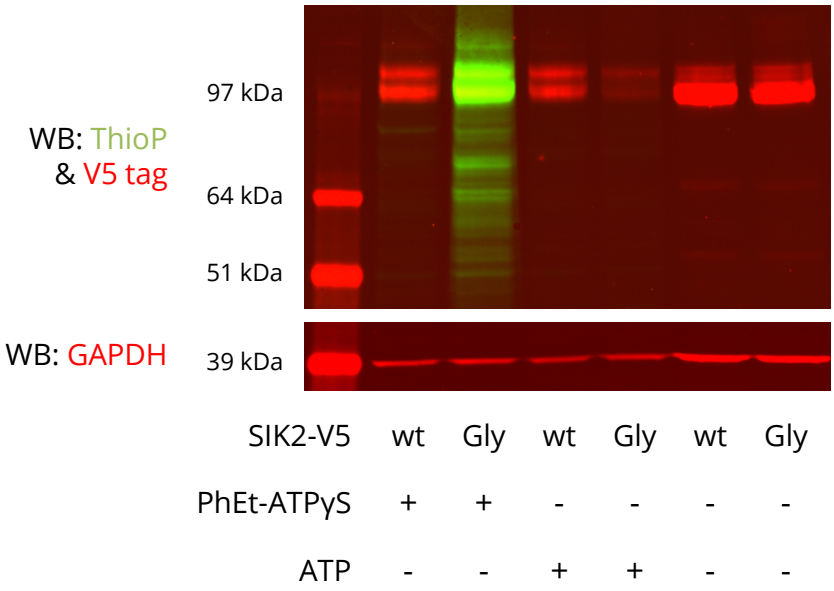

b)

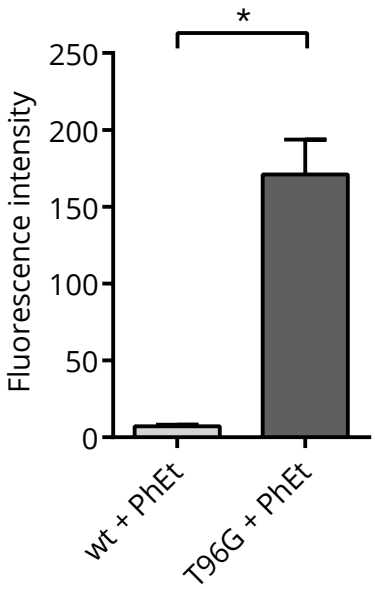

Figure 3.12. Western blot following labelling in SK-OV-3-SIK2 lysates

a) Whole cell lysates from SK-OV-3-SIK2 cells were incubated with either PhEt-ATPγS or ATP. Thiophosphorylation was detected by western blotting after treatment with PNBM. The rightmost two lanes were loaded with untreated whole cell lysate. **b)** Signal from the anti-thiophosphate ester antibody was quantified for each lane using the LI-COR Odyssey Application (LI-COR Biosciences, v3.0.16). Data shown are mean fluorescence intensities (±SEM) from three independent experiments, in arbitrary units. Means were compared using a paired *t*-test (* denotes $p \leq 0.05$).

3.2.8 Preliminary screen data

Having produced a reliable system in which to label SIK2 substrates and demonstrated a means of isolating labelled phosphorylation sites, labelled lysates were used to conduct preliminary screen experiments. Wild-type- and T96G-expressing SK-OV-3 lysates were incubated with PhEt-ATPγS, then digested and purified separately. Phosphopeptides in each sample were then identified by LC-MS/MS. Any peptides identified in the wild-type control were removed from the list of putative substrates discovered in the T96G sample. However, after a series of optimisation experiments, this still only yielded five putative SIK2 phosphorylation sites (Table 3.1), a number which is not consistent with the extensive labelling observable by western blotting (Figure 3.13). Although the approach seems to have worked in principle, identifying a novel SIK2 autophosphorylation site (S674), no canonical SIK2 substrates were detected.

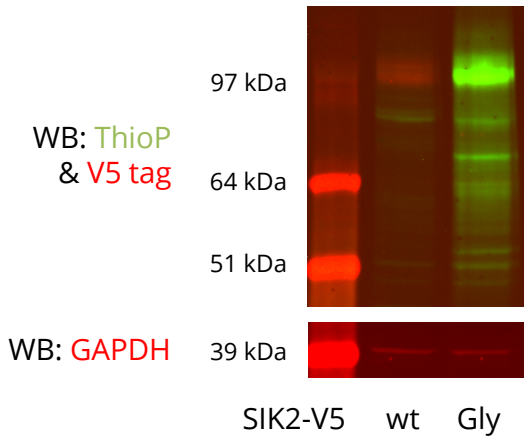

Figure 3.13. Western blot following preliminary screen labelling

SK-OV-3-SIK2 whole cell lysate was incubated with PhEt-ATPγS. Thiophosphorylation was determined by western blotting after treatment with PNBM.

Uniprot accession	Protein name	Peptide sequence	MASCOT score	E value	pSite
Q9H0K1	Serine/threonine-protein kinase SIK2	QSLETQYLQHR	70.45	0.0000062	S674
Q99439	Calponin-2	CDNSSMSLQMGYTQG-ANQSGQVFGLGR	59.73	0.00018	S246
P78562	Phosphate-regulating neutral endopeptidase	KFSLLQTLATFR	48.55	0.0011	S186, T193
Q13283	Ras GTPase-activating protein-binding protein 1	SSSPAPADIAQTVQEDLR	*34.93*	0.00061	S232
Q06210	Glutamine-fructose-6-phosphate aminotransferase	VDSTTCLFPVEEK	*33.01*	0.0022	S261

Table 3.1. Preliminary screen hits

3.3 Discussion

This aim of this project was to optimise a chemical genetic screen to identify novel SIK2 substrates. A similar approach has recently been successfully applied to identify a role in mitotic progression for the related AMPKα2 kinase[105], suggesting that SIK2 might also prove amenable to screening. The SIK2 gatekeeper residue was identified as threonine 96 by alignment with four kinases which have previously been used in chemical genetic approaches. Although threonine is already a relatively small residue, it is the second most commonly occurring gatekeeper residue in animal kinases, after methionine[100].

In order to determine the feasibility of conducting a screen for SIK2, the ability of SIK2 to transfer the γ-thiophosphate from ATPγS was verified, as this is an absolute requirement of the approaches outlined in section 3.1. Given that the SIK sub-family all have threonine gatekeepers rather than the larger residues found in the other aligned kinases (i.e. methionine, phenylalanine or glutamine), it was also necessary to establish that wild-type SIK2 could not already utilise 'bulky' analogues, as this would have meant that wild-type SIK2 would not be a suitable control for use in screening experiments.

Based on autophosphorylation of immunoprecipitated SIK2 (Figure 3.7b), the T96G mutant appears to have a comparable level of kinase activity to the wild-type. Although some of the *in vitro* data (Figure 3.7a) would appear to contradict this interpretation, these assays were conducted with preliminary T96A and T96G protein preparations. It is possible that this anomaly reflects a difference in the effect of the gatekeeper mutation on stability in the GST-tagged kinase domain compared with the V5-tagged full-length protein.

The SIK2 T96G mutant successfully utilised PhEt-ATPγS in live cells and cell lysates, suggesting that this is the optimal mutant/analogue combination to use in screening for SIK2 substrates. Whilst utilisation of Bn-ATPγS was observed *in vitro* (Figure 3.7b), it did not perform as well as PhEt-ATPγS in either permeabilised cells (Figure 3.8) or cell lysates (Figure 3.9).

Of the labelling strategies tested, expression of SIK2 T96G in cells followed by permeabilisation and incubation with PhEt-ATPγS should yield the most physiologically relevant screen results as the cellular architecture remains relatively intact. However, this approach resulted in less efficient labelling compared with SIK2-expressing cell lysates, and as such it had a lower ratio of specific (T96G) to non-specific (wt) signal. One possible explanation for this difference is reduced availability of the analogue in intact cells relative to the cell lysates, potentially due to inefficient permeabilisation. Alternatively, the loss of cellular compartmentalisation upon cell lysis might have allowed SIK2 to label non-physiological substrates, resulting in the observed increase in labelling in the lysates. Despite this possibility, the labelling is the first of several critical steps in the screen

protocol which determine the overall efficacy, so the decision was made to prioritise labelling intensity and specificity by using SIK2-expressing cell lysates for the screen itself. The third approach, supplying recombinant SIK2 kinase domain to cell lysates, did not appear to be an effective approach for labelling SIK2 substrates, although it has been widely applied elsewhere.

The 293T cell line was selected for optimisation experiments due to its fast growth and high efficiency of transfection, but it bears little relevance to the biological question of the role of SIK2 in ovarian cancer. For this reason, SK-OV-3, a widely used ovarian cancer cell line in which SIK2 has been shown to modulate the response to paclitaxel[6], was selected to maximise the probability of identifying biologically relevant substrates. SK-OV-3 is difficult to transiently transfect with high efficiency, so a lentiviral system was used to stably overexpress SIK2 wild-type or T96G. Incubating these cell lysates with PhEt-ATPγS resulted in strong, specific labelling of putative SIK2 substrates, allowing preliminary screen experiments to be conducted.

Although an *in vitro* thiophosphorylated peptide was successfully isolated using a covalent capture approach, the same protocol did not yield good results when used to conduct preliminary screen experiments, despite strong and specific labelling of substrate proteins (Figure 3.13). One of the five identified phosphopeptides specific to the T96G mutant corresponded to a novel SIK2 autophosphorylation site at S674, suggesting that the method had worked in principle. However, given the overexpression of SIK2 and the strong autophosphorylation signal observed throughout the previous experiments, discovery of a single SIK2 autophosphorylation site should be considered an absolute minimum requirement for a successful screen experiment. Of the remaining four phosphopeptides, two contained cysteine residues, suggesting either that they had non-specifically adsorbed to the agarose or that the reactivity of the iodoacetyl resin was compromised, resulting in a low covalent capture efficiency. The site identified at S261 of Glutamine-fructose-6-phosphate aminotransferase has previously been reported to be phosphorylated by AMPK[120,121], suggesting that this may be a genuine screen hit. If this is the case it would support the notion that covalent capture efficiency was very low, as any peptide containing a cysteine as well as a thiophosphorylated residue would be expected to bind to the resin via both[116].

In summary, the data presented here show that the SIK2 T96G gatekeeper mutant can utilise N^6-Phenylethyl-ATPγS to phosphorylate substrates in a robust and reproducible manner *in vitro* and in cell lysates. However, preliminary screen experiments demonstrated a need for further refinements to the covalent capture protocol, which are discussed in the following chapter.

CHAPTER 4: SCREENING AND ANALYSIS

4.1 Introduction

In order to increase the robustness and sensitivity of the screen following the preliminary experiment detailed in Chapter 3, a number of refinements were made to the covalent capture protocol, based on the method published by Carlson & White (2012)[122].

Firstly, a SILAC approach[123] was adopted, meaning that one set of cells were grown in culture media containing heavy isotope-labelled lysine and arginine[124], which are incorporated into proteins. This allows samples to be mixed and subjected to tryptic digestion, and all subsequent downstream processes, together (Figure 4.1), since tryptic peptides from the two samples can be distinguished by their different masses. As a result, any biases introduced by variability in experimental conditions affect both samples equally, enabling quantitative comparisons[125]. This is particularly advantageous in the context of a chemical genetic screen as any difference in the efficiency of tryptic digestion, desalting, or covalent capture steps between separate control and gatekeeper mutant samples could result in a phosphorylation event being wrongly ascribed to the kinase of interest.

Secondly, a number of optimisations were made to buffer conditions in the covalent capture protocol. Carlson *et al*. (2011) determined that a lower pH of 5.5, as opposed to 7.0 in the original Blethrow *et al*. (2008) protocol, improved the selective capture of thiophosphorylated peptides[126]. This is consistent with a previous report suggesting that lower pH favours alkylation of thiophosphate over alkylation of cysteine residues[127]. In addition, the non-thiol reducing agent TCEP was added to the binding and wash buffers to prevent oxidation and premature elution of thiophosphorylated peptides. The authors also recommended using a brand new (i.e. previously unopened) batch of iodoacetyl resin for each experiment, so this procedure was also adopted.

Incorporating these changes to the screen protocol resulted in greatly improved recovery of peptides. This chapter contains the results obtained using the revised workflow, as well as subsequent analysis and consideration of the putative substrates identified.

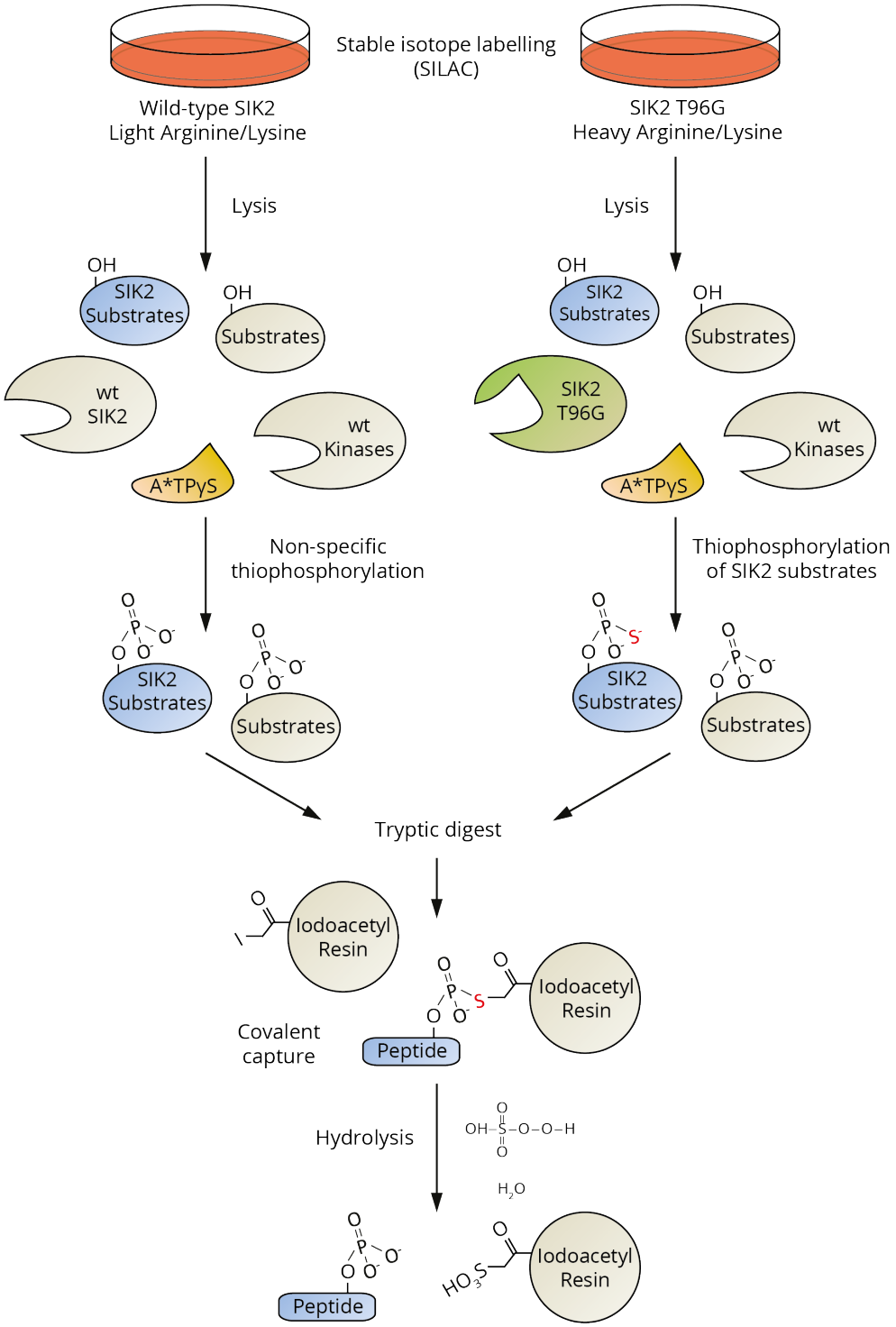

Figure 4.1. Revised screen workflow

SK-OV-3 cells stably overexpressing SIK2 wild-type or T96G are cultured in media containing light or heavy arginine/lysine. Both sets of cells are lysed and equal amounts of each lysate (by protein mass) are separately incubated with 'bulky' PhEt-ATPγS. Following protein precipitation to remove detergents and any remaining PhEt-ATPγS, the two samples are mixed together, denatured, and digested using trypsin. This allows both specifically and non-specifically labelled peptides to be recovered in the same covalent capture reaction, as the eluted light and heavy phosphopeptides can be distinguished in the subsequent LC-MS/MS analysis.

4.2 Results

4.2.1 Labelling of SIK2 substrates

In order to identify novel SIK2 substrates, the revised protocol was used to label substrates in SK-OV-3-SIK2 cell lysates. Aliquots of labelled lysates were taken so that labelling could be checked by western blotting (Figure 4.2) in parallel with the covalent capture protocol. Over the course of four independent screen experiments, labelling in the T96G mutant was between 23.3- and 165.3-fold higher than in wild-type controls, matching or exceeding the specificity achieved in preliminary experiments (Chapter 3).

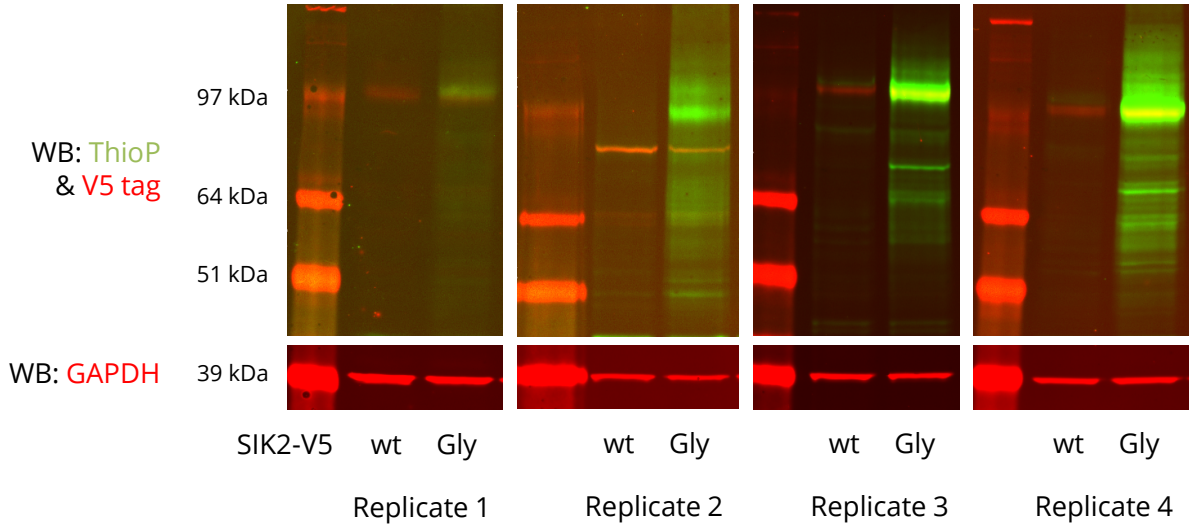

Figure 4.2. Labelling of SIK2 substrates in four independent experiments

Wild-type- or T96G-expressing SK-OV-3-SIK2 whole cell lysates were incubated with PhEt-ATPγS. Thiophosphorylation was detected by western blotting after treatment of lysate aliquots with PNBM.

4.2.2 Identification of putative SIK2 phosphorylation sites

Across four independent screen experiments, 85 putative SIK2 phosphorylation sites were identified on 73 different proteins, including the previously identified SIK2 substrates CRTC1 and CRTC3. These sites correspond to peptides which satisfy a number of criteria.

Firstly, the peptides must contain phosphorylated serine and/or threonine residues. Any detected non-phosphorylated peptides must be either: a) peptides which adsorbed non-specifically to the resin, and were not removed by subsequent wash steps; or b) peptides which covalently bound to and were eluted from the resin, and subsequently lost their phosphate groups. Since there can be no confidence that these peptides were formerly thiophosphorylated, they were not considered for further analysis.

Secondly, the MASCOT score of any given phosphopeptide must exceed the MASCOT homology threshold (calculated on a per-peptide basis), indicating that the match is a significant outlier relative to the distribution of random scores. Where the software could not calculate a homology threshold, the MASCOT identity threshold (based on the absolute *P* values[128]) was used instead.

Thirdly, the phosphopeptides must contain a heavy lysine and/or arginine residue, indicating that they originated from the SIK2 T96G-expressing cell lysate. Phosphopeptides meeting the first two criteria but containing only light residues are the result of background utilisation of PhEt-ATPγS in the wild-type control.

Finally, any phosphopeptides identified in both light and heavy forms were removed from the analysis, leaving a set of statistically significant phosphopeptide identifications corresponding to sites specifically labelled by SIK2 (Table 4.1 and Appendix II).

Uniprot accession	**Protein name**	**pSite**	**MASCOT score**			
			Repl 1	**Repl 2**	**Repl 3**	**Repl 4**
O14974	Protein phosphatase 1 regulatory subunit 12A	S445	79.38	60.79	93.81	112.12
O75122	CLIP-associating protein 2	S370	82.31	72.9	86.99	78.72
O60716	Catenin delta-1	S268	58.46	71.46	80.64	84.68
Q7Z460	CLIP-associating protein 1	S600	73.77	63.34	72.03	*46.42*
P15924	Desmoplakin	S22	50.26	52.66	64.33	50.7
Q9H0K1	Serine/threonine-protein kinase SIK2	S674	71.93		65.02	85.23
P27986	Phosphatidylinositol 3-kinase regulatory subunit alpha	S154	57.72	64.51		76.43
Q9H0B6	Kinesin light chain 2	S582	69.05		*50.03*	64.6
Q9H0K1	Serine/threonine-protein kinase SIK2	S358	51.73	53.59	*46.95*	
Q9BRJ2	39S ribosomal protein L45, mitochondrial	S201	58.5		84.88	
Q32P44	Echinoderm microtubule-associated protein-like 3	S176	60.27	*50.82*		
Q96PK6	RNA-binding protein 14	S620	44.59	64.04		
Q96N67	Dedicator of cytokinesis protein 7	S1438	53.8	53.71		
O14639	Actin-binding LIM protein 1	S452	61.59			45.23
Q9P265	Disco-interacting protein 2 homolog B	S203	67.33	38.92		
Q9H0K1	Serine/threonine-protein kinase SIK2	S587	56.92		*48.09*	
Q9NUL7	Probable ATP-dependent RNA helicase DDX28	S127	59.51	*42.08*		
P48047	ATP synthase subunit O, mitochondrial	S91	44.7	*47.42*		
Q9UPN3	Microtubule-actin cross-linking factor 1, isoforms 1/2/3/5	S7279	*43.04*	*48.02*		
P52298	Nuclear cap-binding protein subunit 2	S13	43.52			47.19
O60716	Catenin delta-1	S346	*37.19*	*47.3*		
Q01804	OTU domain-containing protein 4	S416		*46.18*		*31.11*
P83731	60S ribosomal protein L24	S86				79.66
Q6P597	Kinesin light chain 3	S466				77.35
Q9NSK0	Kinesin light chain 4	S590	72.21			
Q16647	Prostacyclin synthase	S232			72.01	
Q9P0V3	SH3 domain-binding protein 4	S246	70.49			

P11586	C-1-tetrahydrofolate synthase, cytoplasmic	S765	68.99				
Q8IVT2	Mitotic interactor and substrate of PLK1	S394	68.52				
Q9Y3M2	Protein chibby homolog 1	S20	64.67				
P67809	Nuclease-sensitive element-binding protein 1	S176		64.01			
Q9NQT8	Kinesin-like protein KIF13B	S1797	63.93				
Q96PK6	RNA-binding protein 14	S520	62.72				
P40818	Ubiquitin carboxyl-terminal hydrolase 8	S719	57.57				
O00571	ATP-dependent RNA helicase DDX3X	S609		57.21			
Q01813	6-phosphofructokinase type C	S386	56.7				
Q9Y223	Bifunctional UDP-N-acetylglucosamine 2-epimerase/N-acetylmannosamine kinase	S170			*55.83*		
Q9H0K1	Serine/threonine-protein kinase SIK2	S590	55.51				
Q9Y2I7	1-phosphatidylinositol 3-phosphate 5-kinase	S307					53.01
P28290	Sperm-specific antigen 2	S739	52.94				
P36551	Oxygen-dependent coproporphyrinogen-III oxidase, mitochondrial	S129			*52.72*		
Q08380	Galectin-3-binding protein	S444	52.08				
Q6UUV7	CREB-regulated transcription coactivator 3	S370	51.72				
Q07157	Tight junction protein ZO-1	S617	51.21				
Q9H0K1	Serine/threonine-protein kinase SIK2	T359	51.18				
Q92974	Rho guanine nucleotide exchange factor 2	T152	49.92				
Q9H6H4	Receptor expression-enhancing protein 4	S152					49.52
Q9NQT8	Kinesin-like protein KIF13B	S1381					*49.14*
O95239	Chromosome-associated kinesin KIF4A	S801	48.49				
P39023	60S ribosomal protein L3	S13	48.21				
P25705	ATP synthase subunit alpha, mitochondrial	S198	48.02				
Q29RF7	Sister chromatid cohesion protein PDS5 homolog A	T1162	48.01				
P78371	T-complex protein 1 subunit beta	S413			*47.6*		
P42704	Leucine-rich PPR motif-containing protein, mitochondrial	S1330	45.57				
Q9HAU0	Pleckstrin homology domain-containing family A member 5	S382	45.54				
Q9Y446	Plakophilin-3	S180	45.19				
P26045	Tyrosine-protein phosphatase non-receptor type 3	S359					*45.05*
P07900	Heat shock protein HSP 90-alpha	S52		*44.29*			
P62277	40S ribosomal protein S13	S12	44.02				
Q15785	Mitochondrial import receptor subunit TOM34	S280	*43.85*				
Q9Y5P4	Collagen type IV alpha-3-binding protein	S380					*43.78*
Q9BVS5	tRNA (adenine(58)-N(1))-methyltransferase, mitochondrial	T115		*43.15*			
P30622	CAP-Gly domain-containing linker protein 1	S193		*42.98*			
Q15477	Helicase SKI2W	S256	*41.87*				
Q1KMD3	Heterogeneous nuclear ribonucleoprotein U-like protein 2	T609	*41.31*				
P27816	Microtubule-associated protein 4	S928	*40.54*				
P25705	ATP synthase subunit alpha, mitochondrial	S76	*39.8*				
P14625	Endoplasmin	S306		*39.28*			

Q76N89	E3 ubiquitin-protein ligase HECW1	S68		*39.09*	
Q9H0K1	Serine/threonine-protein kinase SIK2	T592	*38.45*		
Q9H7P9	Pleckstrin homology domain-containing family G member 2	S1278	*38.37*		
Q86W92	Liprin-beta-1	S601			*37.39*
Q6L8Q7	2~,5~-phosphodiesterase 12	S533	*37.36*		
Q86W92	Liprin-beta-1	S466	*36.83*		
Q6UUV9	CREB-regulated transcription coactivator 1	S48	*36.35*		
P62701	40S ribosomal protein S4, X isoform	S223	*35.82*		
Q96N67	Dedicator of cytokinesis protein 7	S900	*35.42*		
Q15678	Tyrosine-protein phosphatase non-receptor type 14	S465	*32.83*		
Q8TF72	Protein Shroom3	S664	*31.85*		
Q01850	Cerebellar degeneration-related protein 2	S310	*31.02*		
Q8IVF2	Protein AHNAK2	S5497	*30.7*		
Q9Y305	Acyl-coenzyme A thioesterase 9, mitochondrial	S244	*29.09*		
P15924	Desmoplakin	S2598	*27.31*		
P07437	Tubulin beta chain	T285	*26.7*		
Q8IZQ1	WD repeat and FYVE domain-containing protein 3	S1027	*24.05*		

Table 4.1. Screen hits from four independent experiments

SIK2 substrates were labelled using the revised screen protocol presented in section 4.1, and eluted peptides were identified using LC-MS/MS. Putative SIK2 phosphorylation sites are shown, along with the protein name, Uniprot accession number, and MASCOT score for the corresponding peptide. Sites are sorted primarily by number of independent identifications (descending from 4 to 1) and secondarily by MASCOT score (descending from high to low). Scores shown in italics are those which exceeded the homology threshold but did not reach the identity threshold. Peptide sequences can be found in Appendix II.

4.2.3 Gene ontology analysis

To infer possible biological functions of SIK2 from the screen data, the list of putative substrates was subjected to a gene ontology over-representation analysis. The set of 72 putative substrates (SIK2 itself was excluded from the analysis) was significantly enriched for a number of biological processes involved in microtubule regulation and mitosis (Table 4.2). Microtubule-binding proteins and proteins localised to microtubules and focal adhesions were also significantly over-represented (Table 4.3 & Table 4.4), suggesting a possible role for SIK2 in microtubule regulation. This was still supported when the analysis was restricted to the 18 proteins identified in multiple screen replicates, although the exact ontologies varied. Full GO analysis results for both sets of proteins are contained in Appendix IV.

GO Biological process (Experimental only)	Hits	+/-	Fold enrichment	*p*-value
Regulation of microtubule polymerisation or depolymerisation	4	+	> 5	9.83E-03
Mitotic spindle organisation	4	+	> 5	1.49E-02
Regulation of microtubule cytoskeleton organisation	5	+	> 5	2.82E-02
Mitotic cell cycle	8	+	> 5	9.00E-03

Table 4.2. Selected biological processes enriched in 72 putative substrates

GO Molecular function (Experimental only)	Hits	+/-	Fold enrichment	*p*-value
Microtubule plus-end binding	3	+	> 5	6.19E-03
Tubulin binding	5	+	> 5	4.03E-02

Table 4.3. Selected molecular functions enriched in 72 putative substrates

GO Cellular component (Experimental only)	Hits	+/-	Fold enrichment	*p*-value
Microtubule	8	+	> 5	1.88E-05
Focal adhesion	11	+	> 5	1.82E-05

Table 4.4. Selected cellular components enriched in 72 putative substrates

The list of putative substrates was subjected to a gene ontology (GO) over-representation analysis. Selected GO terms enriched in the list of 72 putative substrates are shown. The list was analysed for enrichment of GO terms relative to a background database of 20,814 human proteins.

4.2.4 Canonical and non-canonical phosphorylation sites

Twelve of the proteins identified as putative SIK2 substrates contain canonical SIK substrate motifs with the sequence LX[H/K/R][S/T]XpSXXXL. Curiously, the motifs only match the sites identified in the screen in three of these proteins (Table 4.5). Although the canonical motif has previously been applied successfully in the identification of novel SIK2 substrates[2,5,51], this demonstrates that it is neither necessary nor sufficient for phosphorylation by SIK2.

Protein name	pSite	-7	-6	-5	-4	-3	-2	-1	0	+1	+2	+3	+4	+5	+6	+7
Canonical SIK consensus motif				**L**	X	**HKR**	**ST**	X	**S**	X	X	X	**L**			
Protein phosphatase 1 regulatory subunit 12A	S445	L	G	**L**	R	**K**	**T**	G	**S**	Y	G	A	**L**	A	E	I
Phosphatidylinositol 3-kinase regulatory subunit alpha	S154	S	T	**L**	Y	**R**	**T**	Q	**S**	S	S	N	**L**	A	E	L
Liprin-beta-1	S466	S	S	**L**	Q	**K**	**S**	S	**S**	L	G	N	**L**	K	K	E

Table 4.5. Sites containing a canonical SIK consensus sequence

The amino acid sequences of the three identified phosphorylation sites which conform to the canonical SIK consensus sequence are shown, along with the consensus sequence itself. Residues specified by the consensus sequence are shown in bold.

To determine whether the canonical motif could be improved upon using the putative phosphorylation sites from the screen, the sequences surrounding each site (-7 to +7 residues) were analysed for over- and under-representation of amino acids using PSPlogo[115] (Figure 4.3). This analysis confirmed a strong preference for arginine at the -3 position and leucine at the +4 position, consistent with the published motif. Although leucine is also over-represented at the -5 position as expected, the results suggest that methionine may be tolerated. The canonical requirement for a serine or threonine at the -2 position has some support, although this is reduced when only the 22 most reliable sites are analysed (Figure 4.3b). At the +3 position, which is not specified by the published motif, aspartic acid and asparagine are strongly favoured.

a)

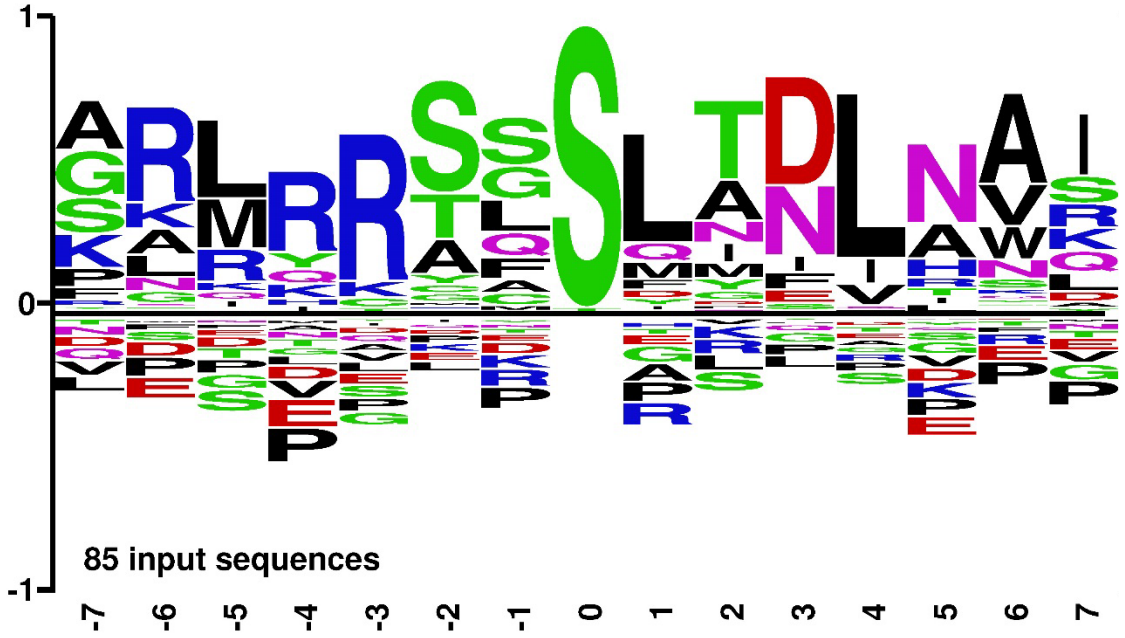

b)

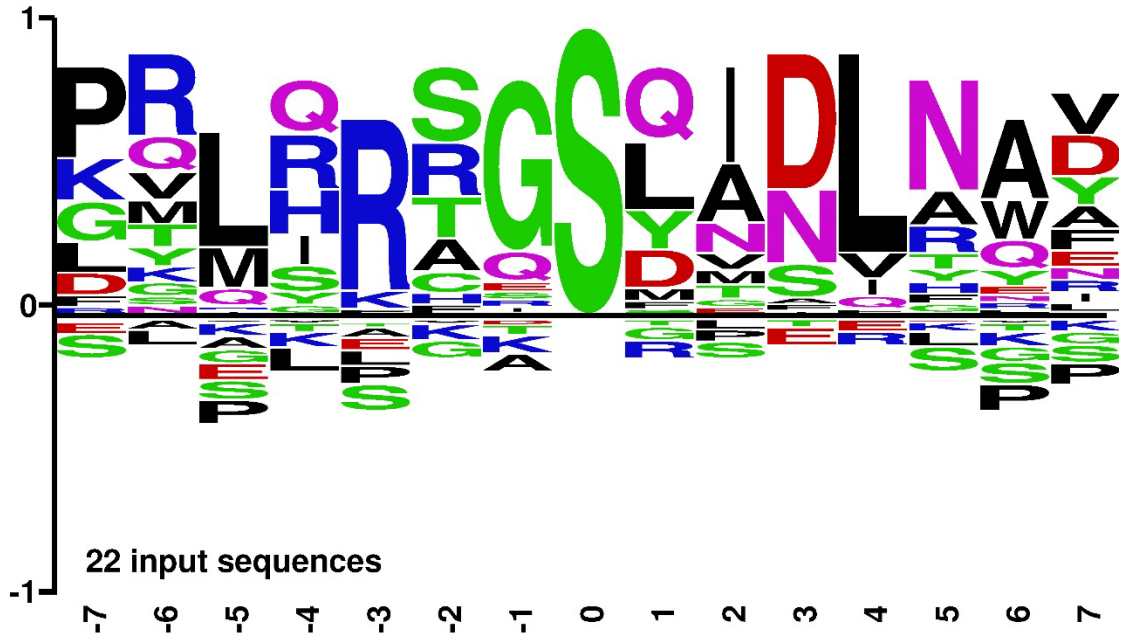

Figure 4.3. Amino acid bias in putative SIK2 phosphorylation sites

Phosphorylation site logos show the degree of over- or under-representation (indicated by positive or negative values, respectively) of particular amino acid residues surrounding **a)** all 85 identified sites, or **b)** the 22 sites identified in multiple independent experiments, relative to known serine phosphorylation sites. Logos were produced and rendered in PSPlogo (Cell Signaling Technologies, USA). The y-axis represents the relative frequency change for each depicted amino acid.

4.3 Discussion

One of the primary aims of this project was to identify novel SIK2 substrates. This chemical genetic screen identified 73 putative substrates, 18 of which were present in multiple independent experiments. 5 of the phosphorylation sites were identified in all four replicates, suggesting that these are the most reliable candidate substrates. They also had good quality MS/MS spectra (See Appendix III) and tended to be amongst the highest scoring peptides.

The first of these was Protein phosphatase 1 regulatory subunit 12A (PPP1R12A) S445, a site known to be phosphorylated by NUAK1, which is also a member of the AMPK-related kinase family[129]. Phosphorylation at this site has been shown to result in 14-3-3 binding, preventing the PPP1R12A-PP1β complex from dephosphorylating myosin light chain 2 and promoting cell detachment[129]. PPP1R12A was also the strongest hit detected in a chemical genetic screen for AMPKα2 substrates[105]. Although the method used in that study did not identify the exact phosphorylation site, the sequence surrounding S445 matches the published substrate motif for AMPK[130], as well as that of SIK2 (Table 4.5). Together with the screen data, this suggests that SIK2 is also capable of phosphorylating PPP1R12A at this site. However, further experimentation will be required to establish that this interaction occurs under physiological conditions.

Also present in all four replicates were CLIP-associating protein 1 (CLASP1) S600 and CLIP-associating protein 2 (CLASP2) S370. Although the sites are almost identical in sequence, the tryptic peptides included a single amino acid difference allowing the two to be distinguished. Both sites are listed in the PhosphoSite database[131] as having been identified in a large number of global phosphoproteomics experiments, but neither have been functionally characterised. Both CLASP1 and CLASP2 associate with and stabilise microtubules[132,133], so they might be of interest in the context of paclitaxel resistance. Furthermore, CLASP2 undergoes extensive phosphorylation, including at S370, upon insulin treatment[134]. This is consistent with regulation by SIK2, which is activated downstream of insulin signalling[52].

Catenin delta-1 (also known as p120-catenin or p120) is a component of adherens junctions which associates with and stabilises E-cadherin, promoting strong adhesion[135]. Phosphorylation of p120 by CK1 at the site identified in the screen, S268, has previously been shown to disrupt this association, destabilising adherens junctions and releasing p120 into the cytoplasm[136]. Cytoplasmic p120 has been shown to activate oncogenic processes, including proliferation, invasion and metastasis, in a variety of cancers[137]. The availability of a phosphorylation-specific antibody for this site[138] makes it a convenient target for validation.

Finally, Desmoplakin (DSP) is a large multi-domain adaptor protein which links intermediate filaments to the desmosomal subunits plakoglobin and plakophilin[139]. Similar to the two CLASP phosphorylation sites, the S22 site identified in the screen has been detected in a large number of high-throughput phosphoproteomics studies[131], but has not been functionally characterised. The N-terminal head region of desmoplakin is responsible for the binding of plakoglobin and plakophilin, so it is possible that S22 phosphorylation might influence this interaction. A nearby V30M mutation reportedly abolished plakoglobin binding, resulting in aberrant desmoplakin localisation[140]. As with all of the above substrates, further investigation will be required to confirm phosphorylation by SIK2.

Three of the screen replicates identified a putative SIK2 phosphorylation site at S154 of phosphatidylinositol 3-kinase regulatory subunit alpha (p85α, also known as PIK3R1), which interacts with[141] and inhibits the activity of[142] the catalytic p110α subunit of phosphatidylinositol 3-kinase (PI3K). This is the same site which was identified in an *in silico* screen and successfully used as a peptide substrate in the previous chapter, so it is likely to be a genuine screen hit. The PI3K-AKT pathway is a key oncogenic signalling pathway which is overactive in a wide range of different tumour types[44,117], including ovarian cancer[143–145], so the possibility that SIK2 feeds into this pathway is potentially very significant. This hypothesis is investigated in Chapter 5.

The results of the gene ontology analyses reflect the functions of the screen hits mentioned above, highlighting a variety of ontologies involved in microtubule regulation as well as focal adhesion. Of particular interest is the possibility that SIK2 is involved in regulation of microtubule polymerisation or depolymerisation, an ontology which was significantly enriched in both the full data set and the subset of reproducible screen hits. This is potentially very significant, as it may account for the role of SIK2 in paclitaxel resistance. It has been well established that microtubule stability is an important modulator of the response to paclitaxel[146–152]; proteins which negatively regulate microtubule stability confer resistance to paclitaxel[153,154].

Six of the identified phosphorylation sites were located on SIK2 itself (Table 4.6), indicating autophosphorylation. This finding is consistent with several results in Chapter 3, in which SIK2 was shown to autophosphorylate *in vitro* and in cell lysates. Hashimoto *et al*. (2008) demonstrated that SIK1 and SIK2 are able to autophosphorylate their activation loops at S186 and S179 respectively[155]. However, this site was not identified in the screen because the tryptic fragment containing S179 also contains multiple cysteine residues, preventing elution from the iodoacetyl resin, and has a mass of 6250.1053 Da, which is beyond the mass range of the LC-MS/MS setup used for analysis. Of the reproducible autophosphorylation sites, S358 and S587 have been reported previously as substrates

of other kinases, whilst S674 phosphorylation is a novel observation. These are discussed further in Chapter 5, and may have utility as biomarkers of SIK2 activity.

pSite	Site sequence (-7 to +7)	Number of replicates
S358	DGRQRRP**S**TIAEQTV	3
T359	GRQRRPS**T**IAEQTVA	1
S587	FREGRRA**S**DTSLTQG	2
S590	GRRASDT**S**LTQGIVA	1
T592	RASDTSL**T**QGIVAFR	1
S674	PQLSPRQ**S**LETQYLQ	3

Table 4.6. SIK2 autophosphorylation sites

Putative SIK2 autophosphorylation sites are shown, along with the sequence surrounding each site and the number of independent experiments in which each was identified. The phosphorylated residue is indicated in bold.

Analysis of the amino acid sequences surrounding the sites identified in the screen broadly supported the canonical substrate motif LX[H/K/R][S/T]XpSXXXL, although the serine/threonine at position -2 did not appear to be an absolute requirement. Despite this, only 3 of the sites actually conform to the motif, demonstrating that it is neither necessary nor sufficient for the identification of novel substrates, and suggesting that mismatches are to some extent tolerated. It should be noted that the method used here, in which full-length SIK2 thiophosphorylates whole proteins, is very different from the method originally used to elucidate the motif, in which recombinant SIK1 kinase domain was incubated with different substrate peptides[51]. This may account for the large number of non-canonical sites, as the chemical genetic approach would detect phosphorylation events which are mediated by distal recognition events and scaffolding proteins, in addition to those mediated by primary structure alone[156].

Although the results of the screen have identified a number of significant avenues for further study, they must nonetheless be approached with a degree of caution, as they are subject to a number of caveats associated with chemical genetic screening in general, and with the protocol used here in particular.

Firstly, it is possible that some of the proteins identified are not physiological substrates of SIK2, despite being specifically labelled in the SIK2 T96G cell lysate. This could occur due to loss of cellular compartmentalisation prior to incubation with PhEt-ATPγS, allowing SIK2 to come into contact with substrates which it is able to phosphorylate, but would not naturally co-localise with. SIK2 is predominantly localised in the cytoplasm[1,46] and at the centrosome[6], so the identification of proteins which normally localise at the plasma membrane such as p120 and desmoplakin is somewhat surprising. However, both

proteins can localise to the cytoplasm under certain conditions[135,157], so this does not necessarily mean they are experimental artefacts. The solution to this problem would be to label SIK2 substrates in permeabilised cells, but this approach resulted in a relatively poor ratio of specific to non-specific labelling, as shown in Chapter 3.

Secondly, in order to achieve sufficient thiophosphorylation of substrate proteins for identification, the screen was conducted with overexpression of SIK2. As with any overexpression approach, this carries the risk that the observed interactions would not occur at endogenous protein levels. For example, it could lead to the detection of substrates usually phosphorylated by other AMPK-related kinases, which have similar phosphorylation site motifs. PPP1R12A S445 is a possible example of this phenomenon, as discussed above, but it may also represent a genuine overlap of function between the AMPK-related kinases. Such an overlap has been reported between the AMPK, MARK and SIK families for phosphorylation of CRTC2[51,158,159] and Class IIa histone deacetylases (HDACs)[62,160,161]. Apart from PPP1R12A there is no overlap between the results of this screen and the results of a published screen for AMPKα2 substrates using the immunoprecipitation protocol[105]. However, the authors have since published a second screen for AMPK substrates using a covalent capture approach, which also identified p120 S268, kinesin light chain 4 (KLC4) S590 and ABLIM1 S452, and distinct sites on Rho guanine nucleotide exchange factor 2 (ARHGEF2) and kinesin light chain 2 (KLC2). In total, they identified 74 putative phosphorylation sites which were present in 2 or more out of 12 biological replicates[162], so an overlap of 4 phosphorylation sites with the SIK2 screen is actually surprisingly limited.

Two screen hits, KIF13B and ARHGEF2, are reportedly phosphorylated by MARK2[163–165], but again these events occur at different sites to those identified in this screen. This relatively small overlap with AMPK screen results and other AMPK family members suggests that if overexpression of SIK2 has resulted in non-physiological substrate identifications, this has not been simply by labelling substrates of related kinases.

Since many functional experiments (both in this work and more generally) also make use of overexpression, rigorous experimentation and access to high-quality reagents (e.g. phosphorylation-specific antibodies) will be required to confirm phosphorylation of any of the identified sites under endogenous expression of SIK2.

A potential solution to the problems associated with overexpression would be to produce genetically engineered cell lines encoding the gatekeeper mutant of the kinase of interest. Whilst this has been achieved by Allen *et al*. (2007) using a mouse embryonic fibroblast (MEF) cell line derived from a 'gene knock-in' mouse model[104], recent advances in genetic engineering using TALENs or CRISPR/Cas9 mean that a wide range of cell lines can now be modified more quickly and easily[166,167]. Although the authors were only able to identify

a single Erk2 substrate using this MEF cell line[104], suggesting that there is a significant trade-off in terms of sensitivity, scaling up the experiment could help to alleviate this.

Thirdly, several previously identified SIK2 substrates, including IRS1, CEP250 and HDAC4, were not identified in the screen. None of the tryptic peptides corresponding to the SIK2 phosphorylation sites on these proteins contain cysteine residues, so all should be detectable using the covalent capture method. Whilst it is possible that these previously identified interactions simply do not occur in SK-OV-3 cells (e.g. if the substrates are not expressed), there are a number of potential sources of false negative results.

With this type of screen it can be difficult to detect relatively low abundance substrates from a complex mixture such as a cell lysate[116]. Possible solutions to this problem include increased sample fractionation prior to covalent capture, or sub-cellular fractionation to purify compartments of interest for labelling in isolation[116].

Since the SIK2 T96G mutant appears to be active *in vitro* without any particular stimulus (see section 3.2.3), its overexpression could mean that these known sites were already phosphorylated at high stoichiometry prior to incubation with PhEt-ATPγS, rendering them unavailable for thiophosphorylation. One option would be to exclude the phosphatase inhibitor from the lysis buffer, allowing endogenous phosphatases to render such sites available for thiophosphorylation. This would in principle lead to an accumulation of thiophosphorylated products, as thiophosphates are >20-fold more resistant to phosphatase activity than phosphate groups[168]. However, in a preliminary experiment conducted with or without phosphatase inhibitors, there was not a significant difference in global thiophosphorylation (data not shown), which suggests that phosphorylation site occupancy did not negatively influence the results presented here.

One known SIK2 autophosphorylation site at S179 was not detectable due to the large size of the corresponding tryptic peptide, so parallel experiments using alternative proteases would allow the detection of such peptides and generally increase coverage of the proteome[169]. This would also improve the detection of phosphorylation sites whose tryptic peptides contain cysteine residues, as these cannot be eluted from the iodoacetyl resin[116].

Finally, a significant issue which is apparent from the screen results is that of reproducibility. Of the 85 sites identified, only 22 (25.9%) were present in more than one independent experiment, indicating significant variability between replicates (Figure 4.4a). However, 44 of the 63 sites that were only identified once are accounted for by a single screen experiment (replicate 1), which identified many more sites than any of the other replicates (Figure 4.4b). Given that this replicate successfully identified a previously reported SIK2 phosphorylation site on CRTC3 at S370[4,170], and an additional site on CRTC1, these appear to be true positive results. It was on this basis that these results were

included in the data set, but all subsequent analyses were also carried out on the subset of 22 reproducible sites as a precautionary measure. It is not clear why one replicate proved significantly more sensitive than the others, as the signal to background ratio in that replicate was 77.5 – neither the highest nor the lowest observed. The most likely explanation is that this is due to cumulative variability in the substrate labelling, tryptic digest and covalent capture steps, amongst others. It is noteworthy that a recent screen for AMPK substrates using a similar methodology identified 478 phosphorylation sites from 12 biological replicates, and only 74 (15.5%) of these were present in 2 or more replicates[162], so limited reproducibility appears to be an inherent issue with this approach, rather than a problem with this specific implementation.

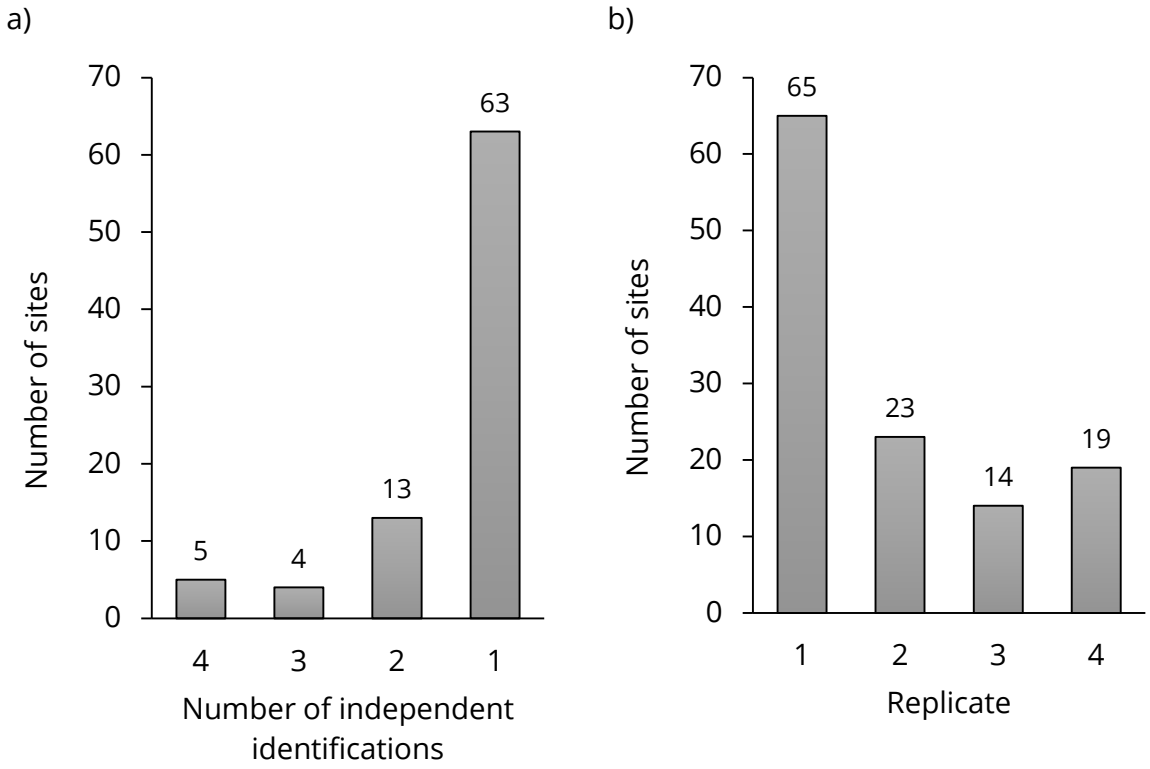

Figure 4.4. Site identifications and reproducibility

a) Bar chart showing the number of sites identified in multiple independent experiments. **b)** Bar chart showing the number of sites identified in each individual replicate.

Given these caveats, the list of putative substrates must be considered a list of candidates for further study, rather than an exhaustive list of SIK2 substrates. Unfortunately, there is not currently a suitable high-throughput method for validating (either biochemically or phenotypically) all of the identified phosphorylation sites at once, so they would have to be validated individually based on their potential biological significance. A quantitative global phosphoproteomics experiment with SIK2 inhibition or depletion would provide

additional evidence which might help to eliminate false positive sites, but this would be relatively costly and would not confirm direct phosphorylation by SIK2.

In summary, this screen has identified a large number of putative SIK2 phosphorylation sites for further study, some of which may prove to be useful biomarkers of SIK2 activity. Furthermore, the screen results have identified a number of potential functions of SIK2 which have not previously been described, as they included a number of proteins with important roles in cell adhesion. The data set was also significantly enriched in microtubule regulatory proteins, suggesting a possible explanation for the role of SIK2 in paclitaxel resistance.

CHAPTER 5: SIK2 ACTIVATION PROMOTES TUMOUR GROWTH AND METASTASIS

5.1 Introduction

One of the aims of this project was to identify potential biomarkers of SIK2 activity. The screen for novel SIK2 substrates (Chapter 4) identified a number of SIK2 autophosphorylation sites which may have such utility. Of these sites, S358 and S674 (Figure 5.1) were the most reliable, each appearing in three independent screen replicates.

Whilst phosphorylation of S674 is a novel finding, S358 has previously been functionally characterised. Henriksson *et al*. (2012) demonstrated that S358 is phosphorylated by PKA in response to cAMP in adipocytes. They showed that this phosphorylation event is dependent on phosphorylation of S343, is responsible for binding to 14-3-3 proteins, and does not affect SIK2 kinase activity[54]. Dentin *et al*. (2007) showed that S358 lies within a canonical AKT phosphorylation site motif and is phosphorylated by AKT2 upon exposure to insulin[52]. The authors also showed that prior treatment with insulin greatly increases autophosphorylation of wild-type SIK2 immunoprecipitates, but not the S358A mutant, concluding that S358 phosphorylation increases SIK2 kinase activity and leads to increased CRTC2 phosphorylation[52]. However, the possibility that S358 itself was the site of autophosphorylation was not considered, so this result may simply reflect the effect of abolishing the autophosphorylation site rather than a change in kinase activity.

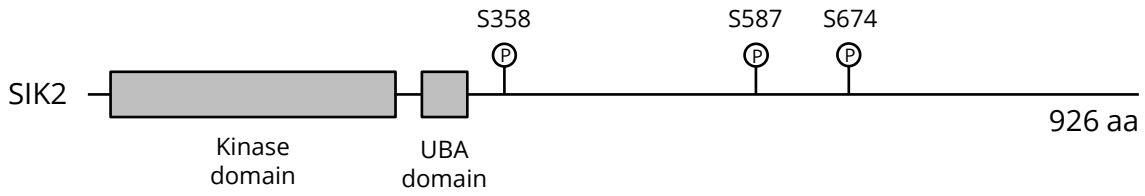

Figure 5.1. SIK2 domain structure

Schematic representation of SIK2 showing the position of autophosphorylation sites which were identified in multiple screen replicates.

Although S587 was identified as an autophosphorylation site in the screen, phosphorylation of this residue has previously been shown to have an inhibitory effect on SIK2 activity[171], suggesting a possible negative feedback loop which may complicate the use of this site as a biomarker.

Another of the screen hits meriting further investigation is S154 on phosphatidylinositol 3-kinase regulatory subunit alpha (p85α, Figure 5.2), which interacts with[141] and inhibits

the activity of[142] the catalytic p110α subunit of phosphatidylinositol 3-kinase (PI3K). If SIK2 regulates the activity of PI3K then this would be a significant finding, as the PI3K-AKT pathway is a key oncogenic signalling pathway which is overactive in a wide range of different tumour types[44,117], including ovarian cancer[143–145].

This chapter will discuss autophosphorylation of SIK2 as a marker of SIK2 activity, and the effects of SIK2 activation on downstream signalling via phosphorylation of p85α.

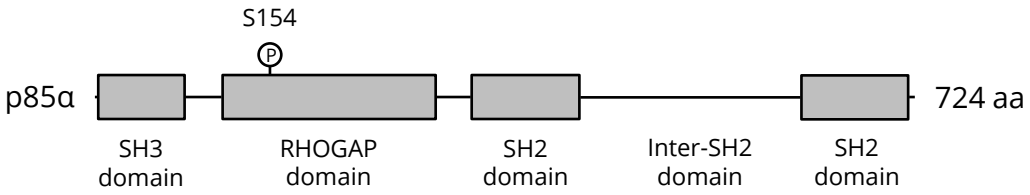

Figure 5.2. p85α domain structure

Schematic representation of the p85α regulatory subunit of PI3K, including the putative SIK2 phosphorylation site S154.

5.2 Results

5.2.1 SIK2 undergoes autophosphorylation at serine 358

In order to investigate autophosphorylation of SIK2 at S358, a polyclonal antibody was raised against the phosphopeptide RQRRPpSTIAEQ. To test this antibody, SIK2 mutants were expressed in 293T cells (Figure 5.3a). The pS358 antibody successfully detected phosphorylation of wild-type SIK2, but not of the S358A mutant, suggesting that it is specific for this site. Furthermore, phosphorylation was not detected in either the K49M or T175A mutants, which have both been reported to be catalytically inactive.

Since S358 may be phosphorylated by other kinases in live cells, SIK2 immunoprecipitates were incubated with ATP *in vitro* (Figure 5.3b) to determine their ability to autophosphorylate. This mirrored the results from cell lysates, with strong phosphorylation of S358 in wild-type SIK2, and little or no phosphorylation in the S358A mutant or either of the inactive mutants (ANOVA, $p \leq 0.01$ for each) (Figure 5.3c). This demonstrates that SIK2 activity is required for S358 phosphorylation, consistent with the hypothesis that S358 is an autophosphorylation site.

Whilst some of the phosphorylation detected at S358 following incubation *in vitro* clearly occurred prior to immunoprecipitation (see Figure 5.3a), the fluorescence signal is much stronger than in the cell lysates, suggesting that further autophosphorylation occurred *in vitro*. In addition, an increase in the molecular weight of wild-type and S358A SIK2 relative to that of the K49M and T175A mutants is visible in the kinase assays, but not the cell lysates. This is also indicative of autophosphorylation occurring *in vitro*, although this may be occurring at additional sites.

To confirm that the detected autophosphorylation indeed occurred *in vitro*, SIK2 immunoprecipitates were incubated with ATPγS (Figure 5.4b). This resulted in strong thiophosphorylation of both wild-type SIK2 and the S358A mutant, indicating that the S358A mutant remains active and that autophosphorylation occurs at additional sites, consistent with the results of the screen. As expected, significantly less thiophosphorylation was observed in both of the inactive mutants (ANOVA, $p \leq 0.05$ for both) (Figure 5.4c).

Unfortunately, a polyclonal antibody raised against a phosphopeptide corresponding to S674 proved unsuccessful in preliminary experiments, failing to recognise phosphorylation of recombinant full-length SIK2 following incubation with ATP *in vitro* (data not shown). As such, it was not possible to investigate the potential of this site as a biomarker of SIK2 activity.

a)

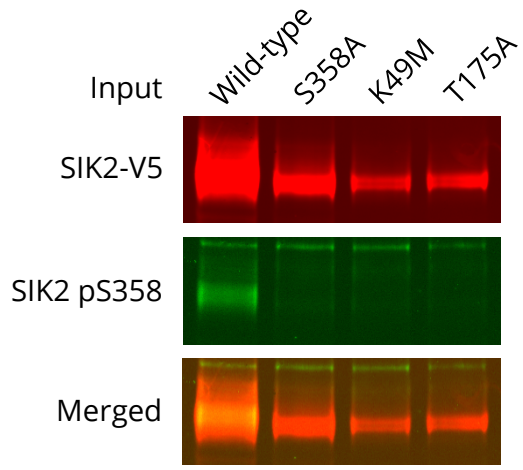

b)

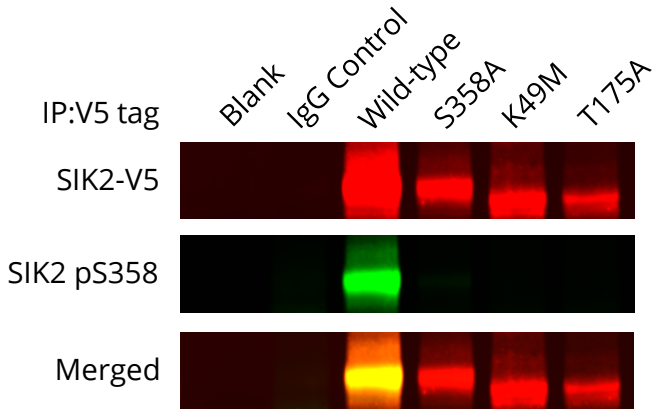

c)

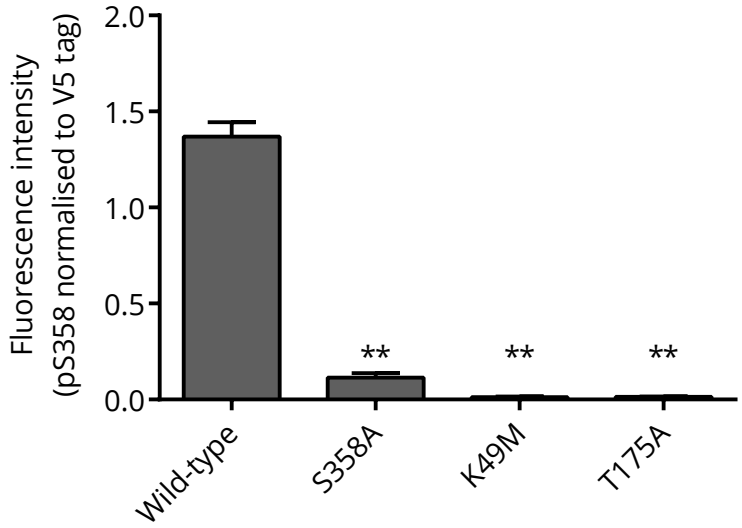

Figure 5.3. *In vitro* kinase assays with immunoprecipitated SIK2 and ATP

a) Western blot showing transient expression of SIK2 constructs in 293T cells. **b)** Western blot following immunoprecipitation of SIK2 and incubation with ATP. **c)** Bar chart showing mean fluorescence intensity (±SEM) for the pS358 antibody shown in b). Bands from triplicate experiments were quantified using the LI-COR Odyssey Application (LI-COR Biosciences, v3.0.16). ANOVA with Dunnett's Multiple Comparison Test was used to test for significant differences between each treatment and the wild-type control (** denotes $p \leq 0.01$).

a)

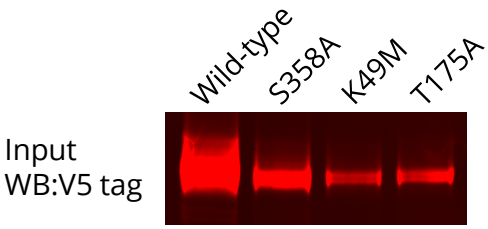

b)

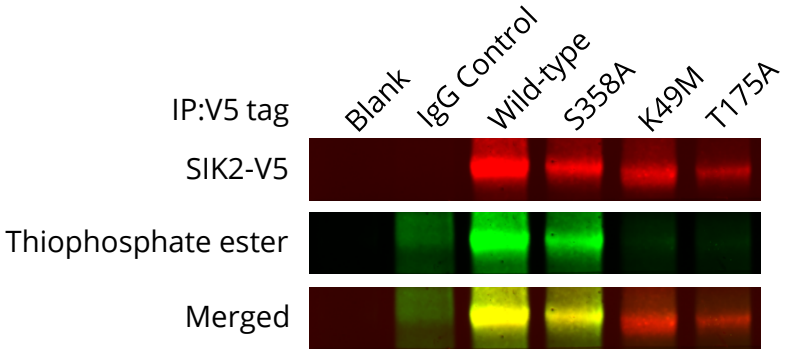

c)

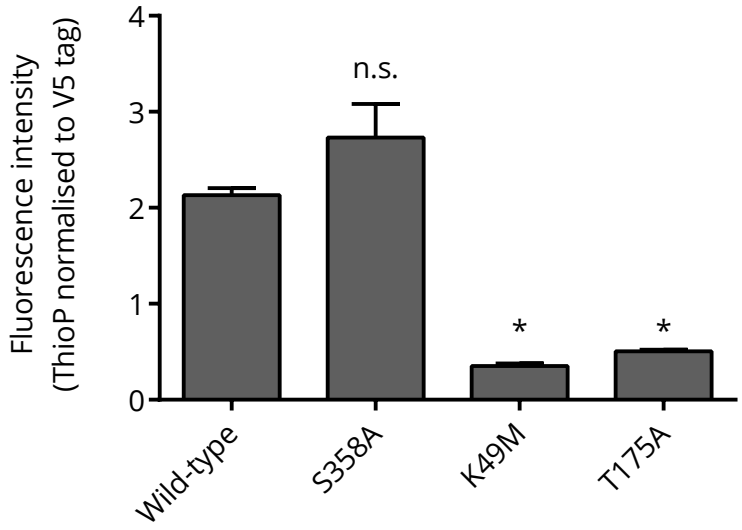

Figure 5.4. *In vitro* kinase assays with immunoprecipitated SIK2 and ATPγS

a) Western blot showing transient expression of SIK2 constructs in 293T cells. **b)** Western blot following immunoprecipitation of SIK2 and incubation with ATPγS. **c)** Bar chart showing mean fluorescence intensity (±SEM) for the ThioP antibody shown in b). Bands from duplicate experiments were quantified using the LI-COR Odyssey Application (LI-COR Biosciences, v3.0.16). ANOVA with Dunnett's Multiple Comparison Test was used to test for significant differences between each treatment and the wild-type control (* denotes $p \leq 0.05$, n.s. denotes $p > 0.05$).

5.2.2 SIK2 S358 phosphorylation increases in response to adipocytes

Having established that SIK2 activity results in autophosphorylation at S358, the anti-pS358 antibody was used to investigate SIK2 activation in SK-OV-3-SIK2 cell lines. SIK2 has previously been shown to be highly expressed in high-grade serous ovarian tumours[6], but further work in our laboratory showed that expression is higher still in metastases at the omentum (F. Miranda, D. Mannion, & A.A. Ahmed, unpublished data), an adipocyte-rich tissue found in the abdominal cavity which is a common site of ovarian cancer metastasis. Furthermore, it has been reported that omental adipocytes transfer free fatty acids to ovarian cancer cells, resulting in activation of AMPK and β-oxidation, and enhanced tumour growth[18]. Given the high levels of SIK2 in omental metastases and its relatedness with AMPK, we hypothesised that SIK2 might play a role in the establishment of omental metastases.

To investigate this possibility, primary adipocytes were isolated from freshly excised normal omentum of women who were undergoing surgery for benign ovarian cysts (Figure 5.5). Staining with Oil Red O, a lipid stain, confirmed that the isolated cells were adipocytes, whilst staining with Calcein AM showed that the majority of the adipocytes remained viable following isolation. These primary adipocytes were then used in co-culture experiments with SK-OV-3-SIK2 cells (Figure 5.6). Cells which were co-cultured with adipocytes showed an increase in SIK2 S358 phosphorylation relative to controls, suggesting activation (Figure 5.6a). Addition of adipocytes also resulted in activation of AKT, as indicated by an increase in S473 phosphorylation. AKT activation did not occur when SIK2 was depleted using a specific siRNA, demonstrating that SIK2 is required for AKT activation upon adipocyte treatment.

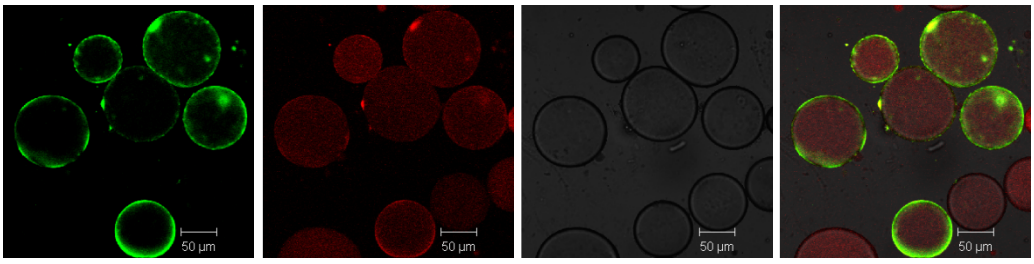

Figure 5.5. Isolation of primary omental adipocytes

Representative microscope images of adipocytes following isolation. Live cells are indicated by Calcein AM staining, whilst adipocytes are indicated using the Oil Red O lipid stain.

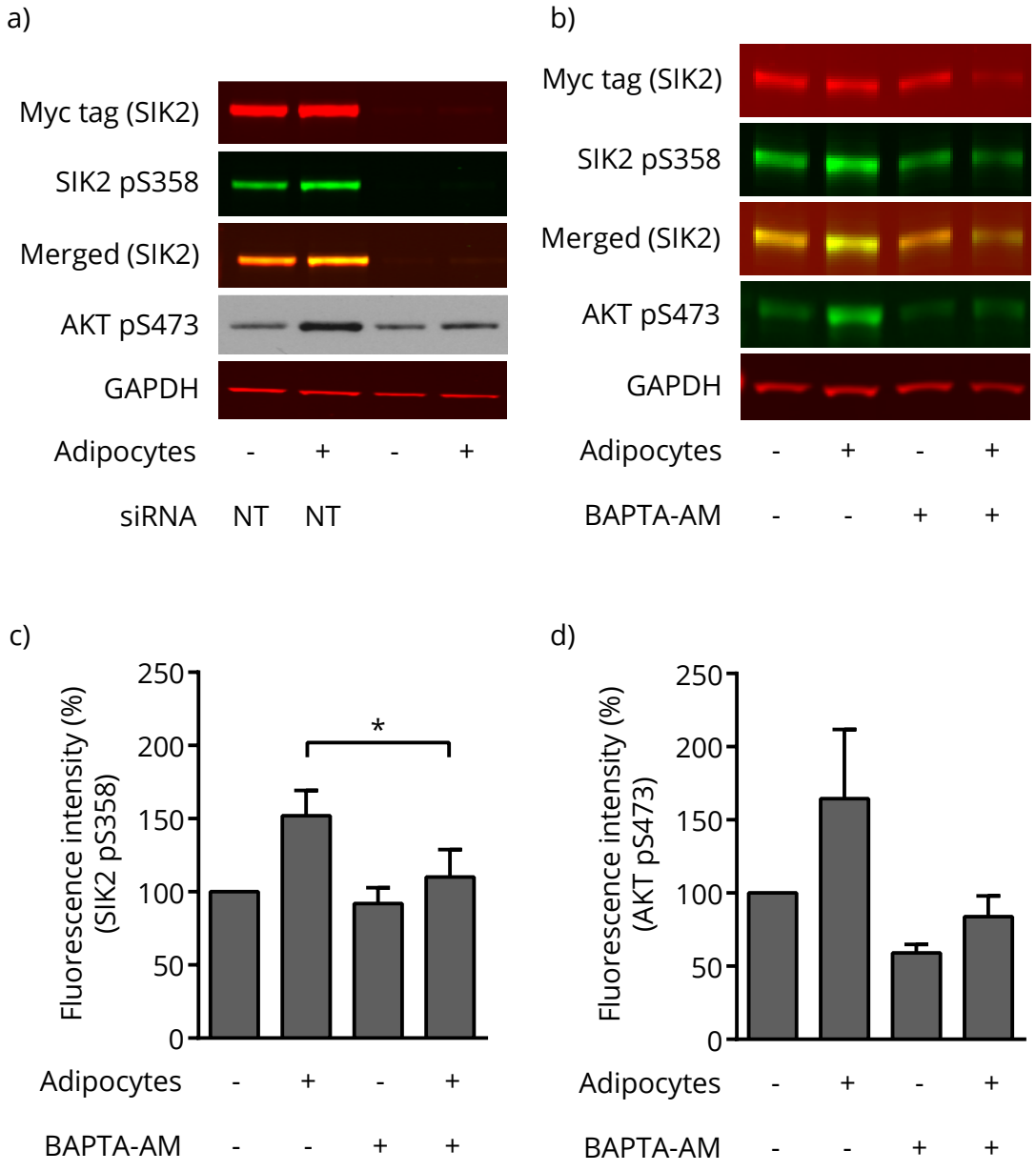

Figure 5.6. Western blots following incubation of SK-OV-3-SIK2 cells with primary adipocytes

a) Western blots following treatment of SK-OV-3-SIK2 cells with siRNA and co-culture with primary adipocytes. **b)** Western blots following treatment of SK-OV-3-SIK2 cells with BAPTA-AM and co-culture with adipocytes. **c)** Bar graph of SIK2 pS358 signal from b). **d)** Bar graph of AKT pS473 signal from b). Bands from triplicate experiments were quantified using the LI-COR Odyssey Application (LI-COR Biosciences, v3.0.16). All values were normalised to the corresponding GAPDH intensity. Mean fluorescence intensity (±SEM) is expressed as a percentage of the negative control. The indicated treatments were compared using a paired *t*-test (* denotes $p \leq 0.05$).

Activation of free fatty acid receptors (FFARs) results in increased intracellular calcium[172], which has previously been shown to activate SIK1 via CaMK1[173], and AMPK via CaMKK[174]. Since SIK2, SIK1 and AMPK are closely related, this suggested that SIK2 might also be activated by calcium signalling when co-cultured with adipocytes. To determine if this is the case, SK-OV-3-SIK2 cells were treated with 50 mM BAPTA-AM, an intracellular calcium chelator, for 1 hour prior to adipocyte treatment (Figure 5.6b). This prevented the increase in levels of phosphorylated SIK2 (Figure 5.6c), as well as the increase in AKT S473 phosphorylation (Figure 5.6d), indicating that calcium signalling is required for the response of SIK2 to adipocyte treatment.

5.2.3 Phosphorylation of p85α by SIK2 increases PI3K activity

The finding that SIK2 activation results in an increase in AKT pS473 is of particular interest as AKT activation is associated with a range of oncogenic processes in ovarian cancer, including cellular proliferation, migration[175], and paclitaxel resistance[176]. The identification of p85α, the regulatory subunit of the upstream PI3 Kinase, as a potential SIK2 substrate suggests a possible mechanism for this activation of AKT.

First, it was necessary to confirm the phosphorylation of p85α S154 by SIK2. Purified recombinant p85α was incubated with SIK2 *in vitro* and S154 phosphorylation was detected using a custom polyclonal antibody (Figure 5.7a). As anticipated, a large increase in S154 phosphorylation was detected in the presence of SIK2 relative to the negative control. Furthermore, no signal was detected when SIK2 was incubated with the p85α S154A mutant, demonstrating that the antibody is specific for this residue. Unfortunately, this antibody did not prove sensitive enough to detect reproducibly S154 phosphorylation in cell lysates (data not shown).

To establish whether phosphorylation of p85α by SIK2 affects PI3K activity, recombinant p85α and p110α were incubated with SIK2 and ATP *in vitro*. These complexes were then used in a commercially available, ELISA-based assay of PI3K activity (see section 2.1.19). In this assay, PIP3 converted from PIP2 by PI3K competes with biotinylated PIP3 for binding to a capture protein, so subsequent detection of the captured, biotinylated PIP3 allows PI3K activity to be quantified.

PI3K activity was 4-10 times higher after incubation with SIK2 than in control reactions containing PI3K alone (Figure 5.7b), demonstrating that phosphorylation by SIK2 increases PI3K activity. Whilst the measured PI3K activity increases with the amount of PI3K in the control reactions, this is not the case after incubation with SIK2, suggesting that the increased activity has saturated the assay. This would mean that the fold increases observed are conservative estimates. A control reaction containing SIK2 alone did not contain any detectable PI3K activity, so the increase is not due to conversion of PIP2 to PIP3 by contaminants in the SIK2 protein preparation.

a)

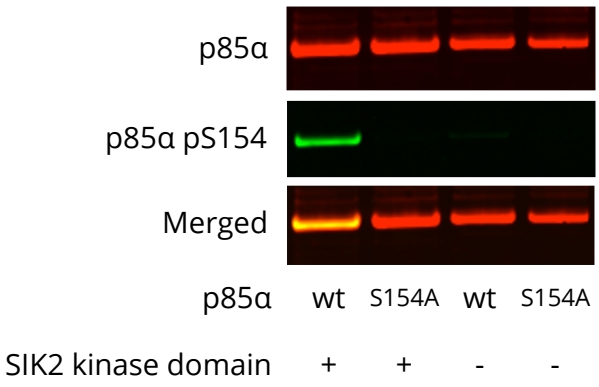

b)

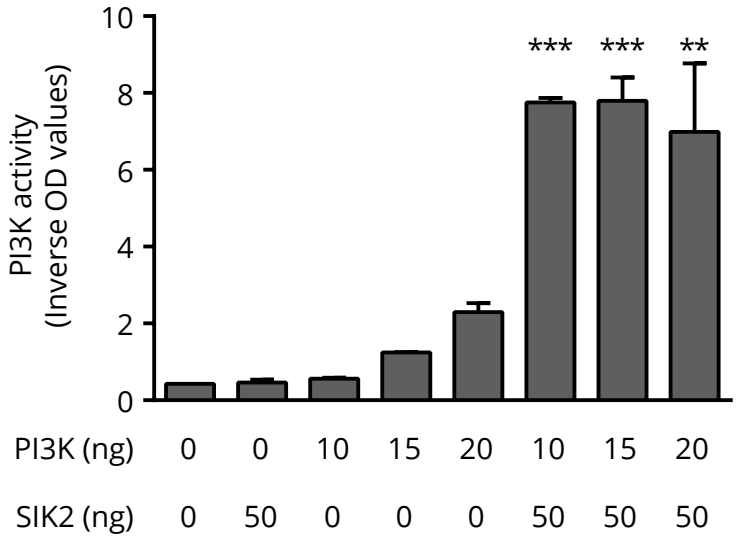

Figure 5.7. Phosphorylation of p85α and PI3K activity

a) Western blot following incubation of recombinant p85α with SIK2 kinase domain. S154 phosphorylation was detected using a specific polyclonal antibody. **b)** Bar graph showing the effect of SIK2 on PI3K activity *in vitro*. Results shown are the means ± SEM of three independent experiments. Treatments were each compared to their corresponding negative control using one-way ANOVA with Sidak correction (** denotes $p \leq 0.01$, *** denotes $p \leq 0.001$).

5.2.4 SIK2 overexpression affects cell spreading

During routine passaging of SK-OV-3-pLX302 cell lines, it was noted that cells overexpressing SIK2 (Figure 5.8a) attached and spread more quickly when plated. To confirm this phenotype, cells overexpressing wild-type SIK2, the overactive T96M mutant, or empty vector were re-plated and imaged every 5 minutes using time-lapse microscopy. Cells undergoing spreading, defined for the purposes of this experiment as cells with visible lamellipodia (Figure 5.8b), were counted within each field.

SK-OV-3 cells overexpressing wild-type SIK2 spread at a faster rate than empty vector controls, whilst expression of the T96M mutant resulted in even faster spreading (Figure 5.8c). Due to a high degree of variability between experimental replicates, the differences in the gradients of the regression lines of the wild-type compared with either the T96M or empty vector cell lines were not statistically significant (ANCOVA, $p = 0.258$ and $p = 0.111$ respectively). However, the difference between the T96M mutant and the empty-vector control was statistically significant (ANCOVA, $p = 0.00473$). Taken together, these results suggest that SIK2 activity promotes the early stages of cell spreading following attachment.

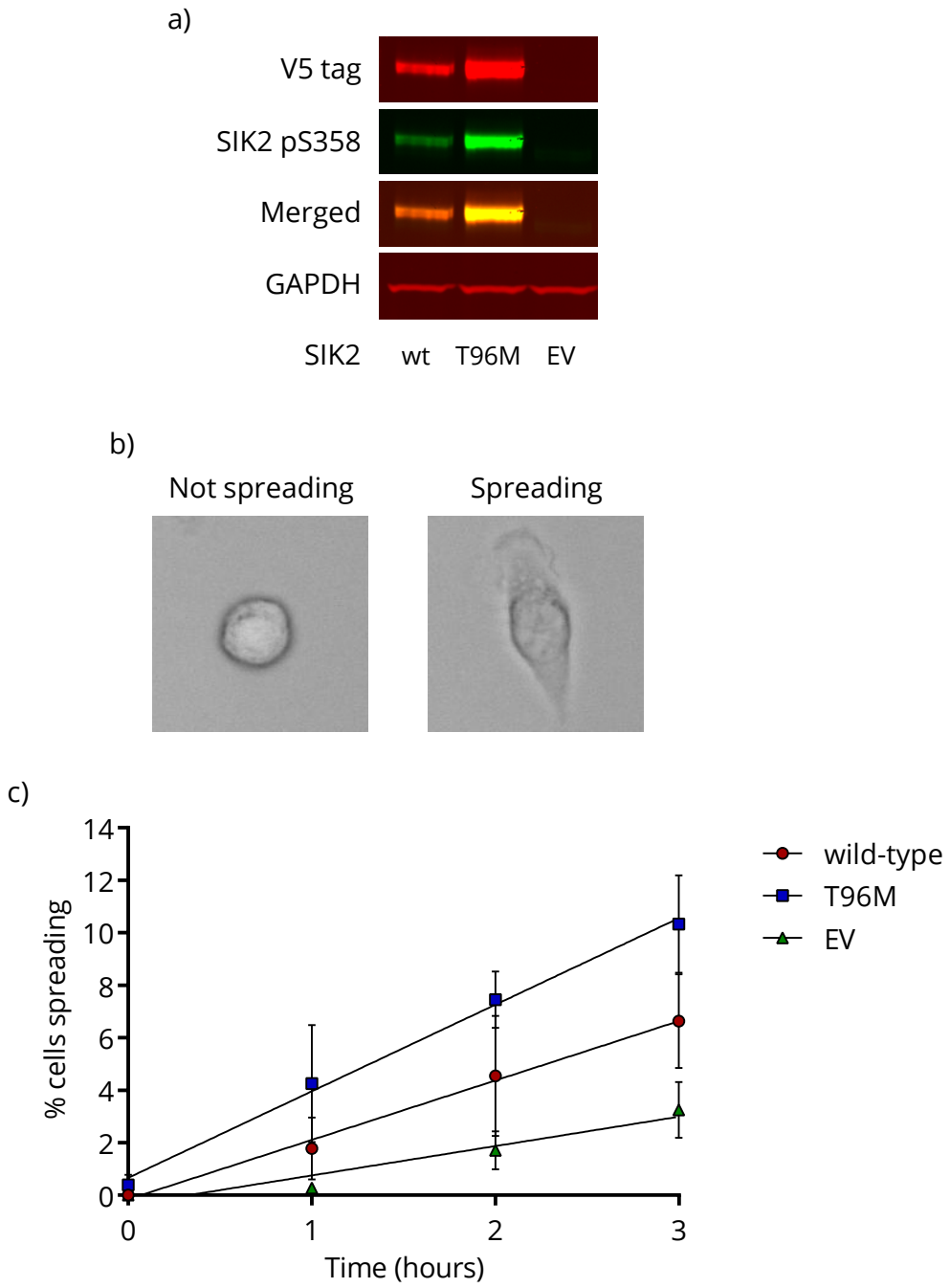

Figure 5.8. Cell spreading in SK-OV-3-SIK2 cell lines

SK-OV-3-SIK2 cell lines were disaggregated and re-plated, and were imaged using time-lapse microscopy. **a)** Western blot showing stable overexpression of SIK2 in SK-OV-3 cells. **b)** Example images to illustrate scoring criteria, showing a cell which is not spreading (left), and the same cell 90 mins later undergoing spreading (right). **c)** Graph showing the rate of cell spreading in SK-OV-3 cell lines. Data shown are the means ± SEM of three independent experiments, each comprising four technical replicates. The gradients of the regression lines were compared using ANCOVA.

5.2.5 Overexpression of SIK2 promotes peritoneal metastasis *in vivo*

To determine if SIK2 overexpression influences metastasis throughout the peritoneum (which includes the omentum), mice were orthotopically transplanted with ovarian cancer cell lines in the ovarian bursa, using an established xenograft model of ovarian cancer metastasis[177] (Figure 5.9). Transplantation with SK-OV-3 cells stably expressing wild-type SIK2 resulted in significantly increased peritoneal metastasis in terms of both tumour mass (Figure 5.11a) and number of tumour nodules (Figure 5.11b).

In order to validate this finding using another cell line, mice were also transplanted with OVCA432 cells stably overexpressing SIK2, or empty vector controls (Figure 5.10). Consistent with the previous experiment, metastatic tumour burden was significantly increased in terms of both tumour mass (Figure 5.11c) and number of tumour nodules (Figure 5.11d) in mice transplanted with wild-type SIK2 expressing cells. Crucially, no significant difference was observed between OVCA432 cells expressing the catalytically inactive SIK2 K49M mutant and empty vector controls, showing that SIK2 activity is necessary for the effect.

Finally, mice were transplanted with SK-OV-3 cells stably expressing wild-type SIK2 or empty vector controls and survival was monitored over a period of 88 days (Figure 5.12). Transplantation with SIK2-expressing cells significantly decreased survival compared to the control group (Log-rank test, $p = 0.0111$). Taken together, these results demonstrate that SIK2 activity promotes metastasis and tumour growth within the peritoneum, with a detrimental effect on survival.

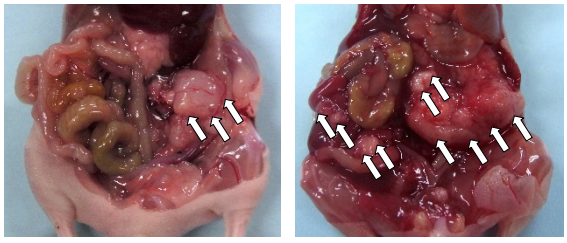

Figure 5.9. An *in vivo* model of ovarian cancer metastasis

Representative images of omental metastasis in female mice that were orthotopically transplanted with SK-OV-3-SIK2 cells or empty vector controls. Metastases are indicated by white arrows.

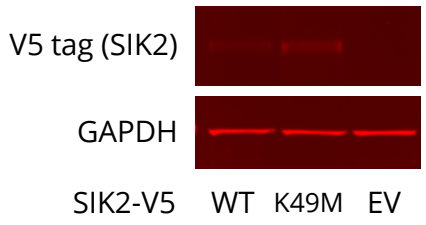

Figure 5.10. Overexpression of SIK2 in OVCA432 cells

Western blot showing stable overexpression of SIK2 in OVCA432 cell lines used in *in vivo* experiments. GAPDH indicates equal loading.

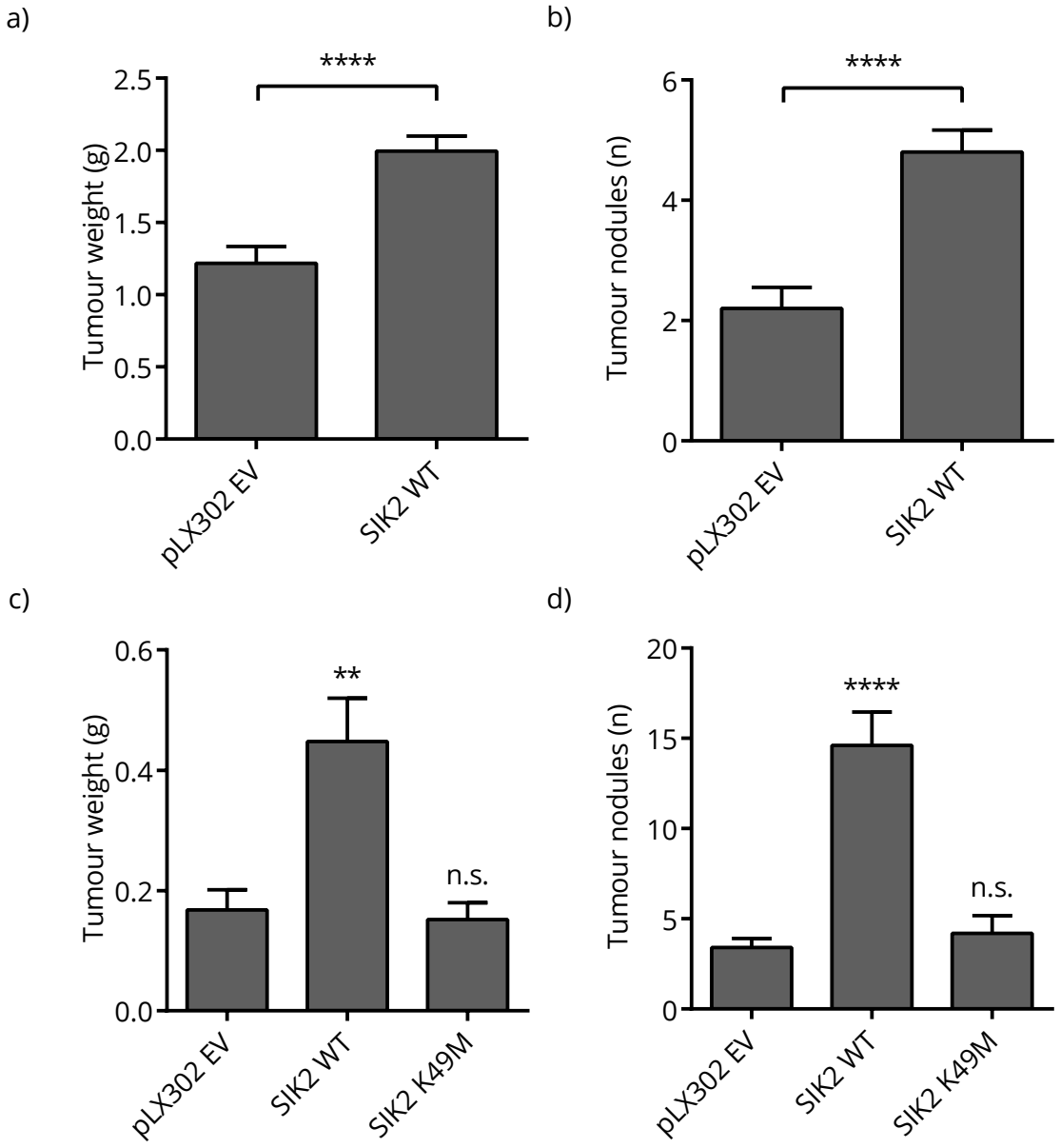

Figure 5.11. Metastatic tumour burden following orthotopic transplantation

Female mice were orthotopically transplanted with ovarian cancer cell lines. **a)** Bar graphs showing the mean tumour mass (±SEM) and **b)** number of tumour nodules (±SEM) of metastases removed from mice transplanted with SK-OV-3 cells (*n* = 15 per group) stably expressing the indicated constructs. Means were compared using *t*-tests (**** denotes $p \leq 0.0001$). **c)** Bar graphs showing the mean tumour mass (±SEM) and **d)** number of tumour nodules (±SEM) of metastases removed from mice transplanted with OVCA432 cells (*n* = 5 per group) stably expressing the indicated constructs. Each mean was compared to that of the negative control using one-way ANOVA with Dunnett's Multiple Comparison Test (** denotes $p \leq 0.01$, **** denotes $p \leq 0.0001$, and n.s. denotes $p > 0.05$).

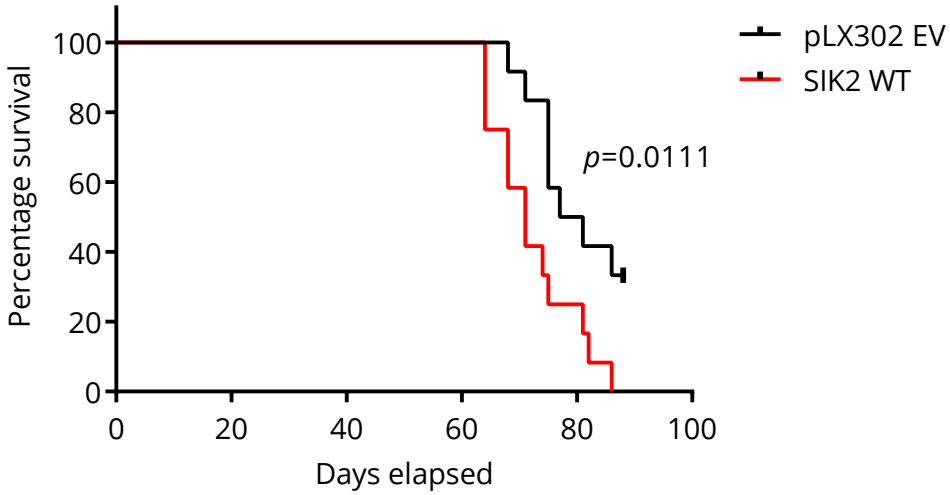

Figure 5.12. SIK2 overexpression and survival *in vivo*

Female mice were orthotopically transplanted with SK-OV-3-SIK2 cells or empty vector controls (*n* = 12 per group). Figure shows a Kaplan-Meier plot of survival in the two groups. The two groups were compared using a Log-rank test.

5.3 Discussion

Having achieved the aim of identifying novel SIK2 phosphorylation sites in Chapter 4, the next step was to determine if any of these would be suitable for use as biomarkers of SIK2 activity. Whilst a polyclonal antibody against SIK2 pS674 was not capable of recognising phosphorylation at this site, a polyclonal antibody against pS358 proved to be specific. S358 phosphorylation appears to be indicative of SIK2 activity *in vitro* and in SK-OV-3-SIK2 cells co-cultured with primary adipocytes. Whilst the possibility that this residue is phosphorylated by another kinase in cells cannot be excluded, depletion of SIK2 prevents increased AKT activation upon adipocyte treatment, suggesting that AKT is downstream rather than upstream of SIK2 in this context. The absence of S358 phosphorylation in inactive SIK2 mutants means that if another kinase is responsible for S358 phosphorylation in this system, then it must be the result of a feedback loop.

Whilst it is clear that SIK2 phosphorylates p85α at S154, the molecular interactions underpinning the effect on PI3K activity remain unclear. Structural analyses have previously shown that it is the inter-SH2 (iSH2) domain of p85α which physically binds to p110α[142], and that this interaction is disrupted by binding of tyrosine-phosphorylated proteins to the N-terminal SH2 domain[178]. S154 lies approximately 170 residues away from this SH2 domain, in the RhoGAP domain (also known as the BH domain), so phosphorylation at this residue is unlikely to be directly influencing this well-established mechanism. The RhoGAP domain is capable of interacting with and activating the GTPase activity of Rac1, Cdc42, and Rab proteins[179]. The binding of Cdc42 or Rac1 to p85α has been shown to increase PI3K activity[180] and promote cell motility and invasiveness[181], so it is possible that S154 phosphorylation promotes this interaction. Another possibility which cannot be excluded is that there are additional sites of SIK2 phosphorylation on p85α which are being phosphorylated prior to the *in vitro* PI3K activity assay.

Rac1 and Cdc42 are both key regulators of the actin cytoskeleton that are responsible for cell adhesion and formation of the filopodia and lamellipodia[182,183], and their binding to the RhoGAP domain also activates their GTPase activity[179]. As such, modulation of these interactions by S154 phosphorylation may contribute to the effect of SIK2 overexpression on cell spreading identified here. Although this potential mechanism was not investigated further, it represents an avenue for future study.

Experiments using the calcium chelator BAPTA-AM demonstrated that calcium signalling is necessary for activation of SIK2 in response to incubation with adipocytes. Activation of SIK2 can also be stimulated by treatment of cells with m-3M3FBS, a phospholipase C agonist[184], or thapsigargin, which inhibits transport of calcium from the cytoplasm into the endoplasmic reticulum[185] (F. Miranda, D. Mannion, & A.A. Ahmed, unpublished data). Both of these treatments increase the cytoplasmic calcium concentration, demonstrating that calcium signalling is sufficient for SIK2 activation. This activation likely occurs via

CaMKK, which is able to activate the related kinase AMPK by phosphorylating its activation loop in response to increased intracellular Ca^{2+} concentration[174], although further experimentation will be necessary to confirm that this is also the case for SIK2. In the context of incubation with adipocytes, calcium signalling is probably activated downstream of FFARs, although omental adipocytes have been shown to interact with ovarian cancer cells by releasing adipokines including IL-8[18], which can also activate calcium signalling[186].

The activation of PI3K/AKT signalling in ovarian cancer cells by SIK2 when exposed to adipocytes has significant implications for the biology of ovarian cancer. Despite the presence of circulating tumour cells in the blood of ovarian cancer patients, metastases tend to be localised within the peritoneal cavity, with a clear predilection for the omentum[14,15,18]. The adipocytes in this fat-rich tissue release fatty acids when incubated with ovarian cancer cells, leading to the activation of AMPK and the β-oxidation pathway, and providing a source of energy which promotes tumour growth[18]. Activation of PI3K/AKT signalling via SIK2 appears to be a parallel mechanism which also contributes to the establishment and growth of metastases in this adipocyte-rich niche, as activation of AKT is associated with increased cell growth[144,187], invasion[175], and chemotherapy resistance[176,188,189] in ovarian cancers. Consistent with this idea, overexpression of SIK2 resulted in significantly increased metastatic tumour burden in an *in vivo* model of ovarian cancer metastasis, and a significant decrease in survival.

The main weakness of the biochemical data presented here is that the experiments were conducted using SIK2-overexpressing cells. Since the screen was also performed with overexpression of SIK2, it is therefore possible that the observed SIK2 autophosphorylation does not occur naturally. Unfortunately, it was not possible to use unmodified cell lines as the pS358 antibody is not able to detect reliably S358 phosphorylation at endogenous levels of SIK2 expression.

In summary, these experiments have confirmed that SIK2 undergoes autophosphorylation at S358, and that this phosphorylation can be detected using a polyclonal antibody to infer SIK2 activity. SIK2 is activated in ovarian cancer cells upon incubation with primary adipocytes, with a concomitant increase in AKT activity. SIK2 was also shown to phosphorylate the p85α regulatory subunit of PI3K, which increased PI3K activity *in vitro*. In an *in vivo* model of ovarian cancer metastasis, overexpression of SIK2 led to increased metastatic tumour burden. Taken together, these findings suggest that SIK2 is capable of activating the oncogenic PI3K-AKT signalling pathway in response to adipocytes, promoting survival and proliferation of ovarian cancer cells in the adipocyte-rich microenvironment of the omentum.

CHAPTER 6: PRELIMINARY INVESTIGATION OF CLASPS AND P120 CATENIN

6.1 Introduction

The gene ontology analysis presented in Chapter 4 identified a potential role for SIK2 in the regulation of microtubule polymerisation. Two of the hits which were identified in all four screen replicates are the cytoplasmic linker associated proteins, CLASP1 and CLASP2, both of which are microtubule plus-end binding proteins which have been shown to stabilise microtubules[132,133].

This stabilisation is dependent on recruitment of the microtubule end-binding protein EB1 to the serine-arginine rich domain of CLASPs[133], which can undergo phosphorylation to prevent this interaction[190]. This domain contains the site identified in the screen, which is conserved in both CLASP1 and CLASP2 (Figure 6.1), suggesting that phosphorylation by SIK2 might also influence EB1 binding and negatively regulate microtubule stability. Since decreased microtubule stability increases resistance to paclitaxel[149], this represents a possible mechanism for the contribution of SIK2 to paclitaxel resistance. In yeast, PKA activity negatively regulates the microtubule stabilising effect of CLASP to limit cell size during glucose starvation[191], which is also consistent with this hypothesis as PKA has been reported to inhibit SIK2 activity[51].

Furthermore, CLASP2 undergoes extensive phosphorylation upon insulin stimulation, including the S370 site identified here[134] (the residue number varies between isoforms), which is of interest as SIK2 is thought to be activated downstream of insulin[52]. The authors also showed that CLASP2 is required for insulin-stimulated delivery of the GLUT4 glucose transporter to the plasma membrane, which is interesting as SIK2 activity has been shown to promote GLUT4 expression in adipocytes[64]. It was also recently reported that CLASP1 S600 and the equivalent site on CLASP2 can be phosphorylated by the related MARK kinases *in vitro*[192].

Gene ontology analysis of the screen results also identified a number of proteins involved in focal adhesion. p120 catenin (also known as p120 or catenin delta-1) is a component of adherens junctions which associates with and stabilises E-cadherin, promoting strong adhesion[135]. The S268 phosphorylation site was detected as a SIK2 substrate in all four screen replicates, and a phosphorylation-specific antibody[138] is available, making it an attractive target for validation.

Phosphorylation of S268 by CK1 has previously been shown to disrupt E-cadherin binding, destabilising adherens junctions and releasing p120 into the cytoplasm[136]. Cytoplasmic p120 has been shown to activate oncogenic processes, including proliferation, invasion

and metastasis, in a variety of cancers[137]. It is possible that loss of E-cadherin-mediated adhesion facilitates detachment of cells from the primary ovarian tumours into the peritoneal fluid[15], so regulation of p120 by SIK2 might contribute to the promotion of metastasis by SIK2 shown in the previous chapter.

This chapter contains the results of preliminary functional experiments to investigate the effect of the identified sites on CLASP1/2 localisation and to confirm phosphorylation of p120 by SIK2.

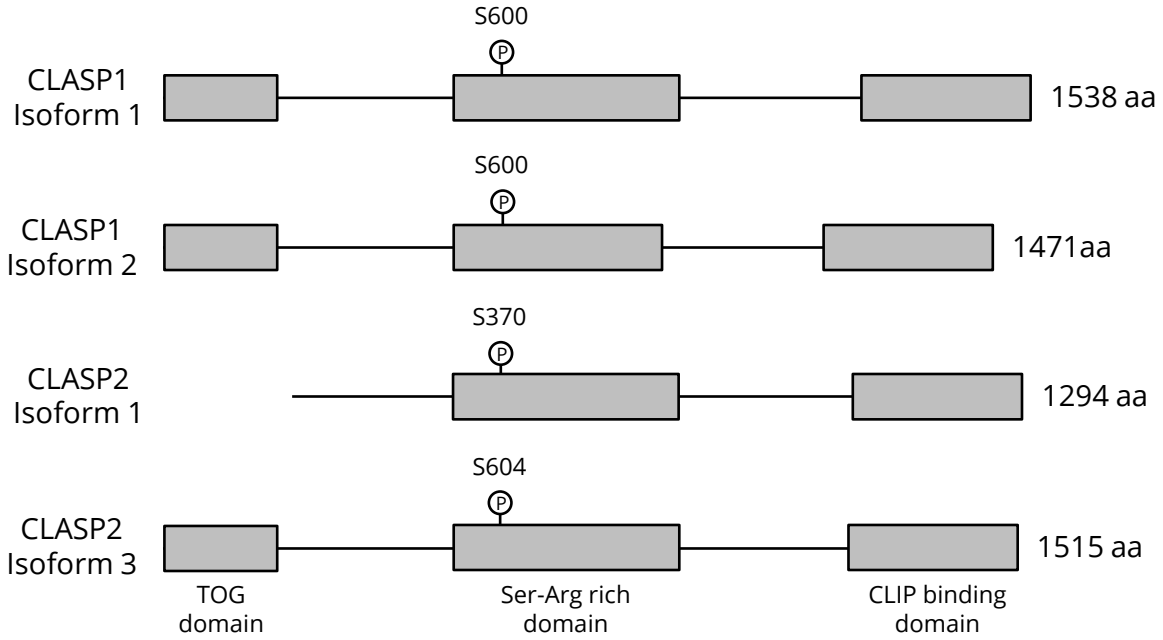

Figure 6.1. CLASP1 and CLASP2 domain structures

Schematic representation of CLASP1 isoform 1 and CLASP2 isoform 1 showing the positions of the putative SIK2 phosphorylation sites at S600 and S370, respectively. The isoforms used in preliminary experiments are also shown. Note that in the longer CLASP2 isoform 3 the phosphorylation site corresponds to S604 rather than S370.

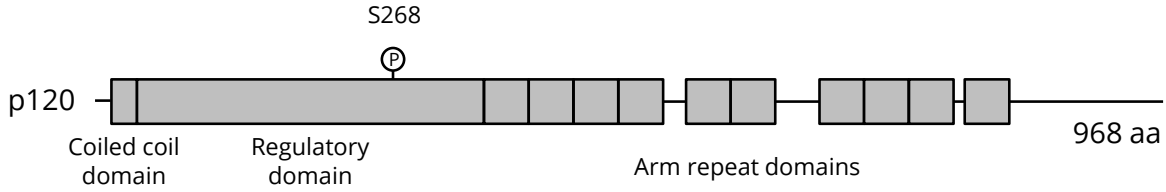

Figure 6.2. p120 domain structure

Schematic representation of p120 showing the position of the S268 phosphorylation site identified as a potential SIK2 substrate in Chapter 4.

6.2 Results

6.2.1 Mutagenesis of CLASP1 S600 does not affect localisation

In order to determine if phosphorylation of S600 affects localisation of CLASP1 to microtubules, S600A and S600E mutants were generated to abolish phosphorylation or mimic phosphorylation, respectively. These mutants were successfully expressed in 293T cells (Figure 6.3a), although the presence of additional lower molecular weight bands suggests some protein degradation.

CLASP1 was stably overexpressed in SK-OV-3 cells using lentiviral transduction (Figure 6.3b). These cell lines were then grown on glass cover slips and a scratch assay was used to induce polarisation and migration of cells bordering the scratch. Immunofluorescence staining using V5-tag and α-tubulin antibodies (Figure 6.4) showed clear co-localisation of CLASP1 and α-tubulin, although this did not appear to be affected in either the S600A or S600E mutant. The striking localisation of CLASP1 to the microtubule plus-end[133] observed by Mimori-Kiyosue *et al*. (2005) was not evident in any of the cell lines, suggesting that this is not mediated by S600 phosphorylation status. However, it is possible that the quality of these images is not sufficient to detect plus-end localisation, so a higher resolution approach along with a positive control could yield additional information.

Unfortunately, although exogenous CLASP2 expressed properly in 293T cells, attempts to generate a stable cell line were unsuccessful, meaning it was not possible to investigate the equivalent phosphorylation site in this protein.

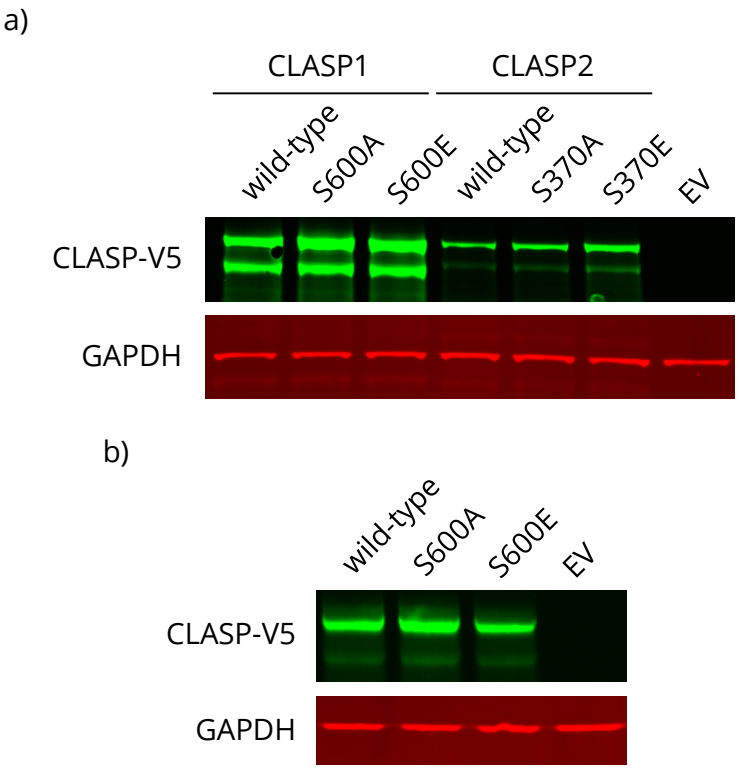

Figure 6.3. Expression of CLASP mutants

a) Western blot showing transient expression of CLASP1 and CLASP2 in 293T cells. GAPDH confirms equal loading. **b)** Western blot showing stable expression of CLASP1 in SK-OV-3 cells. GAPDH confirms equal loading.

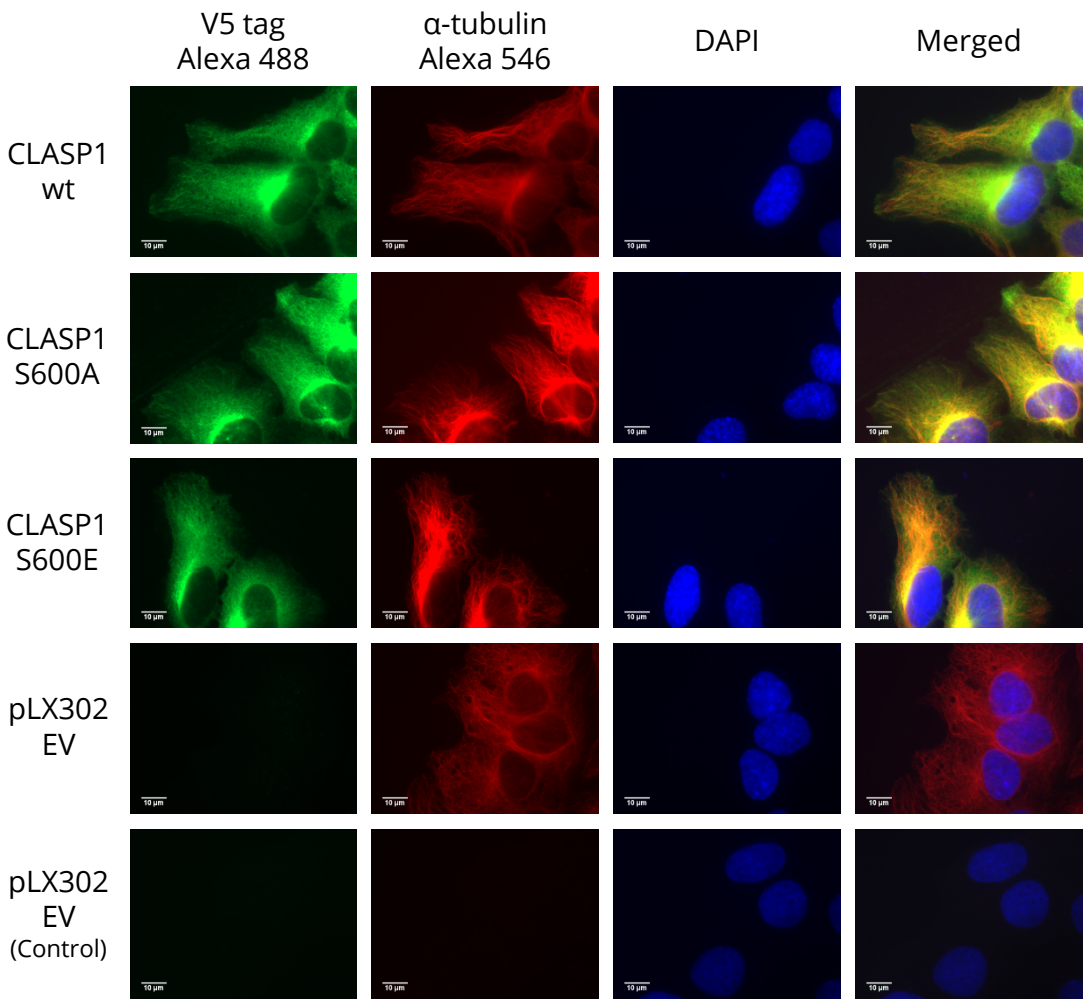

Figure 6.4. Immunofluorescence staining in SK-OV-3-CLASP1 cells

Representative fluorescence microscopy images following scratch assays in SK-OV-3-CLASP1 cell lines. Exposure settings were kept constant for each channel. Scale bars represent 10 µm. The bottom row shows a control stained with secondary antibodies only.

6.2.2 SIK2 does not influence p120 S268 phosphorylation

Since p120 can promote a number of oncogenic processes[137], as well as playing a role in cell adhesion[135], the commercially available antibody against phosphorylated S268 was used to determine whether phosphorylation at this site correlates with SIK2 activity. SK-OV-3 cells stably overexpressing wild-type SIK2, the overactive T96M mutant, or empty vector were treated with siRNA targeting the coding sequence of SIK2 (10) or a non-targeting control. As a further control, a third siRNA targeting the 3' untranslated region (UTR) of SIK2 (23) was used to deplete the endogenous SIK2 whilst leaving the exogenous expression unaffected (Figure 6.5a).

Contrary to expectations, stable overexpression of SIK2 did not result in increased S268 phosphorylation compared to empty-vector controls (Figure 6.5b). Furthermore, depletion of SIK2 did not reduce S268 phosphorylation. In fact, effective depletion of SIK2 actually resulted in a modest increase in phosphorylation. Unusually, treatment with the 3'UTR siRNA lead to an even greater increase in phosphorylation. These increases were exacerbated by an unexplained decrease in p120 protein levels in the cells treated with SIK2 specific siRNAs, since the signal from anti-pS268 antibody was normalised using the signal from the anti-p120 antibody. Nonetheless, all of these observations suggest that, under these conditions, S268 phosphorylation is independent of SIK2.

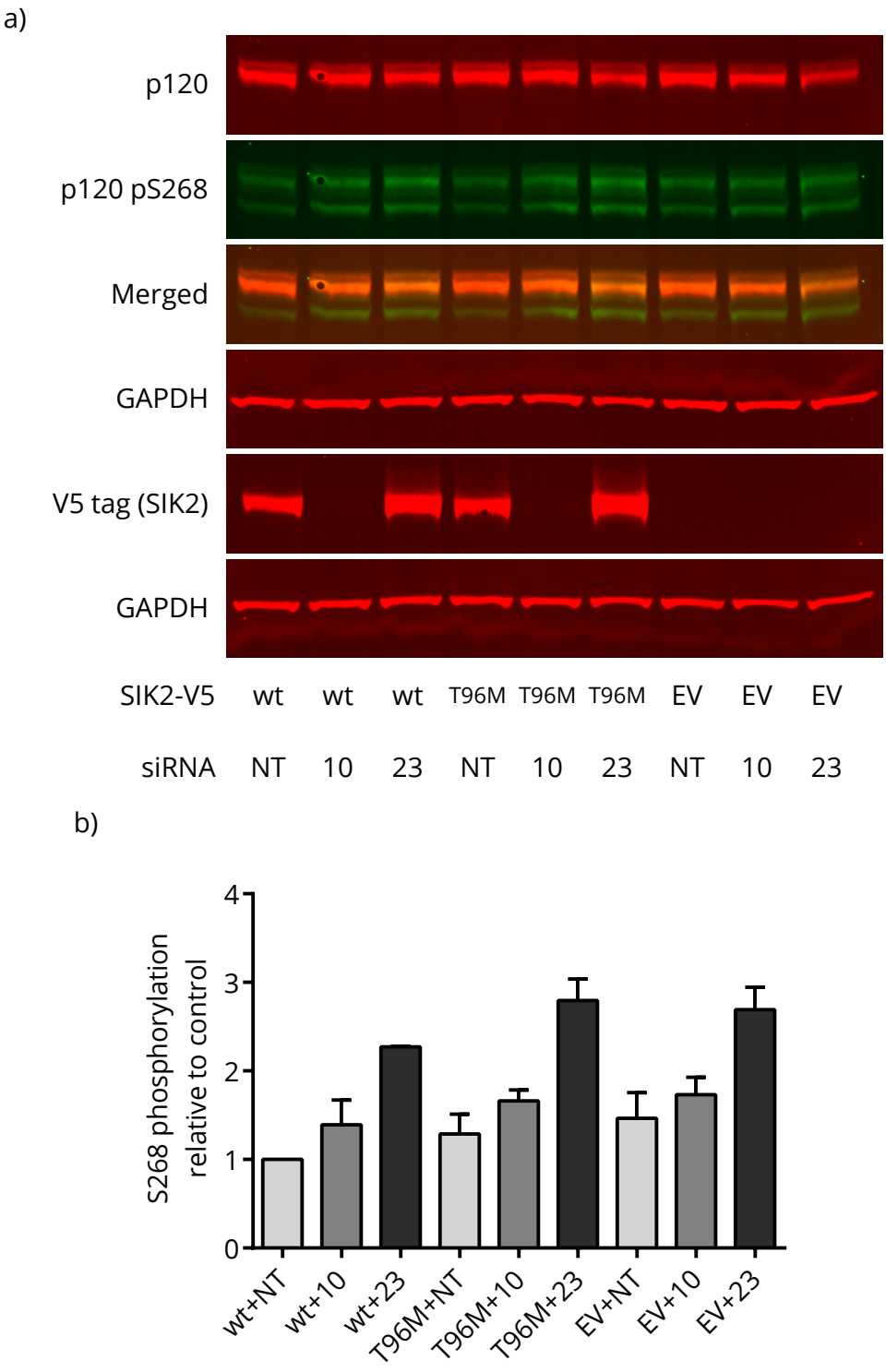

Figure 6.5. SIK2 overexpression, depletion, and p120 phosphorylation

SK-OV-3-SIK2 cell lines were treated with siRNAs to deplete SIK2. **a)** Western blots showing depletion of SIK2 and phosphorylation of p120 in SK-OV-3-SIK2 cell lines. **b)** Graph showing levels of p120 S268 phosphorylation as a proportion of the wild-type/non-targeting (NT) control. Data shown are the means ± SEM from two independent experiments.

6.3 Discussion

CLASP1 and CLASP2 were selected for validation on the basis that they have been shown to bind to and stabilise microtubules[132,133], so modulation of this interaction could conceivably contribute to the paclitaxel resistance phenotype associated with high SIK2 expression[6]. Modification of the newly identified CLASP1 S600 site to prevent (S600A) or mimic (S600E) phosphorylation did not result in a clear redistribution of CLASP1 with respect to microtubules. However, the clear localisation of CLASP to the microtubule plus-end, associated with EB1 binding[133], was not observed in this system, so further experimentation will be required to rule out the possibility of S600 phosphorylation affecting this interaction (e.g. in HeLa cells where plus-end localisation has been demonstrated). An alternative approach would be to investigate the effect of mutant CLASP expression on microtubule stability directly by measuring glu-tubulin levels, an indicator of microtubule stability[193]. These experiments were trialled (data not shown), but it was not possible to fully optimise the assays within the time constraints of this project.

Since p120 has previously been implicated in oncogenic processes[137], the effect of SIK2 overexpression and depletion on phosphorylation at S268 was investigated. However, there was no evidence that overexpression of SIK2 results in increased S268 phosphorylation, or that depletion has the opposite effect. Treatment with an siRNA targeting the 3'UTR of SIK2 actually resulted in a large increase in p120 S268 phosphorylation, although this is partly due to a decrease in the level of p120 protein, to which the signal from the pS268 antibody was normalised. It is possible that this reflects an off-target effect of this particular siRNA, which appeared to be more toxic than the others (data not shown), resulting in decreased cell confluence which could affect p120 through differences in cell-cell adhesion.

The apparent independence of S268 phosphorylation status from SIK2 expression in this context makes it unlikely that p120 contributes to the increased metastasis of SIK2 overexpressing cells shown in the previous chapter.

The failure to validate S268 phosphorylation by SIK2 might suggest that it was a false positive screen hit. However, p120 S268 was also the most commonly identified phosphorylation site in a recent screen for AMPK substrates by Schaffer *et al*. (2015). This screen used intact permeabilised cells for substrate labelling, so it is unlikely that the identification of p120 as a SIK2 substrate is an artefact resulting from cell lysis. It is also unlikely that it is an artefact of SIK2 overexpression, as the same SIK2-overexpressing cell lines were used in the validation experiments. It may be the case that phosphorylation of p120 by SIK2 is dependent on a particular context (e.g. cell spreading) or stimulus which was absent in these functional experiments, but SIK2 was not deliberately stimulated prior to the screen experiments which identified S268 as a putative SIK2 phosphorylation site.

In summary, a preliminary experiment investigating the function of a newly identified phosphorylation site on CLASP1 was inconclusive, but may merit further investigation. Although p120 has previously been shown to activate oncogenic processes, including proliferation, invasion and metastasis, in multiple cancers[137], there was no evidence to suggest that p120 is regulated by SIK2.

CHAPTER 7: DISCUSSION & CONCLUSION

7.1 Overview

Salt-inducible kinase 2 is an AMPK-related protein kinase which has previously been identified as a potential therapeutic target in high-grade serous ovarian cancer. It has previously been shown that increased SIK2 expression is associated with increased risk of progression following paclitaxel therapy, whilst depletion of SIK2 increases sensitivity of ovarian cancer cells to paclitaxel both *in vitro* and in xenograft models[6]. This evidence suggests that pharmacological inhibition of SIK2 represents a plausible clinical strategy to enhance the response of HGSOC to paclitaxel therapy. However, the molecular mechanisms underpinning this effect remain unclear and cannot be accounted for by previously identified SIK2 substrates.

The main aim of this project was to discover novel substrates of SIK2 using a chemical genetic screen, an approach which allows large-scale identification of substrates for a kinase of interest. Furthermore, the project aimed to use the information from the screen to elucidate the role of SIK2 in HGSOC biology and paclitaxel resistance, and provide potential biomarkers of SIK2 activity to assist in the development of small-molecule inhibitors.

Whilst chemical genetic screening has previously been applied to AMPKα2 to identify substrates[105,162], the approach had not been used to investigate any of the SIK kinases. Following a programme of preliminary experimentation, an analogue-sensitive SIK2 mutant was shown to be able to utilise N^6-phenylethyl-ATPγS to label substrates in the SK-OV-3 ovarian cancer cell line. This system was then used to conduct screen experiments in conjunction with a covalent capture technique[116] to isolate thiophosphorylated peptides.

Four independent screen experiments identified a total of 85 putative phosphorylation sites on 73 different proteins, 22 of which were present in multiple replicates. There was significant variability between replicates, although this was consistent with studies using the same approach on other kinases[162]. The vast majority of the proteins identified are previously unrecognised SIK2 substrates, providing targets for further study. This represents a significant step forward in the study of SIK2, as only a handful of direct substrates have previously been identified (see Chapter 1), and only one of these has been validated in an ovarian cancer system.

Only 3 of the sites conform exactly to the SIK phosphorylation site consensus motif, demonstrating that this motif is neither necessary nor sufficient for phosphorylation by SIK2. Gene ontology analysis of the screen data showed that the identified substrates were significantly enriched in proteins involved in cytoskeletal regulation, particularly

microtubule regulatory proteins, suggesting that SIK2 might influence the response to paclitaxel by regulating microtubule stability. The list of putative substrates was also enriched in proteins involved in cell adhesion, mirroring the results of a recent screen for AMPK substrates[162]. However, the overlap between the two sets of screen results was only 4 phosphorylation sites, so it is possible that SIK2 and AMPK act in parallel in a complimentary manner.

The screen hits also included a number of phosphorylation sites on SIK2 itself, supporting observations from *in vitro* kinase assays which suggested that SIK2 can autophosphorylate. The putative autophosphorylation site at S358 was validated using a custom phosphorylation-specific polyclonal antibody, showing that S358 undergoes autophosphorylation *in vitro*, and can be used as a biomarker of SIK2 activity. Using this antibody it was established that SIK2 is activated in a calcium-dependent manner upon incubation of SK-OV-3-SIK2 cells with primary adipocytes, suggesting that SIK2 might be activated during metastasis to adipocyte-rich tissues in the peritoneum, including the omentum. Further work in our group has established that activation of SIK2 in this context leads to up-regulation of β-oxidation (F. Miranda, D. Mannion, & A.A. Ahmed, unpublished data), which would allow ovarian cancer cells to utilise adipocyte-derived fatty acids to fuel cell growth and proliferation.

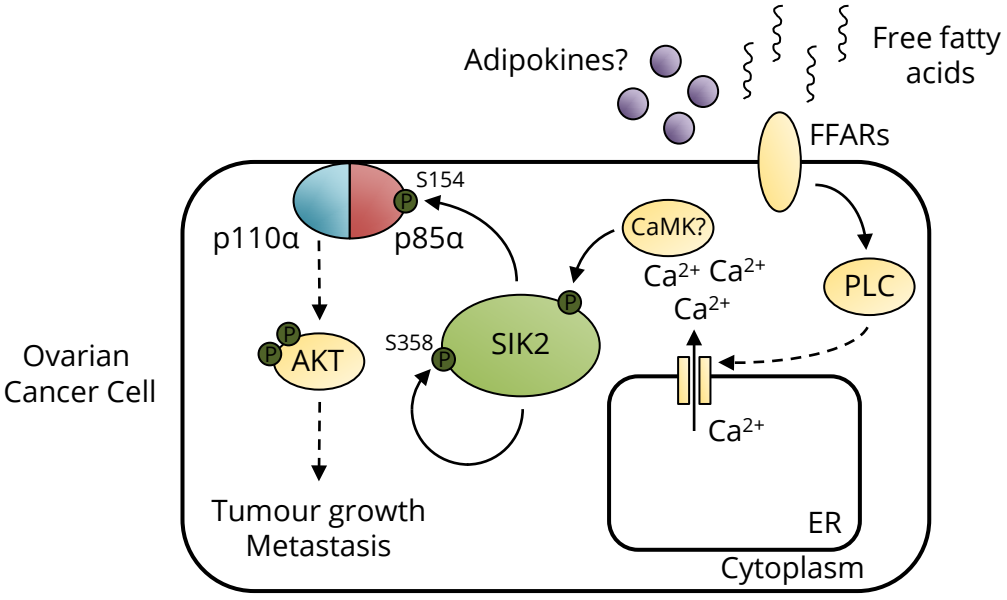

Figure 7.1. A model of SIK2 activation by omental adipocytes

Co-incubation of ovarian cancer cells with adipocytes results in exposure to free fatty acids and adipokines, activating calcium release from the endoplasmic reticulum (ER) via phospholipase C (PLC). Calcium leads to activation of SIK2, probably via a CaMK family kinase, resulting in increased SIK2 autophosphorylation at S358. SIK2 in turn activates PI3 kinase by phosphorylating the regulatory p85α subunit at S154, leading to downstream activation of AKT signalling, promoting metastasis and tumour growth.

One of the three SIK consensus motifs identified in the screen is located at S154 of p85α, the regulatory subunit of the PI3K complex[141,142]. SIK2 was shown to phosphorylate this residue and increase the activity of the PI3K complex *in vitro*, consistent with the activation of the downstream kinase AKT observed upon incubation with adipocytes. Activation of this critical oncogenic signalling pathway[44,117] further suggested a role for SIK2 in metastatic spread to the omentum (Figure 7.1). This was confirmed using an *in vivo* model of ovarian cancer metastasis, which showed that SIK2 activity promotes increased tumour size and increased number of tumour nodules in mice transplanted with either SK-OV-3 or OVCA432 cells, with a significant effect on survival.

There is already a strong rationale for the pursuit of SIK2 as a therapeutic target in ovarian cancer on the basis that its expression is strongly associated with paclitaxel resistance. These results demonstrate a clear role for SIK2 in metastasis and tumour growth at the omentum, and suggest that in addition to sensitising ovarian cancer cells to paclitaxel, clinical use of a SIK2 inhibitor might slow metastatic tumour growth in the peritoneum. If well tolerated, such an inhibitor could be used as a maintenance therapy following first-line chemotherapy to prevent or delay relapse. This would be of significant benefit in the treatment of ovarian cancer, as metastatic burden in the peritoneum is a major cause of morbidity, promoting abdominal adhesions which obstruct the small and large intestines, causing significant discomfort and leading to malnutrition[15,19].

7.2 Future directions

Having identified novel SIK2 substrates with various different functions, there is clearly a great deal of scope for further investigation. However, individual validation of all of the identified substrates would be relatively laborious and resource-intensive, requiring at a minimum the cloning and expression of alanine and phosphomimetic point mutants of each substrate protein, and ideally the creation of phosphorylation-specific antibodies for each phosphorylation site.

An alternative approach would be to use the SIK2-overexpressing cell lines generated for this project to investigate phenotypes of interest suggested by gene ontology analysis. For example, microtubule stability can be inferred from detyrosination of α-tubulin[193], so if levels of detyrosinated tubulin are lower under SIK2 overexpression, then this could well account for the effect on paclitaxel resistance. This should be a priority as a positive result would further strengthen the rationale for development of SIK2 inhibitors for clinical use. A similar methodology has recently been used to show that spleen tyrosine kinase (SYK) modulates microtubule stability, and the response to paclitaxel, in ovarian cancer cells[154].

Since preliminary experiments using CLASP1 S600 mutants proved inconclusive, in part due to the absence of a clear microtubule tip localisation in SK-OV-3 cells, these experiments could be repeated in the HeLa cell line in which this was originally

observed[133]. The CLASP1 overexpressing cell lines could also be used in assays of microtubule stability to help determine if the S600 phosphorylation site (and CLASP2 S370) has any functional significance.

The discovery that SIK2 activates PI3K/AKT signalling via phosphorylation of p85α creates an another avenue for further investigation, as this could also be responsible for paclitaxel resistance[176]. This could be investigated by expressing a phosphomimetic mutant of p85α in ovarian cancer cells and assaying cell proliferation or survival following paclitaxel treatment. Alternatively, an S154A mutant could be expressed to see if this rescues the paclitaxel resistance phenotype associated with SIK2 expression.

Given that PI3K/AKT signalling is also known to promote invasive behaviour in ovarian cancer cells[175], it would be of interest to know if this occurs downstream of SIK2, as this may be contributing to the increased metastatic potential of SIK2-overexpressing cells described in Chapter 5.

Since SIK2 is considered an attractive therapeutic target in HGSOC, as well as in inflammatory and autoimmune diseases[4], there is active interest in producing specific small molecule inhibitors. Clark *et al*. (2012) reported a number of compounds with SIK inhibitory activity, including KIN112 and HG-9-91-01. Arrien Pharmaceuticals (USA) used a fragment-based design strategy to produce ARN-3236, a potent SIK2 inhibitor with favourable pharmacokinetic properties, which is currently in pre-clinical development[194]. Furthermore, the MRC recently funded a drug discovery project to identify novel SIK2 inhibitors in a collaboration between the University of Glasgow and the University of Oxford[195]. The anti-SIK2 pS358 antibody described in Chapter 5 could facilitate such drug discovery efforts by providing a measure of SIK2 kinase activity, allowing the on-target activity of novel SIK2 inhibitors to be determined in cell culture experiments or xenograft models (if SIK2 is overexpressed in these systems).

A recent paper by Sundberg *et al*. (2015) found that the anti-inflammatory effects of the clinically approved Src inhibitors dasatinib and bosutinib are actually mediated by inhibition of SIKs[170]. Whether pan-SIK inhibition or SIK2-specific inhibition is more desirable in a therapeutic context remains an open question. Having optimised the required techniques, it would be feasible to conduct chemical genetic screens to identify substrates of SIK1 and SIK3 to help determine the extent to which their functions overlap with those of SIK2. The constructs required for these experiments have already been produced as part of this project.

7.3 Conclusions

In summary, this work has identified a large number of putative SIK2 substrates for further study, and a potential role for SIK2 in cytoskeletal regulation. Phosphorylation of one such substrate, p85α, results in activation of PI3K/AKT signalling in ovarian cancer cells upon exposure to adipocytes. Consistent with this finding, overexpression of SIK2 led to increased tumour growth and metastasis of ovarian cancer cells in xenograft models. In addition to the previously identified effect on paclitaxel resistance[6], this further reinforces the case for development of SIK2 inhibitors for use in the treatment of ovarian cancer.

REFERENCES

1. Horike, N., Takemori, H., Katoh, Y., Doi, J., Min, L., Asano, T., Sun, X. J., Yamamoto, H., Kasayama, S., Muraoka, M., Nonaka, Y. & Okamoto, M. Adipose-specific expression, phosphorylation of Ser794 in insulin receptor substrate-1, and activation in diabetic animals of salt-inducible kinase-2. *J. Biol. Chem.* **278,** 18440–18447 (2003).

2. Bricambert, J., Miranda, J., Benhamed, F., Girard, J., Postic, C. & Dentin, R. Salt-inducible kinase 2 links transcriptional coactivator p300 phosphorylation to the prevention of ChREBP-dependent hepatic steatosis in mice. *J. Clin. Invest.* **120,** 4316–4331 (2010).

3. Sasaki, T., Takemori, H., Yagita, Y., Terasaki, Y., Uebi, T., Horike, N., Takagi, H., Susumu, T., Teraoka, H., Kusano, K., Hatano, O., Oyama, N., Sugiyama, Y., Sakoda, S. & Kitagawa, K. SIK2 Is a Key Regulator for Neuronal Survival after Ischemia via TORC1-CREB. *Neuron* **69,** 106–119 (2011).

4. Clark, K., MacKenzie, K. F., Petkevicius, K., Kristariyanto, Y., Zhang, J., Choi, H. G., Peggie, M., Plater, L., Pedrioli, P. G. A., McIver, E., Gray, N. S., Arthur, J. S. C. & Cohen, P. Phosphorylation of CRTC3 by the salt-inducible kinases controls the interconversion of classically activated and regulatory macrophages. *Proc. Natl. Acad. Sci.* **109,** 16986–16991 (2012).

5. Sakamaki, J.-I., Fu, A., Reeks, C., Baird, S., Depatie, C., Al Azzabi, M., Bardeesy, N., Gingras, A.-C., Yee, S.-P. & Screaton, R. A. Role of the SIK2-p35-PJA2 complex in pancreatic β-cell functional compensation. *Nat. Cell Biol.* **16,** 234–244 (2014).

6. Ahmed, A. A., Lu, Z., Jennings, N. B., Etemadmoghadam, D., Capalbo, L., Jacamo, R. O., Barbosa-Morais, N., Le, X. F., Vivas-Mejia, P., Lopez-Berestein, G., Grandjean, G., Bartholomeusz, G., Liao, W., Andreeff, M., Bowtell, D., Glover, D. M., Sood, A. K. & Bast, R. C. SIK2 Is a Centrosome Kinase Required for Bipolar Mitotic Spindle Formation that Provides a Potential Target for Therapy in Ovarian Cancer. *Cancer Cell* **18,** 109–121 (2010).

7. Bon, H., Wadhwa, K., Schreiner, A., Osborne, M., Carroll, T., Ramos-Montoya, A., Ross-Adams, H., Visser, M., Hoffmann, R., Ahmed, A. A., Neal, D. E. & Mills, I. G. Salt-inducible Kinase 2 Regulates Mitotic Progression and Transcription in Prostate Cancer. *Mol. Cancer Res.* **13,** 620–636 (2014).

8. Ovarian cancer statistics. *Cancer Res. UK* at <http://www.cancerresearchuk.org/health-professional/cancer-statistics/statistics-by-cancer-type/ovarian-cancer>

9. Cooper, N., Quinn, M. J., Rachet, B., Mitry, E. & Coleman, M. P. Survival from cancer of the ovary in England and Wales up to 2001. *Br. J. Cancer* **99,** S70–S72 (2008).

10. Vaughan, S., Coward, J. I., Bast, R. C., Berchuck, A., Berek, J. S., Brenton, J. D., Coukos, G., Crum, C. C., Drapkin, R., Etemadmoghadam, D., Friedlander, M., Gabra, H., Kaye, S. B., Lord, C. J., Lengyel, E., Levine, D. A., McNeish, I. A., Menon, U., Mills, G. B., Nephew, K. P., Oza, A. M., Sood, A. K., Stronach, E. A., Walczak, H., Bowtell, D. D. &

Balkwill, F. R. Rethinking ovarian cancer: recommendations for improving outcomes. *Nat. Rev. Cancer* **11,** 719–725 (2011).

11. Sehouli, J., Senyuva, F., Fotopoulou, C., Neumann, U., Denkert, C., Werner, L. & Gülten, O. Ö. Intra-abdominal tumor dissemination pattern and surgical outcome in 214 patients with primary ovarian cancer. *J. Surg. Oncol.* **99,** 424–427 (2009).

12. Prat, J. Staging classification for cancer of the ovary, fallopian tube, and peritoneum. *Int. J. Gynecol. Obstet.* **124,** 1–5 (2014).

13. Phillips, K. G., Velasco, C. R., Li, J., Kolatkar, A., Luttgen, M., Bethel, K., Duggan, B., Kuhn, P. & McCarty, O. J. T. Optical Quantification of Cellular Mass, Volume, and Density of Circulating Tumor Cells Identified in an Ovarian Cancer Patient. *Front. Oncol.* **2,** 1–8 (2012).

14. Pradeep, S., Kim, S. S. J., Wu, S., Nishimura, M., Chaluvally-Raghavan, P., Miyake, T., Pecot, C., Kim, S. S. J., Choi, H., Bischoff, F., Mayer, J., Huang, L., Nick, A., Hall, C., Rodriguez-Aguayo, C., Zand, B., Dalton, H., Arumugam, T., Lee, H., Han, H., Cho, M., Rupaimoole, R., Mangala, L., Sehgal, V., Oh, S., Liu, J., Lee, J. S., Coleman, R., Ram, P., Lopez-Berestein, G., Fidler, I. & Sood, A. Hematogenous Metastasis of Ovarian Cancer: Rethinking Mode of Spread. *Cancer Cell* **26,** 77–91 (2014).

15. Lengyel, E. Ovarian Cancer Development and Metastasis. *Am. J. Pathol.* **177,** 1053–1064 (2010).

16. Kenny, H. A., Krausz, T., Yamada, S. D. & Lengyel, E. Use of a novel 3D culture model to elucidate the role of mesothelial cells, fibroblasts and extra-cellular matrices on adhesion and invasion of ovarian cancer cells to the omentum. *Int. J. Cancer* **121,** 1463–1472 (2007).

17. McGrail, D. J., Kieu, Q. M. N. & Dawson, M. R. The malignancy of metastatic ovarian cancer cells is increased on soft matrices through a mechanosensitive Rho-ROCK pathway. *J. Cell Sci.* **127,** 2621–2626 (2014).

18. Nieman, K. M., Kenny, H. A., Penicka, C. V, Ladanyi, A., Buell-Gutbrod, R., Zillhardt, M. R., Romero, I. L., Carey, M. S., Mills, G. B., Hotamisligil, G. S., Yamada, S. D., Peter, M. E., Gwin, K. & Lengyel, E. Adipocytes promote ovarian cancer metastasis and provide energy for rapid tumor growth. *Nat. Med.* **17,** 1498–1503 (2011).

19. Tan, D. S., Agarwal, R. & Kaye, S. B. Mechanisms of transcoelomic metastasis in ovarian cancer. *Lancet Oncol.* **7,** 925–934 (2006).

20. King, M.-C., Marks, J. H., Mandell, J. B. & New York Breast Cancer Study, G. Breast and ovarian cancer risks due to inherited mutations in BRCA1 and BRCA2. *Science (80-.).* **302,** 643–646 (2003).

21. Chen, S. & Parmigiani, G. Meta-Analysis of BRCA1 and BRCA2 Penetrance. *J. Clin. Oncol.* **25,** 1329–1333 (2007).

22. Ramus, S. J. & Gayther, S. A. The Contribution of BRCA1 and BRCA2 to Ovarian Cancer. *Mol. Oncol.* **3,** 138–150 (2009).

23. Group, C. & Cancer, O. Menopausal hormone use and ovarian cancer risk: individual participant meta-analysis of 52 epidemiological studies. *Lancet* **385,** 1835–1842 (2015).

24. Collaborative Group on Epidemiological Studies of Ovarian Cancer. Ovarian cancer and body size: individual participant meta-analysis including 25,157 women with ovarian cancer from 47 epidemiological studies. *PLoS Med.* **9,** e1001200 (2012).

25. Adami, H. O., Hsieh, C. C., Lambe, M., Trichopoulos, D., Leon, D., Persson, I., Ekbom, A. & Janson, P. O. Parity, age at first childbirth, and risk of ovarian cancer. *Lancet* **344,** 1250–1254 (1994).

26. Beral, V., Doll, R., Hermon, C., Peto, R. & Reeves, G. Ovarian cancer and oral contraceptives: collaborative reanalysis of data from 45 epidemiological studies including 23,257 women with ovarian cancer and 87,303 controls. *Lancet* **371,** 303–14 (2008).

27. Prat, J. Ovarian carcinomas: Five distinct diseases with different origins, genetic alterations, and clinicopathological features. *Virchows Arch.* **460,** 237–249 (2012).

28. Fathalla, M. F. Incessant ovulation - a factor in ovarian neoplasia? *Lancet* **2,** 163 (1971).

29. Levanon, K., Crum, C. & Drapkin, R. New insights into the pathogenesis of serous ovarian cancer and its clinical impact. *J. Clin. Oncol.* **26,** 5284–5293 (2008).

30. Dubeau, L. The cell of origin of ovarian epithelial tumors and the ovarian surface epithelium dogma: does the emperor have no clothes? *Gynecol. Oncol.* **72,** 437–442 (1999).

31. Kindelberger, D. W., Lee, Y., Miron, A., Hirsch, M. S., Feltmate, C., Medeiros, F., Callahan, M. J., Garner, E. O., Gordon, R. W., Birch, C., Berkowitz, R. S., Muto, M. G. & Crum, C. P. Intraepithelial carcinoma of the fimbria and pelvic serous carcinoma: Evidence for a causal relationship. *Am. J. Surg. Pathol.* **31,** 161–9 (2007).

32. Kuhn, E., Kurman, R. J., Vang, R., Sehdev, A. S., Han, G., Soslow, R., Wang, T. L. & Shih, I. M. TP53 mutations in serous tubal intraepithelial carcinoma and concurrent pelvic high-grade serous carcinoma-evidence supporting the clonal relationship of the two lesions. *J. Pathol.* **226,** 421–426 (2012).

33. Karst, A. M., Levanon, K. & Drapkin, R. Modeling high-grade serous ovarian carcinogenesis from the fallopian tube. *Proc. Natl. Acad. Sci.* **108,** 7547–7552 (2011).

34. Kim, J., Coffey, D. M., Creighton, C. J., Yu, Z., Hawkins, S. M. & Matzuk, M. M. High-grade serous ovarian cancer arises from fallopian tube in a mouse model. *Proc. Natl. Acad. Sci.* **109,** 3921–3926 (2012).

35. Perets, R., Wyant, G., Muto, K., Bijron, J., Poole, B., Chin, K., Chen, J., Ohman, A., Stepule, C., Kwak, S., Karst, A., Hirsch, M., Setlur, S., Crum, C., Dinulescu, D. & Drapkin, R. Transformation of the Fallopian Tube Secretory Epithelium Leads to High-Grade Serous Ovarian Cancer in Brca;Tp53;Pten Models. *Cancer Cell* **24,** 751–765 (2013).

36. Ahmed, A. A., Etemadmoghadam, D., Temple, J., Lynch, A. G., Riad, M., Sharma, R., Stewart, C., Fereday, S., Caldas, C., Defazio, A., Bowtell, D. & Brenton, J. D. Driver mutations in TP53 are ubiquitous in high grade serous carcinoma of the ovary. *J. Pathol.* **221,** 49–56 (2010).

37. Bell, D., Berchuck, A., Birrer, M., Chien, J., Cramer, D. W., Dao, F., Dhir, R., DiSaia, P., Gabra, H., Glenn, P., Godwin, A. K., Gross, J., Hartmann, L., Huang, M., Huntsman, D. G., Iacocca, M., Imielinski, M., Kalloger, S., Karlan, B. Y., Levine, D. A., Mills, G. B., Morrison, C., Mutch, D., Olvera, N., Orsulic, S., Park, K., Petrelli, N., Rabeno, B., Rader, J. S., Sikic, B. I., Smith-McCune, K., Sood, A. K., Bowtell, D., Penny, R., Testa, J. R., Chang, K., Dinh, H. H., Drummond, J. A., Fowler, G., Gunaratne, P., Hawes, A. C., Kovar, C. L., Lewis, L. R., Morgan, M. B., Newsham, I. F., Santibanez, J., Reid, J. G., Trevino, L. R., Wu, Y.-Q., Wang, M., Muzny, D. M., Wheeler, D. A., Gibbs, R. A., Getz, G., Lawrence, M. S., Cibulskis, K., Sivachenko, A. Y., Sougnez, C., Voet, D., Wilkinson, J., Bloom, T., Ardlie, K., Fennell, T., Baldwin, J., Gabriel, S., Lander, E. S., Ding, L., Fulton, R. S., Koboldt, D. C., McLellan, M. D., Wylie, T., Walker, J., O'Laughlin, M., Dooling, D. J., Fulton, L., Abbott, R., Dees, N. D., Zhang, Q., Kandoth, C., Wendl, M., Schierding, W., Shen, D., Harris, C. C., Schmidt, H., Kalicki, J., Delehaunty, K. D., Fronick, C. C., Demeter, R., Cook, L., Wallis, J. W., Lin, L., Magrini, V. J., Hodges, J. S., Eldred, J. M., Smith, S. M., Pohl, C. S., Vandin, F., Raphael, B. J., Weinstock, G. M., Mardis, E. R., Wilson, R. K., Meyerson, M., Winckler, W., Getz, G., Verhaak, R. G. W., Carter, S. L., Mermel, C. H., Saksena, G., Nguyen, H., Onofrio, R. C., Lawrence, M. S., Hubbard, D., Gupta, S., Crenshaw, A., Ramos, A. H., Ardlie, K., Chin, L., Protopopov, A., Zhang, J. J. J., Kim, T. M., Perna, I., Xiao, Y., Zhang, H., Ren, G., Sathiamoorthy, N., Park, R. W., Lee, E., Park, P. J., Kucherlapati, R., Absher, D. M., Waite, L., Sherlock, G., Brooks, J. D., Li, J. Z., Xu, J., Myers, R. M., Laird, P. W., Cope, L., Herman, J. G., Shen, H., Weisenberger, D. J., Noushmehr, H., Pan, F., Triche Jr, T., Berman, B. P., Van Den Berg, D. J., Buckley, J., Baylin, S. B., Spellman, P. T., Purdom, E., Neuvial, P., Bengtsson, H., Jakkula, L. R., Durinck, S., Han, J., Dorton, S., Marr, H., Choi, Y. G., Wang, V., Wang, N. J., Ngai, J., Conboy, J. G., Parvin, B., Feiler, H. S., Speed, T. P., Gray, J. W., Levine, D. A., Socci, N. D., Liang, Y., Taylor, B. S., Schultz, N., Borsu, L., Lash, A. E., Brennan, C., Viale, A., Sander, C., Ladanyi, M., Hoadley, K. A., Meng, S., Du, Y., Shi, Y., Li, L., Turman, Y. J., Zang, D., Helms, E. B., Balu, S., Zhou, X., Wu, J., Topal, M. D., Hayes, D. N., Perou, C. M., Getz, G., Voet, D., Saksena, G., Zhang, J. J. J., Zhang, H., Wu, C. J., Shukla, S., Cibulskis, K., Lawrence, M. S., Sivachenko, A. Y., Jing, R., Park, R. W., Liu, Y., Park, P. J., Noble, M., Chin, L., Carter, H., Kim, D., Karchin, R., Spellman, P. T., Purdom, E., Neuvial, P., Bengtsson, H., Durinck, S., Han, J., Korkola, J. E., Heiser, L. M., Cho, R. J., Hu, Z., Parvin, B., Speed, T. P., Gray, J. W., Schultz, N., Cerami, E., Taylor, B. S., Olshen, A., Reva, B., Antipin, Y., Shen, R., Mankoo, P., Sheridan, R., Ciriello, G., Chang, W. K., Bernanke, J. A., Borsu, L., Levine, D. A., Ladanyi, M., Sander, C., Haussler, D., Benz, C. C., Stuart, J. M., Benz, S. C., Sanborn, J. Z., Vaske, C. J., Zhu, J., Szeto, C., Scott, G. K., Yau, C., Hoadley, K. A., Du, Y., Balu, S., Hayes, D. N., Perou, C. M., Wilkerson, M. D., Zhang, N., Akbani, R., Baggerly, K. A., Yung, W. K., Mills, G. B., Weinstein, J. N., Penny, R., Shelton, T., Grimm, D., Hatfield, M., Morris, S., Yena, P., Rhodes, P., Sherman, M., Paulauskis, J., Millis, S., Kahn, A., Greene, J. M., Sfeir, R., Jensen, M. A., Chen, J., Whitmore, J., Alonso, S., Jordan, J., Chu, A., Zhang, J. J. J., Barker, A., Compton, C., Eley, G., Ferguson, M., Fielding, P., Gerhard, D. S., Myles, R., Schaefer, C., Mills

Shaw, K. R., Vaught, J., Vockley, J. B., Good, P. J., Guyer, M. S., Ozenberger, B., Peterson, J. & Thomson, E. Integrated genomic analyses of ovarian carcinoma. *Nature* **474,** 609–615 (2011).

38. Bowtell, D. D. L. The genesis and evolution of high-grade serous ovarian cancer. *Nat. Rev. Cancer* **10,** 803–808 (2010).

39. Bowtell, D. D., Böhm, S., Ahmed, A. A., Aspuria, P.-J., Bast, R. C., Beral, V., Berek, J. S., Birrer, M. J., Blagden, S., Bookman, M. A., Brenton, J. D., Chiappinelli, K. B., Martins, F. C., Coukos, G., Drapkin, R., Edmondson, R., Fotopoulou, C., Gabra, H., Galon, J., Gourley, C., Heong, V., Huntsman, D. G., Iwanicki, M., Karlan, B. Y., Kaye, A., Lengyel, E., Levine, D. A., Lu, K. H., McNeish, I. A., Menon, U., Narod, S. A., Nelson, B. H., Nephew, K. P., Pharoah, P., Powell, D. J., Ramos, P., Romero, I. L., Scott, C. L., Sood, A. K., Stronach, E. A. & Balkwill, F. R. Rethinking ovarian cancer II: reducing mortality from high-grade serous ovarian cancer. *Nat. Rev. Cancer* **15,** 668–679 (2015).

40. Siddik, Z. H. Cisplatin: mode of cytotoxic action and molecular basis of resistance. *Oncogene* **22,** 7265–79 (2003).

41. Hennessy, B. T. J., Hennessy, B. T., Coleman, R. L., Coleman, R. L., Markman, M. & Markman, M. Ovarian cancer. *Lancet* **374,** 1371–82 (2009).

42. Yap, T. A., Carden, C. P. & Kaye, S. B. Beyond chemotherapy: targeted therapies in ovarian cancer. *Nat. Rev. Cancer* **9,** 167–181 (2009).

43. Mayor, T., Stierhof, Y. D., Tanaka, K., Fry, A. M. & Nigg, E. A. The centrosomal protein C-Nap1 is required for cell cycle-regulated centrosome cohesion. *J. Cell Biol.* **151,** 837–846 (2000).

44. Vivanco, I. & Sawyers, C. L. The phosphatidylinositol 3-Kinase–AKT pathway in human cancer. *Nat. Rev. Cancer* **2,** 489–501 (2002).

45. Nagel, S., Leich, E., Quentmeier, H., Meyer, C., Kaufmann, M., Zaborski, M., Rosenwald, A., Drexler, H. G. & Macleod, R. A. F. Amplification at 11q23 targets protein kinase SIK2 in diffuse large B-cell lymphoma. *Leuk. Lymphoma* **51,** 881–91 (2010).

46. Yang, F.-C., Lin, Y.-H., Chen, W.-H., Huang, J.-Y., Chang, H.-Y., Su, S.-H., Wang, H.-T., Chiang, C.-Y., Hsu, P.-H., Tsai, M.-D., Tan, B. C.-M. & Lee, S.-C. Interaction between salt-inducible kinase 2 (SIK2) and p97/valosin-containing protein (VCP) regulates endoplasmic reticulum (ER)-associated protein degradation in mammalian cells. *J. Biol. Chem.* **288,** 33861–72 (2013).

47. Yang, F.-C., Tan, B. C.-M., Chen, W.-H., Lin, Y.-H., Huang, J.-Y., Chang, H.-Y., Sun, H.-Y., Hsu, P.-H., Liou, G.-G., Shen, J., Chang, C.-J., Han, C.-C., Tsai, M.-D. & Lee, S.-C. Reversible Acetylation Regulates Salt-inducible Kinase (SIK2) and Its Function in Autophagy. *J. Biol. Chem.* **288,** 6227–6237 (2013).

48. Mathew, R., Karantza-Wadsworth, V. & White, E. Role of autophagy in cancer. *Nat. Rev. Cancer* **7,** 961–7 (2007).

49. Wehr, M. C., Holder, M. V., Gailite, I., Saunders, R. E., Maile, T. M., Ciirdaeva, E.,

Instrell, R., Jiang, M., Howell, M., Rossner, M. J. & Tapon, N. Salt-inducible kinases regulate growth through the Hippo signalling pathway in Drosophila. *Nat. Cell Biol.* **15,** 61–71 (2013).

50. Hall, C. A., Wang, R., Miao, J., Oliva, E., Shen, X., Wheeler, T., Hilsenbeck, S. G., Orsulic, S. & Goode, S. Hippo pathway effector Yap is an ovarian cancer oncogene. *Cancer Res.* **70,** 8517–8525 (2010).

51. Screaton, R. A., Conkright, M. D., Katoh, Y., Best, J. L., Canettieri, G., Jeffries, S., Guzman, E., Niessen, S., Yates, J. R., Takemori, H., Okamoto, M., Montminy, M., Iii, J. R. Y., Takemori, H., Okamoto, M., Montminy, M. & Jolla, L. The CREB coactivator TORC2 functions as a calcium- and cAMP-sensitive coincidence detector. *Cell* **119,** 61–74 (2004).

52. Dentin, R., Liu, Y., Koo, S.-H., Hedrick, S., Vargas, T., Heredia, J., Yates, J. & Montminy, M. Insulin modulates gluconeogenesis by inhibition of the coactivator TORC2. *Nature* **449,** 366–369 (2007).

53. Altarejos, J. Y. & Montminy, M. CREB and the CRTC co-activators: sensors for hormonal and metabolic signals. *Nat. Rev. Mol. Cell Biol.* **12,** 141–151 (2011).

54. Henriksson, E., Jones, H. A., Patel, K., Peggie, M., Morrice, N., Sakamoto, K. & Göransson, O. The AMPK-related kinase SIK2 is regulated by cAMP via phosphorylation at Ser ^{358} in adipocytes. *Biochem. J.* **444,** 503–514 (2012).

55. Lizcano, J. M., Göransson, O., Toth, R., Deak, M., Morrice, N. a, Boudeau, J., Hawley, S. a, Udd, L., Mäkelä, T. P., Hardie, D. G. & Alessi, D. R. LKB1 is a master kinase that activates 13 kinases of the AMPK subfamily, including MARK/PAR-1. *EMBO J.* **23,** 833–843 (2004).

56. Patel, K., Foretz, M., Marion, A., Campbell, D. G., Gourlay, R., Boudaba, N., Tournier, E., Titchenell, P., Peggie, M., Deak, M., Wan, M., Kaestner, K. H., Göransson, O., Viollet, B., Gray, N. S., Birnbaum, M. J., Sutherland, C. & Sakamoto, K. The LKB1-salt-inducible kinase pathway functions as a key gluconeogenic suppressor in the liver. *Nat. Commun.* **5,** 4535 (2014).

57. Park, J., Yoon, Y.-S., Han, H.-S., Kim, Y.-H., Ogawa, Y., Park, K.-G., Lee, C.-H., Kim, S.-T. & Koo, S.-H. SIK2 is critical in the regulation of lipid homeostasis and adipogenesis in vivo. *Diabetes* **63,** 3659–73 (2014).

58. Du, J., Chen, Q., Takemori, H. & Xu, H. SIK2 can be activated by deprivation of nutrition and it inhibits expression of lipogenic genes in adipocytes. *Obesity (Silver Spring).* **16,** 531–538 (2008).

59. Horike, N., Kumagai, A., Shimono, Y., Onishi, T., Itoh, Y., Sasaki, T., Kitagawa, K., Hatano, O., Takagi, H., Susumu, T., Teraoka, H., Kusano, K. I., Nagaoka, Y., Kawahara, H. & Takemori, H. Downregulation of SIK2 expression promotes the melanogenic program in mice. *Pigment Cell Melanoma Res.* **23,** 809–819 (2010).

60. Kumagai, A., Horike, N., Satoh, Y., Uebi, T., Sasaki, T., Itoh, Y., Hirata, Y., Uchio-Yamada, K., Kitagawa, K., Uesato, S., Kawahara, H., Takemori, H. & Nagaoka, Y. A

potent inhibitor of SIK2, 3, 3', 7-trihydroxy-4'-methoxyflavon (4'-O-methylfisetin), promotes melanogenesis in B16F10 melanoma cells. *PLoS One* **6,** e26148 (2011).

61. Ozanne, J., Prescott, A. R. & Clark, K. The clinically approved drugs dasatinib and bosutinib induce anti-inflammatory macrophages by inhibiting the salt-inducible kinases. *Biochem. J.* **465,** 271–279 (2015).

62. Walkinshaw, D. R., Weist, R., Kim, G. W., You, L., Xiao, L., Nie, J., Li, C. S., Zhao, S., Xu, M. & Yang, X. J. The tumor suppressor kinase LKB1 activates the downstream kinases SIK2 and SIK3 to stimulate nuclear export of class IIa histone deacetylases. *J. Biol. Chem.* **288,** 9345–9362 (2013).

63. Weems, J. C., Griesel, B. A. & Olson, A. L. Class II Histone Deacetylases Downregulate GLUT4 Transcription in Response to Increased cAMP Signaling in Cultured Adipocytes and Fasting Mice. *Diabetes* **61,** 1404–1414 (2012).

64. Henriksson, E., Sall, J., Gormand, A., Wasserstrom, S., Morrice, N. A., Fritzen, A. M., Foretz, M., Campbell, D. G., Sakamoto, K., Ekelund, M., Degerman, E., Stenkula, K. G. & Goransson, O. SIK2 regulates CRTCs, HDAC4 and glucose uptake in adipocytes. *J. Cell Sci.* **128,** 472–486 (2014).

65. Hunter, T. A thousand and one protein kinases. *Cell* **50,** 823–829 (1987).

66. Hunter, T. Protein kinases and phosphatases: the yin and yang of protein phosphorylation and signaling. *Cell* **80,** 225–236 (1995).

67. Lander, E. S., Linton, L. M., Birren, B., Nusbaum, C., Zody, M. C., Baldwin, J., Devon, K., Dewar, K., Doyle, M., FitzHugh, W., Funke, R., Gage, D., Harris, K., Heaford, A., Howland, J., Kann, L., Lehoczky, J., LeVine, R., McEwan, P., McKernan, K., Meldrim, J., Mesirov, J. P., Miranda, C., Morris, W., Naylor, J., Raymond, C., Rosetti, M., Santos, R., Sheridan, A., Sougnez, C., Stange-Thomann, N., Stojanovic, N., Subramanian, A., Wyman, D., Rogers, J., Sulston, J., Ainscough, R., Beck, S., Bentley, D., Burton, J., Clee, C., Carter, N., Coulson, A., Deadman, R., Deloukas, P., Dunham, A., Dunham, I., Durbin, R., French, L., Grafham, D., Gregory, S., Hubbard, T., Humphray, S., Hunt, A., Jones, M., Lloyd, C., McMurray, A., Matthews, L., Mercer, S., Milne, S., Mullikin, J. C., Mungall, A., Plumb, R., Ross, M., Shownkeen, R., Sims, S., Waterston, R. H., Wilson, R. K., Hillier, L. W., McPherson, J. D., Marra, M. A., Mardis, E. R., Fulton, L. A., Chinwalla, A. T., Pepin, K. H., Gish, W. R., Chissoe, S. L., Wendl, M. C., Delehaunty, K. D., Miner, T. L., Delehaunty, A., Kramer, J. B., Cook, L. L., Fulton, R. S., Johnson, D. L., Minx, P. J., Clifton, S. W., Hawkins, T., Branscomb, E., Predki, P., Richardson, P., Wenning, S., Slezak, T., Doggett, N., Cheng, J. F., Olsen, A., Lucas, S., Elkin, C., Uberbacher, E., Frazier, M., Gibbs, R. A., Muzny, D. M., Scherer, S. E., Bouck, J. B., Sodergren, E. J., Worley, K. C., Rives, C. M., Gorrell, J. H., Metzker, M. L., Naylor, S. L., Kucherlapati, R. S., Nelson, D. L., Weinstock, G. M., Sakaki, Y., Fujiyama, A., Hattori, M., Yada, T., Toyoda, A., Itoh, T., Kawagoe, C., Watanabe, H., Totoki, Y., Taylor, T., Weissenbach, J., Heilig, R., Saurin, W., Artiguenave, F., Brottier, P., Bruls, T., Pelletier, E., Robert, C., Wincker, P., Smith, D. R., Doucette-Stamm, L., Rubenfield, M., Weinstock, K., Lee, H. M., Dubois, J., Rosenthal, A., Platzer, M., Nyakatura, G., Taudien, S., Rump, A., Yang, H., Yu, J., Wang, J., Huang, G., Gu, J., Hood, L., Rowen, L.,

Madan, A., Qin, S., Davis, R. W., Federspiel, N. A., Abola, A. P., Proctor, M. J., Myers, R. M., Schmutz, J., Dickson, M., Grimwood, J., Cox, D. R., Olson, M. V, Kaul, R., Shimizu, N., Kawasaki, K., Minoshima, S., Evans, G. A., Athanasiou, M., Schultz, R., Roe, B. A., Chen, F., Pan, H., Ramser, J., Lehrach, H., Reinhardt, R., McCombie, W. R., de la Bastide, M., Dedhia, N., Blöcker, H., Hornischer, K., Nordsiek, G., Agarwala, R., Aravind, L., Bailey, J. A., Bateman, A., Batzoglou, S., Birney, E., Bork, P., Brown, D. G., Burge, C. B., Cerutti, L., Chen, H. C., Church, D., Clamp, M., Copley, R. R., Doerks, T., Eddy, S. R., Eichler, E. E., Furey, T. S., Galagan, J., Gilbert, J. G., Harmon, C., Hayashizaki, Y., Haussler, D., Hermjakob, H., Hokamp, K., Jang, W., Johnson, L. S., Jones, T. A., Kasif, S., Kaspryzk, A., Kennedy, S., Kent, W. J., Kitts, P., Koonin, E. V, Korf, I., Kulp, D., Lancet, D., Lowe, T. M., McLysaght, A., Mikkelsen, T., Moran, J. V, Mulder, N., Pollara, V. J., Ponting, C. P., Schuler, G., Schultz, J., Slater, G., Smit, A. F., Stupka, E., Szustakowski, J., Thierry-Mieg, D., Thierry-Mieg, J., Wagner, L., Wallis, J., Wheeler, R., Williams, A., Wolf, Y. I., Wolfe, K. H., Yang, S. P., Yeh, R. F., Collins, F., Guyer, M. S., Peterson, J., Felsenfeld, A., Wetterstrand, K. A., Patrinos, A., Morgan, M. J., de Jong, P., Catanese, J. J., Osoegawa, K., Shizuya, H., Choi, S., Chen, Y. J. & Szustakowki, J. Initial sequencing and analysis of the human genome. *Nature* **409,** 860–921 (2001).

68. Venter, J. C., Adams, M. D., Myers, E. W., Li, P. W., Mural, R. J., Sutton, G. G., Smith, H. O., Yandell, M., Evans, C. A., Holt, R. A., Gocayne, J. D., Amanatides, P., Ballew, R. M., Huson, D. H., Wortman, J. R., Zhang, Q., Kodira, C. D., Zheng, X. H., Chen, L., Skupski, M., Subramanian, G. M., Thomas, P. D., Zhang, J., Gabor Miklos, G. L., Nelson, C., Broder, S., Clark, A. G., Nadeau, J., McKusick, V. A., Zinder, N., Levine, A. J., Roberts, R. J., Simon, M., Slayman, C., Hunkapiller, M., Bolanos, R., Delcher, A., Dew, I., Fasulo, D., Flanigan, M., Florea, L., Halpern, A., Hannenhalli, S., Kravitz, S., Levy, S., Mobarry, C., Reinert, K., Remington, K., Abu-Threideh, J., Beasley, E., Biddick, K., Bonazzi, V., Brandon, R., Cargill, M., Chandramouliswaran, I., Charlab, R., Chaturvedi, K., Deng, Z., Di Francesco, V., Dunn, P., Eilbeck, K., Evangelista, C., Gabrielian, A. E., Gan, W., Ge, W., Gong, F., Gu, Z., Guan, P., Heiman, T. J., Higgins, M. E., Ji, R. R., Ke, Z., Ketchum, K. A., Lai, Z., Lei, Y., Li, Z., Li, J., Liang, Y., Lin, X., Lu, F., Merkulov, G. V, Milshina, N., Moore, H. M., Naik, A. K., Narayan, V. A., Neelam, B., Nusskern, D., Rusch, D. B., Salzberg, S., Shao, W., Shue, B., Sun, J., Wang, Z., Wang, A., Wang, X., Wang, J., Wei, M., Wides, R., Xiao, C., Yan, C., Yao, A., Ye, J., Zhan, M., Zhang, W., Zhang, H., Zhao, Q., Zheng, L., Zhong, F., Zhong, W., Zhu, S., Zhao, S., Gilbert, D., Baumhueter, S., Spier, G., Carter, C., Cravchik, A., Woodage, T., Ali, F., An, H., Awe, A., Baldwin, D., Baden, H., Barnstead, M., Barrow, I., Beeson, K., Busam, D., Carver, A., Center, A., Cheng, M. L., Curry, L., Danaher, S., Davenport, L., Desilets, R., Dietz, S., Dodson, K., Doup, L., Ferriera, S., Garg, N., Gluecksmann, A., Hart, B., Haynes, J., Haynes, C., Heiner, C., Hladun, S., Hostin, D., Houck, J., Howland, T., Ibegwam, C., Johnson, J., Kalush, F., Kline, L., Koduru, S., Love, A., Mann, F., May, D., McCawley, S., McIntosh, T., McMullen, I., Moy, M., Moy, L., Murphy, B., Nelson, K., Pfannkoch, C., Pratts, E., Puri, V., Qureshi, H., Reardon, M., Rodriguez, R., Rogers, Y. H., Romblad, D., Ruhfel, B., Scott, R., Sitter, C., Smallwood, M., Stewart, E., Strong, R., Suh, E., Thomas, R., Tint, N. N., Tse, S., Vech, C., Wang, G., Wetter, J., Williams, S., Williams, M., Windsor, S., Winn-Deen, E., Wolfe, K. H., Zaveri, J., Zaveri, K., Abril, J. F., Guigó, R., Campbell, M. J., Sjolander, K. V, Karlak, B., Kejariwal, A., Mi, H., Lazareva, B., Hatton, T., Narechania, A., Diemer, K., Muruganujan, A., Guo, N., Sato, S., Bafna, V., Istrail, S., Lippert, R.,

Schwartz, R., Walenz, B., Yooseph, S., Allen, D., Basu, A., Baxendale, J., Blick, L., Caminha, M., Carnes-Stine, J., Caulk, P., Chiang, Y. H., Coyne, M., Dahlke, C., Mays, A., Dombroski, M., Donnelly, M., Ely, D., Esparham, S., Fosler, C., Gire, H., Glanowski, S., Glasser, K., Glodek, A., Gorokhov, M., Graham, K., Gropman, B., Harris, M., Heil, J., Henderson, S., Hoover, J., Jennings, D., Jordan, C., Jordan, J., Kasha, J., Kagan, L., Kraft, C., Levitsky, A., Lewis, M., Liu, X., Lopez, J., Ma, D., Majoros, W., McDaniel, J., Murphy, S., Newman, M., Nguyen, T., Nguyen, N., Nodell, M., Pan, S., Peck, J., Peterson, M., Rowe, W., Sanders, R., Scott, J., Simpson, M., Smith, T., Sprague, A., Stockwell, T., Turner, R., Venter, E., Wang, M., Wen, M., Wu, D., Wu, M., Xia, A., Zandieh, A. & Zhu, X. The sequence of the human genome. *Science (80-.).* **291,** 1304–51 (2001).

69. Manning, G., Whyte, D. B., Martinez, R., Hunter, T. & Sudarsanam, S. The protein kinase complement of the human genome. *Science* **298,** 1912–1934 (2002).

70. Zhang, J., Yang, P. L. & Gray, N. S. Targeting cancer with small molecule kinase inhibitors. *Nat. Rev. Cancer* **9,** 28–39 (2009).

71. Lindberg, R. A., Quinn, A. M. & Hunter, T. Dual-specificity protein kinases: will any hydroxyl do? *Trends Biochem. Sci.* **17,** 114–119 (1992).

72. Kornev, A. P., Haste, N. M., Taylor, S. S. & Eyck, L. F. Ten. Surface comparison of active and inactive protein kinases identifies a conserved activation mechanism. *Proc. Natl. Acad. Sci. U. S. A.* **103,** 17783–17788 (2006).

73. Ubersax, J. A. & Ferrell, J. E. Mechanisms of specificity in protein phosphorylation. *Nat. Rev. Mol. Cell Biol.* **8,** 530–41 (2007).

74. Adams, J. A. Kinetic and catalytic mechanisms of protein kinases. *Chem. Rev.* **101,** 2271–2290 (2001).

75. Johnson, L. N. & Barford, D. The effects of phosphorylation on the structure and function of proteins. *Annu. Rev. Biophys. Biomol. Struct.* **22,** 199–232 (1993).

76. Futreal, P. A., Coin, L., Marshall, M., Down, T., Hubbard, T., Wooster, R., Rahman, N. & Stratton, M. R. A census of human cancer genes. *Nat. Rev. Cancer* **4,** 177–183 (2004).

77. Greenman, C., Stephens, P., Smith, R., Dalgliesh, G. L., Hunter, C., Bignell, G., Davies, H., Teague, J., Butler, A., Stevens, C., Edkins, S., O'Meara, S., Vastrik, I., Schmidt, E. E., Avis, T., Barthorpe, S., Bhamra, G., Buck, G., Choudhury, B., Clements, J., Cole, J., Dicks, E., Forbes, S., Gray, K., Halliday, K., Harrison, R., Hills, K., Hinton, J., Jenkinson, A., Jones, D., Menzies, A., Mironenko, T., Perry, J., Raine, K., Richardson, D., Shepherd, R., Small, A., Tofts, C., Varian, J., Webb, T., West, S., Widaa, S., Yates, A., Cahill, D. P., Louis, D. N., Goldstraw, P., Nicholson, A. G., Brasseur, F., Looijenga, L., Weber, B. L., Chiew, Y.-E., DeFazio, A., Greaves, M. F., Green, A. R., Campbell, P., Birney, E., Easton, D. F., Chenevix-Trench, G., Tan, M.-H., Khoo, S. K., Teh, B. T., Yuen, S. T., Leung, S. Y., Wooster, R., Futreal, P. A. & Stratton, M. R. Patterns of somatic mutation in human cancer genomes. *Nature* **446,** 153–8 (2007).

78. Davies, H., Bignell, G. R., Cox, C., Stephens, P., Edkins, S., Clegg, S., Teague, J.,

Woffendin, H., Garnett, M. J., Bottomley, W., Davis, N., Dicks, E., Ewing, R., Floyd, Y., Gray, K., Hall, S., Hawes, R., Hughes, J., Kosmidou, V., Menzies, A., Mould, C., Parker, A., Stevens, C., Watt, S., Hooper, S., Wilson, R., Jayatilake, H., Gusterson, B. a, Cooper, C., Shipley, J., Hargrave, D., Pritchard-Jones, K., Maitland, N., Chenevix-Trench, G., Riggins, G. J., Bigner, D. D., Palmieri, G., Cossu, A., Flanagan, A., Nicholson, A., Ho, J. W. C., Leung, S. Y., Yuen, S. T., Weber, B. L., Seigler, H. F., Darrow, T. L., Paterson, H., Marais, R., Marshall, C. J., Wooster, R., Stratton, M. R. & Futreal, P. A. Mutations of the BRAF gene in human cancer. *Nature* **417,** 949–954 (2002).

79. Shiloh, Y. ATM and related protein kinases: safeguarding genome integrity. *Nat. Rev. Cancer* **3,** 155–168 (2003).

80. Müller, S., Chaikuad, A., Gray, N. S. & Knapp, S. The ins and outs of selective kinase inhibitor development. *Nat. Chem. Biol.* **11,** 818–821 (2015).

81. Fedorov, O., Müller, S. & Knapp, S. The (un)targeted cancer kinome. *Nat. Chem. Biol.* **6,** 166–169 (2010).

82. Capdeville, R., Buchdunger, E., Zimmermann, J. & Matter, A. Glivec (STI571, imatinib), a rationally developed, targeted anticancer drug. *Nat. Rev. Drug Discov.* **1,** 493–502 (2002).

83. Gathmann, I., Sc, M., Kantarjian, H., Gattermann, N., Goldman, J. M., Stone, R. M., Cervantes, F., Hochhaus, A., Powell, B. L., Gabrilove, J. L., Rousselot, P., Reiffers, J., Cornelissen, J. J., Ph, D., Hughes, T., Agis, H., Fischer, T., Verhoef, G., Shepherd, J., Saglio, G., Gratwohl, A., Nielsen, J. L., Radich, J. P., Simonsson, B., Taylor, K., Baccarani, M., So, C., Pharm, D., Letvak, L., Larson, R. A. & Investigators, I. Five-Year Follow-up of Patients Receiving Imatinib for Chronic Myeloid Leukemia. (2014).

84. Zhang, J., Yang, P. L. & Gray, N. S. Targeting cancer with small molecule kinase inhibitors. *Nat. Rev. Cancer* **9,** 28–39 (2009).

85. Johnson, S. A. & Hunter, T. Kinomics: methods for deciphering the kinome. *Nat. Methods* **2,** 17–25 (2005).

86. Gruhler, A., Olsen, J. V, Mohammed, S., Mortensen, P., Faergeman, N. J., Mann, M. & Jensen, O. N. Quantitative phosphoproteomics applied to the yeast pheromone signaling pathway. *Mol. Cell. Proteomics* **4,** 310–27 (2005).

87. Olsen, J. V., Blagoev, B., Gnad, F., Macek, B., Kumar, C., Mortensen, P. & Mann, M. Global, In Vivo, and Site-Specific Phosphorylation Dynamics in Signaling Networks. *Cell* **127,** 635–648 (2006).

88. Oda, Y., Huang, K., Cross, F. R., Cowburn, D. & Chait, B. T. Accurate quantitation of protein expression and site-specific phosphorylation. *Proc. Natl. Acad. Sci. U. S. A.* **96,** 6591–6596 (1999).

89. Zappacosta, F., Scott, G. F., Huddleston, M. J. & Annan, R. S. An Optimized Platform for Hydrophilic Interaction Chromatography–Immobilized Metal Affinity Chromatography Enables Deep Coverage of the Rat Liver Phosphoproteome. *J. Proteome Res.* **14,** 997–1009 (2015).

90. Krüger, M., Kratchmarova, I., Blagoev, B., Tseng, Y.-H., Kahn, C. R. & Mann, M. Dissection of the insulin signaling pathway via quantitative phosphoproteomics. *Proc. Natl. Acad. Sci. U. S. A.* **105,** 2451–2456 (2008).

91. Wilson-Grady, J. T., Haas, W. & Gygi, S. P. Quantitative comparison of the fasted and re-fed mouse liver phosphoproteomes using lower pH reductive dimethylation. *Methods* **61,** 277–286 (2013).

92. Dephoure, N., Zhou, C., Villén, J., Beausoleil, S. A., Bakalarski, C. E., Elledge, S. J. & Gygi, S. P. A quantitative atlas of mitotic phosphorylation. *Proc. Natl. Acad. Sci. U. S. A.* **105,** 10762–10767 (2008).

93. Olsen, J. V, Vermeulen, M., Santamaria, A., Kumar, C., Miller, M. L., Jensen, L. J., Gnad, F., Cox, J., Jensen, T. S., Nigg, E. A., Brunak, S. & Mann, M. Quantitative phosphoproteomics reveals widespread full phosphorylation site occupancy during mitosis. *Sci. Signal.* **3,** ra3 (2010).

94. Allen, J. J., Lazerwith, S. E. & Shokat, K. M. Bio-orthogonal affinity purification of direct kinase substrates. *J. Am. Chem. Soc.* **127,** 5288–5289 (2005).

95. Hornbeck, P. V., Zhang, B., Murray, B., Kornhauser, J. M., Latham, V. & Skrzypek, E. PhosphoSitePlus, 2014: mutations, PTMs and recalibrations. *Nucleic Acids Res.* **43,** D512–20 (2015).

96. Shah, K., Liu, Y., Deirmengian, C. & Shokat, K. M. Engineering unnatural nucleotide specificity for Rous sarcoma virus tyrosine kinase to uniquely label its direct substrates. *Proc. Natl. Acad. Sci. U. S. A.* **94,** 3565–70 (1997).

97. Liu, Y., Shah, K., Yang, F., Witucki, L. & Shokat, K. M. Engineering Src family protein kinases with unnatural nucleotide specificity. *Chem. Biol.* **5,** 91–101 (1998).

98. Ubersax, J. A., Woodbury, E. L., Quang, P. N., Paraz, M., Blethrow, J. D., Shah, K., Shokat, K. M. & Morgan, D. O. Targets of the cyclin-dependent kinase Cdk1. *Nature* **425,** 859–864 (2003).

99. Eblen, S. T., Kumar, N. V., Shah, K., Henderson, M. J., Watts, C. K. W., Shokat, K. M. & Weber, M. J. Identification of novel ERK2 substrates through use of an engineered kinase and ATP analogs. *J. Biol. Chem.* **278,** 14926–14935 (2003).

100. Zhang, C., Kenski, D. M., Paulson, J. L., Bonshtien, A., Sessa, G., Cross, J. V, Templeton, D. J. & Shokat, K. M. A second-site suppressor strategy for chemical genetic analysis of diverse protein kinases. *Nat. Methods* **2,** 435–441 (2005).

101. Witucki, L. A., Huang, X., Shah, K., Liu, Y., Kyin, S., Eck, M. J. & Shokat, K. M. Mutant tyrosine kinases with unnatural nucleotide specificity retain the structure and phospho-acceptor specificity of the wild-type enzyme. *Chem. Biol.* **9,** 25–33 (2002).

102. Azam, M., Seeliger, M. a, Gray, N. S., Kuriyan, J. & Daley, G. Q. Activation of tyrosine kinases by mutation of the gatekeeper threonine. *Nat. Struct. Mol. Biol.* **15,** 1109–1118 (2008).

103. Suwal, S., Senevirathne, C., Garre, S. & Pflum, M. K. H. Structural analysis of ATP

analogues compatible with kinase-catalyzed labeling. *Bioconjug. Chem.* **23,** 2386–2391 (2012).

104. Allen, J. J., Li, M., Brinkworth, C. S., Paulson, J. L., Wang, D., Hübner, A., Chou, W.-H., Davis, R. J., Burlingame, A. L., Messing, R. O., Katayama, C. D., Hedrick, S. M. & Shokat, K. M. A semisynthetic epitope for kinase substrates. *Nat. Methods* **4,** 511–516 (2007).

105. Banko, M. R., Allen, J. J., Schaffer, B. E., Wilker, E. W., Tsou, P., White, J. L., Villén, J., Wang, B., Kim, S. R., Sakamoto, K., Gygi, S. P., Cantley, L. C., Yaffe, M. B., Shokat, K. M. & Brunet, A. Chemical Genetic Screen for AMPKα2 Substrates Uncovers a Network of Proteins Involved in Mitosis. *Mol. Cell* **44,** 878–892 (2011).

106. Schutz-geschwender, A., Zhang, Y., Holt, T., Mcdermitt, D., Olive, D. M. & Biosciences, L. *Quantitative , Two-Color Western Blot Detection With Infrared Fluorescence*. *LI-COR Biosci.* (2004). at <http://cdn.licor.com/bio/PDF/IRquant.pdf>

107. Yang, X., Boehm, J. S., Yang, X., Salehi-Ashtiani, K., Hao, T., Shen, Y., Lubonja, R., Thomas, S. R., Alkan, O., Bhimdi, T., Green, T. M., Johannessen, C. M., Silver, S. J., Nguyen, C., Murray, R. R., Hieronymus, H., Balcha, D., Fan, C., Lin, C., Ghamsari, L., Vidal, M., Hahn, W. C., Hill, D. E. & Root, D. E. A public genome-scale lentiviral expression library of human ORFs. *Nat. Methods* **8,** 659–661 (2011).

108. Fischer, R. & Kessler, B. M. Gel-aided sample preparation (GASP)-A simplified method for gel-assisted proteomic sample generation from protein extracts and intact cells. *Proteomics* **15,** 1224–1229 (2015).

109. Thomas, P. D., Kejariwal, A., Guo, N., Mi, H., Campbell, M. J., Muruganujan, A. & Lazareva-Ulitsky, B. Applications for protein sequence–function evolution data: mRNA/protein expression analysis and coding SNP scoring tools. *Nucleic Acids Res.* **34 ,** W645–W650 (2006).

110. Mi, H., Muruganujan, A. & Thomas, P. D. PANTHER in 2013: Modeling the evolution of gene function, and other gene attributes, in the context of phylogenetic trees. *Nucleic Acids Res.* **41,** (2013).

111. Mi, H., Muruganujan, A., Casagrande, J. T. & Thomas, P. D. Large-scale gene function analysis with the PANTHER classification system. *Nat. Protoc.* **8,** 1551–66 (2013).

112. Papadopoulos, J. S. & Agarwala, R. COBALT: Constraint-based alignment tool for multiple protein sequences. *Bioinformatics* **23,** 1073–1079 (2007).

113. Tarini, M., Cignoni, P. & Montani, C. Ambient occlusion and edge cueing to enhance real time molecular visualization. *IEEE Trans. Vis. Comput. Graph.* **12,** 1237–1244 (2006).

114. de Castro, E., Sigrist, C. J. A., Gattiker, A., Bulliard, V., Langendijk-Genevaux, P. S., Gasteiger, E., Bairoch, A. & Hulo, N. ScanProsite: Detection of PROSITE signature matches and ProRule-associated functional and structural residues in proteins. *Nucleic Acids Res.* **34,** (2006).

115. Hornbeck, P. V., Kornhauser, J. M., Tkachev, S., Zhang, B., Skrzypek, E., Murray, B.,

Latham, V. & Sullivan, M. PhosphoSitePlus: A comprehensive resource for investigating the structure and function of experimentally determined post-translational modifications in man and mouse. *Nucleic Acids Res.* **40,** (2012).

116. Blethrow, J. D., Glavy, J. S., Morgan, D. O. & Shokat, K. M. Covalent capture of kinase-specific phosphopeptides reveals Cdk1-cyclin B substrates. *Proc. Natl. Acad. Sci. U. S. A.* **105,** 1442–1447 (2008).

117. Kang, S., Bader, A. G. & Vogt, P. K. Phosphatidylinositol 3-kinase mutations identified in human cancer are oncogenic. *Proc. Natl. Acad. Sci. U. S. A.* **102,** 802–807 (2005).

118. Nugoor, C., Marx, A., Panneerselvam, S. & Mandelkow, E. Crystal structure of the kinase MARK3/Par-1: T211A-S215A double mutant. *TO BE Publ.* at <http://www.rcsb.org/pdb/explore/explore.do?structureId=3fe3>

119. Hertz, N. T., Wang, B. T., Allen, J. J., Zhang, C., Dar, A. C., Burlingame, A. L. & Shokat, K. M. Chemical Genetic Approach for Kinase-Substrate Mapping by Covalent Capture of Thiophosphopeptides and Analysis by Mass Spectrometry. *Curr. Protoc. Chem. Biol.* **2,** 15–36 (2010).

120. Li, Y., Roux, C., Lazereg, S., LeCaer, J. P., Laprévote, O., Badet, B. & Badet-Denisot, M. A. Identification of a novel serine phosphorylation site in human glutamine:fructose-6-phosphate amidotransferase isoform 1. *Biochemistry* **46,** 13163–13169 (2007).

121. Eguchi, S., Oshiro, N., Miyamoto, T., Yoshino, K. I., Okamoto, S., Ono, T., Kikkawa, U. & Yonezawa, K. AMP-activated protein kinase phosphorylates glutamine: Fructose-6-phosphate amidotransferase 1 at Ser243 to modulate its enzymatic activity. *Genes to Cells* **14,** 179–189 (2009).

122. Carlson, S. M. & White, F. M. Labeling and Identification of Direct Kinase Substrates. *Sci. Signal.* **5,** pl3–pl3 (2012).

123. Ong, S.-E., Blagoev, B., Kratchmarova, I., Kristensen, D. B., Steen, H., Pandey, A. & Mann, M. Stable isotope labeling by amino acids in cell culture, SILAC, as a simple and accurate approach to expression proteomics. *Mol. Cell. Proteomics* **1,** 376–386 (2002).

124. Ibarrola, N., Kalume, D. E., Gronborg, M., Iwahori, A. & Pandey, A. A Proteomic Approach for Quantitation of Phosphorylation Using Stable Isotope Labeling in Cell Culture. *Anal. Chem.* **75,** 6043–6049 (2003).

125. Ong, S.-E. & Mann, M. A practical recipe for stable isotope labeling by amino acids in cell culture (SILAC). *Nat. Protoc.* **1,** 2650–2660 (2006).

126. Carlson, S. M., Chouinard, C. R., Labadorf, A., Lam, C. J., Schmelzle, K., Fraenkel, E. & White, F. M. Large-Scale Discovery of ERK2 Substrates Identifies ERK-Mediated Transcriptional Regulation by ETV3. *Sci. Signal.* **4,** rs11–rs11 (2011).

127. Kwon, S. W., Kim, S. C., Jaunbergs, J., Falck, J. R. & Zhao, Y. Selective enrichment of thiophosphorylated polypeptides as a tool for the analysis of protein phosphorylation. *Mol. Cell. Proteomics* **2,** 242–7 (2003).

128. MS/MS Results Interpretation. at <http://www.matrixscience.com/help/interpretation_help.html>

129. Zagorska, A., Deak, M., Campbell, D. G., Banerjee, S., Hirano, M., Aizawa, S., Prescott, A. R. & Alessi, D. R. New Roles for the LKB1-NUAK Pathway in Controlling Myosin Phosphatase Complexes and Cell Adhesion. *Sci. Signal.* **3,** ra25–ra25 (2010).

130. Weekes, J., Ball, K. L., Caudwell, F. B. & Hardie, D. G. Specificity determinants for the AMP-activated protein kinase and its plant homologue analysed using synthetic peptides. *FEBS Lett.* **334,** 335–339 (1993).

131. Hornbeck, P. V., Chabra, I., Kornhauser, J. M., Skrzypek, E. & Zhang, B. PhosphoSite: A bioinformatics resource dedicated to physiological protein phosphorylation. *Proteomics* **4,** 1551–1561 (2004).

132. Akhmanova, A., Hoogenraad, C. C., Drabek, K., Stepanova, T., Dortland, B., Verkerk, T., Vermeulen, W., Burgering, B. M., De Zeeuw, C. I., Grosveld, F. & Galjart, N. Clasps are CLIP-115 and -170 associating proteins involved in the regional regulation of microtubule dynamics in motile fibroblasts. *Cell* **104,** 923–35 (2001).

133. Mimori-Kiyosue, Y. CLASP1 and CLASP2 bind to EB1 and regulate microtubule plus-end dynamics at the cell cortex. *J. Cell Biol.* **168,** 141–153 (2004).

134. Langlais, P., Dillon, J. L., Mengos, A., Baluch, D. P., Ardebili, R., Miranda, D. N., Xie, X., Heckmann, B. L., Liu, J. & Mandarino, L. J. Identification of a role for CLASP2 in insulin action. *J. Biol. Chem.* **287,** 39245–39253 (2012).

135. Thoreson, M. A., Anastasiadis, P. Z., Daniel, J. M., Ireton, R. C., Wheelock, M. J., Johnson, K. R., Hummingbird, D. K. & Reynolds, A. B. Selective uncoupling of p120(ctn) from E-cadherin disrupts strong adhesion. *J. Cell Biol.* **148,** 189–201 (2000).

136. Casagolda, D., Del Valle-Pérez, B., Valls, G., Lugilde, E., Vinyoles, M., Casado-Vela, J., Solanas, G., Batlle, E., Reynolds, A. B., Casal, J. I., de Herreros, A. G. & Duñach, M. A p120-catenin-CK1epsilon complex regulates Wnt signaling. *J. Cell Sci.* **123,** 2621–2631 (2010).

137. Schackmann, R. C. J., Tenhagen, M., van de Ven, R. A. H. & Derksen, P. W. B. P120-Catenin in Cancer - Mechanisms, Models and Opportunities for Intervention. *J. Cell Sci.* **126,** 3515–25 (2013).

138. Xia, X., Brooks, J., Campos-González, R. & Reynolds, A. B. Serine and threonine phospho-specific antibodies to p120-catenin. *Hybrid. Hybridomics* **23,** 343–351 (2004).

139. Nekrasova, O. & Green, K. J. Desmosome assembly and dynamics. *Trends Cell Biol.* **23,** 537–546 (2013).

140. Yang, Z., Bowles, N. E., Scherer, S. E., Taylor, M. D., Kearney, D. L., Ge, S., Nadvoretskiy, V. V., DeFreitas, G., Carabello, B., Brandon, L. I., Godsel, L. M., Green, K. J., Saffitz, J. E., Li, H., Danieli, G. A., Calkins, H., Marcus, F. & Towbin, J. A. Desmosomal dysfunction due to mutations in desmoplakin causes arrhythmogenic

right ventricular dysplasia/cardiomyopathy. *Circ. Res.* **99,** 646–655 (2006).

141. Dhand, R., Hara, K., Hiles, I., Bax, B., Gout, I., Panayotou, G., Fry, M. J., Yonezawa, K., Kasuga, M. & Waterfield, M. D. PI 3-kinase: structural and functional analysis of intersubunit interactions. *EMBO J.* **13,** 511–21 (1994).

142. Huang, C.-H., Mandelker, D., Schmidt-Kittler, O., Samuels, Y., Velculescu, V. E., Kinzler, K. W., Vogelstein, B., Gabelli, S. B. & Amzel, L. M. The Structure of a Human p110 /p85 Complex Elucidates the Effects of Oncogenic PI3K Mutations. *Science (80-.).* **318,** 1744–1748 (2007).

143. Campbell, I. G., Russell, S. E., Choong, D. Y. H., Montgomery, K. G., Ciavarella, M. L., Hooi, C. S. F., Cristiano, B. E., Pearson, R. B. & Phillips, W. a. Mutation of the PIK3CA gene in ovarian and breast cancer. *Cancer Res.* **64,** 7678–7681 (2004).

144. Altomare, D. A., Wang, H. Q., Skele, K. L., De Rienzo, A., Klein-Szanto, A. J., Godwin, A. K. & Testa, J. R. AKT and mTOR phosphorylation is frequently detected in ovarian cancer and can be targeted to disrupt ovarian tumor cell growth. *Oncogene* **23,** 5853–5857 (2004).

145. Levine, D. a. Frequent Mutation of the PIK3CA Gene in Ovarian and Breast Cancers. *Clin. Cancer Res.* **11,** 2875–2878 (2005).

146. Minotti, a M., Barlow, S. B. & Cabral, F. Resistance to antimitotic drugs in Chinese hamster ovary cells correlates with changes in the level of polymerized tubulin. *J. Biol. Chem.* **266,** 3987–94 (1991).

147. Kavallaris, M., Kuo, D. Y., Burkhart, C. A., Regl, D. L., Norris, M. D., Haber, M. & Horwitz, S. B. Taxol-resistant epithelial ovarian tumors are associated with altered expression of specific beta-tubulin isotypes. *J. Clin. Invest.* **100,** 1282–1293 (1997).

148. Giannakakou, P., Sackett, D. L., Kang, Y. K., Zhan, Z., Buters, J. T. M., Fojo, T. & Poruchynsky, M. S. Paclitaxel-resistant human ovarian cancer cells have mutant β-tubulins that exhibit impaired paclitaxel-driven polymerization. *J. Biol. Chem.* **272,** 17118–17125 (1997).

149. Gonçalves, A., Braguer, D., Kamath, K., Martello, L., Briand, C., Horwitz, S., Wilson, L. & Jordan, M. A. Resistance to Taxol in lung cancer cells associated with increased microtubule dynamics. *Proc. Natl. Acad. Sci. U. S. A.* **98,** 11737–11742 (2001).

150. Hari, M., Loganzo, F., Annable, T., Tan, X., Musto, S., Morilla, D. B., Nettles, J. H., Snyder, J. P. & Greenberger, L. M. Paclitaxel-resistant cells have a mutation in the paclitaxel-binding region of beta-tubulin (Asp26Glu) and less stable microtubules. *Mol. Cancer Ther.* **5,** 270–278 (2006).

151. Ahmed, A. A., Mills, A. D., Ibrahim, A. E. K., Temple, J., Blenkiron, C., Vias, M., Massie, C. E., Iyer, N. G., McGeoch, A., Crawford, R., Nicke, B., Downward, J., Swanton, C., Bell, S. D., Earl, H. M., Laskey, R. A., Caldas, C. & Brenton, J. D. The Extracellular Matrix Protein TGFBI Induces Microtubule Stabilization and Sensitizes Ovarian Cancers to Paclitaxel. *Cancer Cell* **12,** 514–527 (2007).

152. Ahmed, A. A., Wang, X., Lu, Z., Goldsmith, J., Le, X. F., Grandjean, G., Bartholomeusz,

G., Broom, B. & Bast, R. C. Modulating microtubule stability enhances the cytotoxic response of cancer cells to paclitaxel. *Cancer Res.* **71,** 5806–5817 (2011).

153. George, J. A. Src Tyrosine Kinase and Multidrug Resistance Protein-1 Inhibitions Act Independently but Cooperatively to Restore Paclitaxel Sensitivity to Paclitaxel-Resistant Ovarian Cancer Cells. *Cancer Res.* **65,** 10381–10388 (2005).

154. Yu, Y., Gaillard, S., Phillip, J. M., Huang, T.-C., Pinto, S. M., Tessarollo, N. G., Zhang, Z., Pandey, A., Wirtz, D., Ayhan, A., Davidson, B., Wang, T.-L. & Shih, I.-M. Inhibition of Spleen Tyrosine Kinase Potentiates Paclitaxel-Induced Cytotoxicity in Ovarian Cancer Cells by Stabilizing Microtubules. *Cancer Cell* **28,** 82–96 (2015).

155. Hashimoto, Y. K., Satoh, T., Okamoto, M. & Takemori, H. Importance of autophosphorylation at Ser186 in the A-loop of salt inducible kinase 1 for its sustained kinase activity. *J. Cell. Biochem.* **104,** 1724–39 (2008).

156. Turk, B. E. Understanding and exploiting substrate recognition by protein kinases. *Curr. Opin. Chem. Biol.* **12,** 4–10 (2008).

157. Godsel, L. M., Hsieh, S. N., Amargo, E. V., Bass, A. E., Pascoe-McGillicuddy, L. T., Huen, A. C., Thorne, M. E., Gaudry, C. a., Park, J. K., Myung, K., Goldman, R. D., Chew, T. L. & Green, K. J. Desmoplakin assembly dynamics in four dimensions: Multiple phases differentially regulated by intermediate filaments and actin. *J. Cell Biol.* **171,** 1045–1059 (2005).

158. Koo, S.-H., Flechner, L., Qi, L., Zhang, X., Screaton, R. a, Jeffries, S., Hedrick, S., Xu, W., Boussouar, F., Brindle, P., Takemori, H. & Montminy, M. The CREB coactivator TORC2 is a key regulator of fasting glucose metabolism. *Nature* **437,** 1109–1111 (2005).

159. Uebi, T., Tamura, M., Horike, N., Hashimoto, Y. K. & Takemori, H. Phosphorylation of the CREB-specific coactivator TORC2 at Ser(307) regulates its intracellular localization in COS-7 cells and in the mouse liver. *Am. J. Physiol. Endocrinol. Metab.* **299,** E413–25 (2010).

160. McGee, S. L., Van Denderen, B. J. W., Howlett, K. F., Mollica, J., Schertzer, J. D., Kemp, B. E. & Hargreaves, M. AMP-activated protein kinase regulates GLUT4 transcription by phosphorylating histone deacetylase 5. *Diabetes* **57,** 860–867 (2008).

161. Dequiedt, F., Martin, M., Von Blume, J., Vertommen, D., Lecomte, E., Mari, N., Heinen, M.-F., Bachmann, M., Twizere, J.-C., Huang, M. C., Rider, M. H., Piwnica-Worms, H., Seufferlein, T. & Kettmann, R. New role for hPar-1 kinases EMK and C-TAK1 in regulating localization and activity of class IIa histone deacetylases. *Mol. Cell. Biol.* **26,** 7086–7102 (2006).

162. Schaffer, B. E., Levin, R. S., Hertz, N. T., Shaw, R. J., Shokat, K. M., Brunet Correspondence, A., Maures, T. J., Schoof, M. L., Hollstein, P. E., Ré Nice, B., Benayoun, A., Banko, M. R. & Brunet, A. Identification of AMPK Phosphorylation Sites Reveals a Network of Proteins Involved in Cell Invasion and Facilitates Large-Scale Substrate Prediction. *Cell Metab.* **22,** 1–15 (2015).

163. Yoshimura, Y., Terabayashi, T. & Miki, H. Par1b/MARK2 phosphorylates kinesin-like

motor protein GAKIN/KIF13B to regulate axon formation. *Mol. Cell. Biol.* **30,** 2206–2219 (2010).

164. Yamahashi, Y., Saito, Y., Murata-Kamiya, N. & Hatakeyama, M. Polarity-regulating kinase partitioning-defective 1b (PAR1b) phosphorylates guanine nucleotide exchange factor H1 (GEF-H1) to regulate RhoA-dependent actin cytoskeletal reorganization. *J. Biol. Chem.* **286,** 44576–44584 (2011).

165. Yoshimura, Y. & Miki, H. Dynamic regulation of GEF-H1 localization at microtubules by Par1b/MARK2. *Biochem. Biophys. Res. Commun.* **408,** 322–328 (2011).

166. Joung, J. K. & Sander, J. D. TALENs: a widely applicable technology for targeted genome editing. *Nat. Rev. Mol. Cell Biol.* **14,** 49–55 (2013).

167. Ran, F., Hsu, P., Wright, J. & Agarwala, V. Genome engineering using the CRISPR-Cas9 system. *Nat. Protoc.* **8,** 2281–308 (2013).

168. Cassel, D. & Glaser, L. Resistance to phosphatase of thiophosphorylated epidermal growth factor receptor in A431 membranes. *Proc. Natl. Acad. Sci. U. S. A.* **79,** 2231–2235 (1982).

169. Swaney, D. L., Wenger, C. D. & Coon, J. J. Value of using multiple proteases for large-scale mass spectrometry-based proteomics. *J. Proteome Res.* **9,** 1323–1329 (2010).

170. Sundberg, T. B., Choi, H. G., Song, J.-H., Russell, C. N., Hussain, M. M., Graham, D. B., Khor, B., Gagnon, J., O'Connell, D. J., Narayan, K., Dančík, V., Perez, J. R., Reinecker, H.-C., Gray, N. S., Schreiber, S. L., Xavier, R. J. & Shamji, A. F. Small-molecule screening identifies inhibition of salt-inducible kinases as a therapeutic strategy to enhance immunoregulatory functions of dendritic cells. *Proc. Natl. Acad. Sci. U. S. A.* **111,** 12468–12473 (2014).

171. Muraoka, M., Fukushima, A., Viengchareun, S., Lombès, M., Kishi, F., Miyauchi, A., Kanematsu, M., Doi, J., Kajimura, J., Nakai, R., Uebi, T., Okamoto, M. & Takemori, H. Involvement of SIK2/TORC2 signaling cascade in the regulation of insulin-induced PGC-1alpha and UCP-1 gene expression in brown adipocytes. *Am. J. Physiol. Endocrinol. Metab.* **296,** E1430–9 (2009).

172. Kotarsky, K., Nilsson, N. E., Flodgren, E., Owman, C. & Olde, B. A human cell surface receptor activated by free fatty acids and thiazolidinedione drugs. *Biochem. Biophys. Res. Commun.* **301,** 406–410 (2003).

173. Sjöström, M., Stenström, K., Eneling, K., Zwiller, J., Katz, A. I., Takemori, H. & Bertorello, A. M. SIK1 is part of a cell sodium-sensing network that regulates active sodium transport through a calcium-dependent process. *Proc. Natl. Acad. Sci. U. S. A.* **104,** 16922–16927 (2007).

174. Woods, A., Dickerson, K., Heath, R., Hong, S.-P., Momcilovic, M., Johnstone, S. R., Carlson, M. & Carling, D. Ca2+/calmodulin-dependent protein kinase kinase-β acts upstream of AMP-activated protein kinase in mammalian cells. *Cell Metab.* **2,** 21–33 (2005).

175. Meng, Q., Xia, C., Fang, J., Rojanasakul, Y. & Jiang, B. H. Role of PI3K and AKT specific

isoforms in ovarian cancer cell migration, invasion and proliferation through the p70S6K1 pathway. *Cell Signal* **18,** 2262–2271 (2006).

176. Hu, L., Hofmann, J., Lu, Y., Mills, G. B. & Jaffe, R. B. Inhibition of Phosphatidylinositol 3' -Kinase Increases Efficacy of Paclitaxel in in Vitro and in Vivo Ovarian Cancer Models. *Cancer Res.* **62hu,** 1087–1092 (2002).

177. Motohara, T., Masuko, S., Ishimoto, T., Yae, T., Onishi, N., Muraguchi, T., Hirao, A., Matsuzaki, Y., Tashiro, H., Katabuchi, H., Saya, H. & Nagano, O. Transient depletion of p53 followed by transduction of c-Myc and K-Ras converts ovarian stem-like cells into tumor-initiating cells. *Carcinogenesis* **32,** 1597–1606 (2011).

178. Yu, J., Wjasow, C. & Backer, J. M. Regulation of the p85/p110α phosphatidylinositol 3′-kinase: Distinct roles for the N-terminal and C-terminal SH2 domains. *J. Biol. Chem.* **273,** 30199–30203 (1998).

179. Chamberlain, M. D., Berry, T. R., Pastor, M. C. & Anderson, D. H. The p85α subunit of phosphatidylinositol 3′-kinase binds to and stimulates the GTPase activity of Rab proteins. *J. Biol. Chem.* **279,** 48607–48614 (2004).

180. Zheng, Y., Bagrodia, S. & Cerione, R. A. Activation of phosphoinositide 3-kinase activity by Cdc42Hs binding to p85. *J. Biol. Chem.* **269,** 18727–18730 (1994).

181. Keely, P. J., Westwick, J. K., Whitehead, I. P., Der, C. J. & Parise, L. V. Cdc42 and Rac1 induce integrin-mediated cell motility and invasiveness through PI(3)K. *Nature* **390,** 632–636 (1997).

182. Price, L. S., Leng, J., Schwartz, M. A. & Bokoch, G. M. Activation of Rac and Cdc42 by integrins mediates cell spreading. *Mol. Biol. Cell* **9,** 1863–71 (1998).

183. Evers, E. E., Zondag, G. C., Malliri, A., Price, L. S., ten Klooster, J. P., van der Kammen, R. A. & Collard, J. G. Rho family proteins in cell adhesion and cell migration. *Eur. J. Cancer* **36,** 1269–74 (2000).

184. Bae, Y.-S., Lee, T. G., Park, J. C., Hur, J. H., Kim, Y., Heo, K., Kwak, J.-Y., Suh, P.-G. & Ryu, S. H. Identification of a compound that directly stimulates phospholipase C activity. *Mol. Pharmacol.* **63,** 1043–1050 (2003).

185. Treiman, M., Caspersen, C. & Christensen, S. B. A tool coming of age: Thapsigargin as an inhibitor of sarco-endoplasmic reticulum Ca2+-ATPases. *Trends Pharmacol. Sci.* **19,** 131–135 (1998).

186. Tuschil, A., Lam, C., Haslberger, A. & Lindley, I. Interleukin-8 stimulates calcium transients and promotes epidermal cell proliferation. *J. Invest. Dermatol.* **99,** 294–8 (1992).

187. Sun, M., Wang, G., Paciga, J. E., Feldman, R. I., Yuan, Z.-Q., Ma, X.-L., Shelley, S. A., Jove, R., Tsichlis, P. N., Nicosia, S. V & Cheng, J. Q. AKT1/PKBα Kinase Is Frequently Elevated in Human Cancers and Its Constitutive Activation Is Required for Oncogenic Transformation in NIH3T3 Cells. *Am. J. Pathol.* **159,** 431–437 (2001).

188. Kim, S.-H., Juhnn, Y.-S. & Song, Y.-S. Akt Involvement in Paclitaxel Chemoresistance

of Human Ovarian Cancer Cells. *Ann. N. Y. Acad. Sci.* **1095,** 82–89 (2007).

189. Fraser, M., Bai, T. & Tsang, B. K. Akt promotes cisplatin resistance in human ovarian cancer cells through inhibition of p53 phosphorylation and nuclear function. *Int. J. Cancer* **122,** 534–46 (2008).

190. Watanabe, T., Noritake, J., Kakeno, M., Matsui, T., Harada, T., Wang, S., Itoh, N., Sato, K., Matsuzawa, K., Iwamatsu, A., Galjart, N. & Kaibuchi, K. Phosphorylation of CLASP2 by GSK-3beta regulates its interaction with IQGAP1, EB1 and microtubules. *J. Cell Sci.* **122,** 2969–2979 (2009).

191. Kelkar, M. & Martin, S. G. PKA antagonizes CLASP-dependent microtubule stabilization to re-localize Pom1 and buffer cell size upon glucose limitation. *Nat. Commun.* **6,** 8445 (2015).

192. Goodwin, J. M., Svensson, R. U., Lou, H. J., Winslow, M. M., Turk, B. E. & Shaw, R. J. An AMPK-Independent Signaling Pathway Downstream of the LKB1 Tumor Suppressor Controls Snail1 and Metastatic Potential. *Mol. Cell* **55,** 436–450 (2014).

193. Gundersen, G. G., Khawaja, S. & Bulinski, J. C. Postpolymerization detyrosination of alpha-tubulin: a mechanism for subcellular differentiation of microtubules. *J. Cell Biol.* **105,** 251–64 (1987).

194. Alfredi, A., Zhang, S., Mao, W., Wang, Y., Takemori, H., Lu, Z., Bast, R. C. & Vankayalapati, H. Abstract 749: Highly potent and orally available SIK2 inhibitors block growth of human ovarian cancer cells in culture and xenografts. *Cancer Res.* **74 ,** 749 (2014).

195. Drysdale, M., Knapp, S. & Ahmed, A. A. Targeting the Salt Inducible Kinase 2 (SIK2) for cancer therapy. *Res. Counc. UK - Gatew. to Res.* (2015). at <http://gtr.rcuk.ac.uk/projects?ref=MR/M025381/1>

APPENDIX I: *IN SILICO* SCREEN RESULTS

This table contains the full results of an in silico screen for instances of the SIK consensus sequence LX[H/K/R][S/T]XSXXXL in the Swiss-Prot database. 273 hits were found in 241 distinct proteins. Amino acid residues specified by this motif are shown in upper case.

Accession	Name	Start	End	Sequence
Q96P26	5NT1B	107	116	LrKTdSrgyL
P49902	5NTC	440	449	LfRSgSrqtL
Q9UGI9	AAKG3	9	18	LrRTpSwssL
Q6H8Q1	ABLM2	14	23	LeKSpStaiL
Q13023	AKAP6	1562	1571	LsHSsSiesL
Q12802	AKP13	2493	2502	LrRTeSdsgL
O95076	ALX3	233	242	LpRTdShpqL
O15123	ANGP2	161	170	LeHSlStnkL
Q7Z6G8	ANS1B	348	357	LcHTiSdhyL
O14617	AP3D1	266	275	LiHStSamsL
P04114	APOB	639	648	LyKSvSlpsL
Q96P48	ARAP1	750	759	LyKTaSagkL
Q9NZN5	ARHGC	133	142	LiKSgSyvaL
Q96PE2	ARHGH	10	19	LyRSvSfklL
Q969Q4	ARL11	172	181	LlKSrScmcL
P36542	ATPG	141	150	LyRThSdqfL
Q9UIG0	BAZ1B	342	351	LkKSlSgspL
Q8NDZ0	BEND2	679	688	LaKTkScasL
Q6UXY1	BI2L2	294	303	LpRTpSassL
Q9H694	BICC1	798	807	LsRSnSrehL
Q9NR09	BIRC6	4018	4027	LsKTdSykrL
Q9ULD4	BRPF3	793	802	LnKTvSngeL
Q9UPA5	BSN	1146	1155	LyKSgSeynL
Q5T5Y3	CAMP1	495	504	LaRSiSkdsL
Q5T5Y3	CAMP1	1393	1402	LsRTqSgssL
Q9P1Y5	CAMP3	426	435	LlRSvSsdsL
Q6IMN6	CAPR2	180	189	LqKTfSglsL
P43235	CATK	97	106	LsHSrSndtL
Q13191	CBLB	795	804	LnRTpSdydL
Q8NCX0	CC150	230	239	LeKSaSamlL
Q8NDH2	CC168	673	682	LtKStSlpsL
Q5T9S5	CCD18	1350	1359	LrRSiSasdL
Q8N4L8	CCD24	2	11	LrHSpSlweL
Q8TD31	CCHCR	353	362	LeHSdSvkqL
Q15078	CD5R1	86	95	LkKSlScanL
Q01850	CDR2	306	315	LkRSsSetiL
Q86XR8	CEP57	50	59	LrRSpSkptL
Q5JTW2	CEP78	144	153	LnKSaSlvhL
Q9C0B2	CFA74	825	834	LvHTrSkaaL
Q96NL8	CH037	100	109	LgKScSpvyL
Q9P2M7	CING	126	135	LlRShSqasL
Q7Z460	CLAP1	1157	1166	LrRSySpsmL
P30622	CLIP1	307	316	LkRSpSassL
Q6P4Q7	CNNM4	102	111	LhKStScleL
Q96JB2	COG3	528	537	LtKSgStesL
Q9BV73	CP250	2387	2396	LhHSlShslL
O95639	CPSF4	197	206	LqRSsSliqL
Q53ET0	CRTC2	166	175	LnRTsSdsaL
Q6UUV7	CRTC3	157	166	LnRTnSdsaL
Q7Z407	CSMD3	348	357	LtHTtStgeL
O43246	CTR4	194	203	LnHTfSaisL
Q69YQ0	CYTSA	49	58	LsKTkSsddL
Q5M775	CYTSB	909	918	LrKSpSlesL
Q86Y56	DAAF5	444	453	LkKTpSasgL
O60610	DIAP1	967	976	LrKSeSfsnL
O60879	DIAP2	824	833	LkKSeSfnrL
Q9NQL9	DMRT3	376	385	LaRSqSspfL
Q9H4B8	DPEP3	384	393	LsRSwSeeeL
Q9H8V3	ECT2	362	371	LkKSvSmlsL
Q09472	EP300	84	93	LlRSgSspnL
Q9UQ84	EXO1	741	750	LyKSsSadsL
Q8TAG9	EXOC6	525	534	LtRTlSsclL
O43909	EXTL3	496	505	LlRSlSdsdL
Q49AJ0	F135B	1271	1280	LkKSgSllqL
Q96MY7	F161B	434	443	LpRSrSlsgL
Q9Y4F9	FA65B	386	395	LhRSrSfsdL
Q53R41	FAKD1	491	500	LqHSnSldlL
Q53RD9	FBLN7	333	342	LpKTiSfhyL
Q01362	FCERB	38	47	LlKSaSsppL
O14526	FCHO1	580	589	LsRSlSpspL
Q5H8C1	FREM1	1632	1641	LlHSpSqvgL
O94915	FRYL	1973	1982	LaRTrSlssL
Q13480	GAB1	261	270	LpRSyShdvL
P39905	GDNF	13	22	LlHTaSafpL
Q13439	GOGA4	84	93	LfRSsSkesL
Q13439	GOGA4	93	102	LvRTsSresL
Q96CP6	GRM1A	200	209	LeKTlSpreL
Q7Z2Y8	GVIN1	76	85	LsHSkSlsaL
P13807	GYS1	3	12	LnRTlSmssL
P56524	HDAC4	241	250	LrKTaSepnL
Q9UQL6	HDAC5	254	263	LrKTaSepnL
Q8WUI4	HDAC7	150	159	LrKTvSepnL
Q9UKV0	HDAC9	215	224	LrKTaSepnL
Q7Z4Q2	HEAT3	221	230	LlKSfSataL
Q15751	HERC1	1507	1516	LiKSrSesdL
O95714	HERC2	4123	4132	LgHSdSedqL
Q30201	HFE	24	33	LlRShSlhyL
Q8NCD3	HJURP	515	524	LpKSdSsssL
Q14974	IMB1	7	16	LeKTvSpdrL
Q96PE3	INP4A	846	855	LpRSrSqtcL

Q9H0H0	INT2	1070	1079	LpKSlSvarL
Q75QN2	INT8	99	108	LeKSlSvpvL
Q9NZM3	ITSN2	1441	1450	LyKTkSnkeL
Q8WXH2	JPH3	225	234	LrKSeSkssL
Q8IV33	K0825	784	793	LlRTpSaggL
Q9H0B3	K1683	700	709	LtKTpSlahL
Q17RG1	KCD19	910	919	LsRSvSysiL
Q9NS40	KCNH7	258	267	LsHSrSresL
Q9NR82	KCNQ5	826	835	LgKSlSvqnL
Q9ULH0	KDIS	1676	1685	LnRTpStvtL
Q9H1H9	KI13A	1693	1702	LcRTgScseL
Q9H0B6	KLC2	540	549	LrRSgSfgkL
P11801	KPSH1	367	376	LhRSiSqnlL
Q9BXB1	LGR4	875	884	LiKShScpaL
Q6MZP7	LIN54	145	154	LgKSgSpivL
Q86W92	LIPB1	461	470	LqKSsSlgnL
Q8TBB1	LNX1	578	587	LkRTsSsivL
Q8ND23	LR16B	239	248	LsKSgSleeL
Q86X40	LRC28	5	14	LcKTiSvarL
Q96PB8	LRC3B	8	17	LtRSlSmclL
Q96E66	LRC51	41	50	LkRSkSgksL
Q9Y608	LRRF2	197	206	LlRSaSlasL
Q38SD2	LRRK1	569	578	LlKSlSelyL
Q6UWE0	LRSM1	71	80	LpKScSllsL
O94822	LTN1	1503	1512	LrKTkSlnkL
Q99759	M3K3	107	116	LdRSsSmksL
P80192	M3K9	690	699	LqHSpSqsyL
Q3KQU3	MA7D1	308	317	LaRSrSavtL
Q14244	MAP7	237	246	LaRSkStaaL
Q8IVT2	MISP	538	547	LqKSqSsdlL
Q9NYL2	MLTK	588	597	LqRSqSnpiL
Q96DY7	MTBP	750	759	LvKSeSsesL
Q13615	MTMR3	608	617	LpKTrSydnL
Q9NYA4	MTMR4	605	614	LpKTrSmddL
Q9NYA4	MTMR4	624	633	LtRTsSdpnL
Q86WG5	MTMRD	225	234	LfHSaSfqrL
Q8WXI7	MUC16	12896	12905	LfKStSvgpL
Q8WXI7	MUC16	15082	15091	LfKStSvgpL
Q8WXI7	MUC16	15550	15559	LfKStSvgpL
Q8WXI7	MUC16	17264	17273	LfKStSvgpL
Q8WXI7	MUC16	17732	17741	LfKStSvgpL
Q8WXI7	MUC16	18668	18677	LfKStSvgpL
Q8WXI7	MUC16	20383	20392	LfKStSvgpL
Q8WXI7	MUC16	20539	20548	LfKStSvgpL
Q8WXI7	MUC16	20851	20860	LfKStSvgpL
Q8WXI7	MUC16	21319	21328	LfKStSvgpL
Q9NR99	MXRA5	804	813	LiKTtSppsL
Q15746	MYLK	338	347	LqKTsSsitL
Q9UKN7	MYO15	1755	1764	LgKSsSvtrL
O14974	MYPT1	440	449	LrKTgSygaL
O14974	MYPT1	905	914	LgRSgSysyL
O60237	MYPT2	442	451	LrKTgShnmL
Q86W24	NAL14	782	791	LiRSqSlifL
Q9Y2X3	NOP58	142	151	LaHSlSryrL
Q9H340	O51B6	3	12	LnKSaStfqL
Q8NH18	OR5J2	157	166	LiHTiSlrrL
Q8NGQ5	OR9Q1	157	166	LvRTvSaftL
Q96SU4	OSBL9	321	330	LtHSsSgnsL
P27986	P85A	149	158	LyRTqSssnL
Q8TEW8	PAR3L	741	750	LkKSsSlesL
Q8TEW0	PARD3	884	893	LkKSsSlesL
Q6L8Q7	PDE12	294	303	LiRTvSyniL
Q07343	PDE4B	135	144	LyRSdSdydL
Q08493	PDE4C	121	130	LyRSdSdyeL
Q08499	PDE4D	192	201	LyRSdSdydL
P0DJD8	PEPA3	28	37	LrRTlSergL
P0DJD7	PEPA4	28	37	LrRTlSergL
P0DJD9	PEPA5	28	37	LrRTlSergL
P56589	PEX3	196	205	LkHSlSlldL
Q75T13	PGAP1	879	888	LlKTtSqfpL
Q96QT6	PHF12	139	148	LdRSaSkteL
Q6ZVD8	PHLP2	1226	1235	LqKSpStscL
Q8WYR1	PI3R5	427	436	LfKStSqlvL
Q92508	PIEZ1	1641	1650	LmRTaSellL
Q8TEQ8	PIGO	812	821	LeRTkSqgpL
Q9BZ72	PITM2	862	871	LsHTpSvrrL
O94827	PKHG5	929	938	LlKSkSeasL
Q9UKY4	POMT2	166	175	LsKSlSaalL
Q9BZL4	PP12C	422	431	LlKTgSsgaL
Q9BZL4	PP12C	447	456	LqRSaSsswL
Q03181	PPARD	45	54	LsRSsSppsL
Q9UKL6	PPCT	134	143	LaRStSmpqL
O75864	PPR37	329	338	LpHTqSletL
Q96QH2	PRAM	527	536	LrRTrSaagL
Q9ULL5	PRR12	251	260	LlKTsSfhlL
Q9BWN1	PRR14	328	337	LgRSyScpdL
P85299	PRR5	235	244	LrRSrSgdvL
Q9BQI7	PSD2	743	752	LrKThSspaL
Q9NYI0	PSD3	1006	1015	LkKShSspsL
Q8NDX1	PSD4	1014	1023	LkKShSspsL

Q96JH8	RADIL	211	220	LrRTvSetsL
Q5U651	RAIN	323	332	LrRSvSelsL
Q6ZTQ3	RASF6	182	191	LyRTmSeaaL
Q8NDT2	RB15B	344	353	LdHSvSeveL
Q6ZP01	RBM44	729	738	LkKTlSqmsL
Q9H0H5	RGAP1	585	594	LlKTpSsssL
Q9BRR9	RHG09	54	63	LrKTnSdwwL
P57078	RIPK4	401	410	LsRSsSeskL
Q6ZRF8	RN207	402	411	LhRSiStkvL
P34096	RNAS4	3	12	LqRThSlllL
Q5JTH9	RRP12	322	331	LvKScSetlL
Q01196	RUNX1	62	71	LvRTdSpnfL
Q13950	RUNX2	113	122	LvRTdSpnfL
Q13761	RUNX3	66	75	LvRTdSpnfL
Q92736	RYR2	121	130	LrHSySgmyL
Q15413	RYR3	111	120	LrHSfSgmyL
Q9H228	S1PR5	249	258	LlRTlSvvlL
Q96N87	S6A18	375	384	LdKSaSgpgL
Q9UBE0	SAE1	233	242	LkRTtSdyfL
Q8IYX7	SAXO1	182	191	LvKTiSckpL
Q9H5K3	SG196	208	217	LpKTlSqylL
Q9BRG2	SH23A	120	129	LrRSfSedtL
Q9BRG2	SH23A	175	184	LpRTsSdpvL
Q9UPX8	SHAN2	38	47	LlRSnSdnnL
Q9BYB0	SHAN3	370	379	LqRSaSdinL
A0MZ66	SHOT1	456	465	LnKStSsrsL
Q13796	SHRM2	641	650	LqKSrStvaL
Q8TF72	SHRM3	885	894	LlRSqStfqL
O60292	SI1L3	1539	1548	LqRTlSdesL
Q5VYV7	SLX4I	350	359	LaKTtSkeeL
Q8TEV9	SMCR8	484	493	LsKSdSqasL
Q96Q15	SMG1	1213	1222	LkKStSstsL
Q9H9C1	SPE39	204	213	LkRTlSkeiL
Q9NRA0	SPHK2	416	425	LhRSvSdlpL
Q2M3C7	SPKAP	667	676	LaHTlSnviL
P28290	SSFA2	295	304	LmKTlSklnL
Q8WYL5	SSH1	973	982	LkRShSlakL
Q76I76	SSH2	456	465	LwRShSdsdL
P52630	STAT2	590	599	LkKTmSgtfL
Q13586	STIM1	516	525	LtHSdSessL
Q9P246	STIM2	675	684	LeKScSmnqL
Q9BXU1	STK31	620	629	LnKSpSvdhL
Q8IV01	SYT12	128	137	LrKSqSadsL
Q9NYJ8	TAB2	103	112	LtHSiSdgqL
Q8TEA7	TBCK	411	420	LpHSnSnneL
Q9Y4C2	TCAF1	499	508	LaHSgSdlsL
Q15569	TESK1	352	361	LsRSrSdlfL
P10827	THA	302	311	LgKSlSafnL
Q9NV64	TM39A	177	186	LfRShSvlnL
Q9GZU3	TM39B	182	191	LfRTySflnL
Q63HR2	TNS2	115	124	LpRSfSldpL
Q12888	TP53B	1312	1321	LhRTsSgtsL
P48995	TRPC1	286	295	LnHTsSdepL
Q9NZQ8	TRPM5	418	427	LyRSvSrksL
P49815	TSC2	1382	1391	LsKSsSspeL
Q6P2S7	TTC41	913	922	LaKSaSeeyL
P26651	TTP	268	277	LvRTpSvqsL
Q9NRJ4	TULP4	1053	1062	LaHTaSaspL
Q9Y385	UB2J1	201	210	LnHSfSltdL
Q9UK80	UBP21	151	160	LrRStSlrrL
P68543	UBX2A	247	256	LqKTaSfreL
A0JNW5	UH1BL	948	957	LfKSaSdtnL
Q8N2C7	UNC80	1486	1495	LhHSrScarL
P46939	UTRO	1481	1490	LyKTlSevkL
A6NCI4	VWA3A	844	853	LrRTsSsidL
Q9H4A3	WNK1	1294	1303	LsHSaSslsL
O96014	WNT11	30	39	LsKTpSalaL
Q1RN00	YC018	171	180	LsKTcShlkL
Q8NBF4	YG006	81	90	LaHTgSvetL
Q9UF83	YM012	160	169	LtRTpSrasL
Q9UF83	YM012	390	399	LtRTpSrasL
Q9UF83	YM012	399	408	LtRTqSsssL
Q9UF83	YM012	408	417	LtRTpSmasL
Q9UF83	YM012	453	462	LtRTpSmvsL
Q9UF83	YM012	462	471	LkRSpSrasL
Q9UF83	YM012	471	480	LtRTpSrasL
Q9UF83	YM012	489	498	LtRTpStasL
Q9UF83	YM012	525	534	LtRTpStasL
A8MUU9	YV023	61	70	LkRTpSrasL
A8MUU9	YV023	70	79	LtRTlSrasL
A8MUU9	YV023	160	169	LrRTpSrasL
A8MUU9	YV023	169	178	LtRTpSrasL
A8MUU9	YV023	228	237	LrRTpSrasL
A8MUU9	YV023	237	246	LtRTpSrasL
A8MUU9	YV023	246	255	LtRTpSrasL
A8MUU9	YV023	345	354	LtRTpStasL
A8MUU9	YV023	354	363	LtRTpSrasL
A8MUU9	YV023	435	444	LtRSpStasL
Q5HYM0	ZC12B	616	625	LhRSaSqnrL
Q9C0B5	ZDHC5	291	300	LrRTkSkgsL
Q9ULC8	ZDHC8	294	303	LgRSkSkgsL
Q5T1R4	ZEP3	2349	2358	LdRSsSvgcL
P51523	ZNF84	123	132	LrKSnSegdL

APPENDIX II: ADDITIONAL SCREEN DATA

Uniprot accession	Gene name	Repl 1	Repl 2	Repl 3	Repl 4	Peptide sequence	pSite	Site sequence (-7 to +7)
O14974	PPP1R12A	79.38	60.79	93.81	112.1	TGSYGALAEITASK	S445	LGLRKTGSYGALAEI
O75122	CLASP2	82.31	72.9	86.99	78.72	SRSDIDVNAAAGAK	S370	GSLQRSRSDIDVNAA
O60716	CTNND1	58.46	71.46	80.64	84.68	VGGSSVDLHR	S268	PQVRVGGSSVDLHRF
Q7Z460	CLASP1	73.77	63.34	72.03	*46.42*	SRSDIDVNAAASAK	S600	GSLQRSRSDIDVNAA
P15924	DSP	50.26	52.66	64.33	50.7	AESGPDLR	S22	GRMIRAESGPDLRYE
Q9H0K1	SIK2	71.93		65.02	85.23	QSLETQYLQHR	S674	PQLSPRQSLETQYLQ
P27986	PIK3R1	57.72	64.51		76.43	TQSSSNLAELR	S154	STLYRTQSSSNLAEL
Q9H0B6	KLC2	69.05		*50.03*	64.6	ASSLNFLNK	S582	PRMKRASSLNFLNKS
Q9H0K1	SIK2	51.73	53.59	*46.95*		RPSTIAEQTVAK	S358	DGRQRRPSTIAEQTV
Q9BRJ2	MRPL45	58.5		84.88		CSSMMNQGNVYGQITVR	S201	VVQVRCSSMMNQGNV
Q32P44	EML3	60.27	*50.82*			AISSANLLVR	S176	KLSRKAISSANLLVR
Q96PK6	RBM14	44.59	64.04			LSESQLSFR	S620	DYRRLSESQLSFRRS
Q96N67	DOCK7	53.8	53.71			SPSGSAFGSQENLR	S1438	PSGSAFGSQENLRWR
O14639	ABLIM1	61.59			45.23	STSQGSINSPVYSR	S452	RMIHRSTSQGSINSP
Q9P265	DIP2B	67.33	38.92			GTSGSLADVFANTR	S203	EVKGTSGSLADVFAN
Q9H0K1	SIK2	56.92		*48.09*		RASDTSLTQGIVAFR	S587	FREGRRASDTSLTQG
Q9NUL7	DDX28	59.51	*42.08*			GSFADLGLEPR	S127	RKLSSKGSFADLGLE
P48047	ATP5O	44.7	*47.42*			VKSLNDITAK	S91	KRSIKVKSLNDITAK
Q9UPN3	MACF1	*43.04*	*48.02*			RPTPTFHSSR	S7279	PTPTFHSSRTSLAGD
P52298	NCBP2	43.52			47.19	SDSYVELSQYR	S13	LKALRSDSYVELSQY
O60716	CTNND1	*37.19*	*47.3*			GSLASLDSLR	S346	LAQHERGSLASLDSL
Q01804	OTUD4		*46.18*		*31.11*	TPSQIIR	S416	KNLSRTPSQIIRKPD
P83731	RPL24				79.66	AITGASLADIMAK	S86	QRAITGASLADIMAK
Q6P597	KLC3				77.35	AMSLNTLNVDAPR	S466	AGMKRAMSLNTLNVD
Q9NSK0	KLC4	72.21				AASLNYLNQPSAAPLQVSR	S590	SNMKRAASLNYLNQP
Q16647	PTGIS			72.01		GSLSVGDKDHMCSVK	S232	GDKDHMCSVKSRLWK
Q9P0V3	SH3BP4	70.49				SYSLSELSVLQAK	S246	FRSKRSYSLSELSVL
P11586	MTHFD1	68.99				TDTESELDLISR	S765	AFKTDTESELDLISR
Q8IVT2	MISP	68.52				ALSSDSILSPAPDAR	S394	PGLRRALSSDSILSP
Q9Y3M2	CBY1	64.67				SASLSNLHSLDR	S20	TPPRKSASLSNLHSL
P67809	YBX1		64.01			NEGSESAPEGQAQQR	S176	EKNEGSESAPEGQAQ
Q9NQT8	KIF13B	63.93				SATLSGSATNLASLTAALAK	S1797	RSATLSGSATNLASL
Q96PK6	RBM14	62.72				TQSSASLAASYAAQQHPQAAASYR	S520	AAPYRTQSSASLAAS
P40818	USP8	57.57				SYSSPDITQAIQEEEKR	S719	KLKRSYSSPDITQAI
O00571	DDX3X		57.21			QSSGASSSSFSSSR	S609	YRQSSGASSSSFSSS
Q01813	PFKP	56.7				SFAGNLNTYK	S386	AVRLRGRSFAGNLNT
Q9Y223	GNE			*55.83*		SAEQHLISMCEDHDR	S170	SAEQHLISMCEDHDR
Q9H0K1	SIK2	55.51				ASDTSLTQGIVAFR	S590	GRRASDTSLTQGIVA
Q9Y2I7	PIKFYVE				53.01	SASITNLSLDR	S307	PARNRSASITNLSLD
P28290	SSFA2	52.94				SQSLPTTLLSPVR	S739	YPLRRSQSLPTTLLS
P36551	CPOX			*52.72*		CSSFMAPPVTDLGELR	S129	ELAHRCSSFMAPPVT
Q08380	LGALS3BP	52.08				YSSDYFQAPSDYR	S444	GPLVKYSSDYFQAPS

Q6UUV7	CRTC3	51.72			LFSLSNPSLSTTNLSGPSR	S370	SLRLFSLSNPSLSTT
Q07157	TJP1	51.21			SREDLSAQPVQTK	S617	SKRNLRKSREDLSAQ
Q9H0K1	SIK2	51.18			RPSTIAEQTVAK	T359	GRQRRPSTIAEQTVA
Q92974	ARHGEF2	49.92			SVSTTNIAGHFNDESPLGLR	T152	SLAKSVSTTNIAGHF
Q9H6H4	REEP4			49.52	SFSMQDLR	S152	AGRLRSFSMQDLRSI
Q9NQT8	KIF13B			*49.14*	RSISSPNVNR	S1381	KLSRRSISSPNVNRL
O95239	KIF4A	48.49			TFSLTEVR	S801	KLRRRTFSLTEVRGQ
P39023	RPL3	48.21			HGSLGFLPR	S13	FSAPRHGSLGFLPRK
P25705	ATP5A1	48.02			AVDSLVPIGR	S198	TGIKAVDSLVPIGRG
Q29RF7	PDS5A	48.01			STGTETGSNINVNSELNPSTGNR	T1162	PYVRSTGTETGSNIN
P78371	CCT2		*47.6*		TVYGGGCSEMLMAHAVTQLANR	S413	TVYGGGCSEMLMAHA
P42704	LRPPRC	45.57			SYVSEKDVTSAK	S1330	SLMKSYVSEKDVTSA
Q9HAU0	PLEKHA5	45.54			IVNVSLADLR	S382	ENKIVNVSLADLRGG
Q9Y446	PKP3	45.19			ADYDTLSLR	S180	RADYDTLSLRSLRLG
P26045	PTPN3			*45.05*	RSLSVEHLETK	S359	PAMRRSLSVEHLETK
P07900	HSP90AA1		*44.29*		ELISNSSDALDK	S52	LRELISNSSDALDKI
P62277	RPS13	44.02			GLSQSALPYR	S12	HAPGKGLSQSALPYR
Q15785	TOMM34	*43.85*			SSFADISNLLQIEPR	S280	ALKDYKSSFADISNL
Q9Y5P4	COL4A3BP			*43.78*	SSSMSSIDLVSASDDVHR	S380	SRSSSMSSIDLVSAS
Q9BVS5	TRMT61B		*43.15*		CGPTHQGSEDPSMLSQAQSATEVEER	T115	DQGRCGPTHQGSEDP
P30622	CLIP1		*42.98*		TASESISNLSEAGSIK	S193	SNLTKTASESISNLS
Q15477	SKIV2L	*41.87*			ASSLEDLVLK	S256	APLARASSLEDLVLK
Q1KMD3	HNRNPUL2	*41.31*			CDYMDEVTYGELEKEEAQPIVTK	T609	CDYMDEVTYGELEKE
P27816	MAP4	*40.54*			LATNTSAPDLK	S928	SRLATNTSAPDLKNV
P25705	ATP5A1	*39.8*			VLSIGDGIAR	S76	EETGRVLSIGDGIAR
P14625	HSP90B1		*39.28*		EESDDEAAVEEEEEEKKPK	S306	AKEEKEESDDEAAVE
Q76N89	HECW1		*39.09*		STSDTDLVTSDSR	S68	VTIPRSTSDTDLVTS
Q9H0K1	SIK2	*38.45*			ASDTSLTQGIVAFR	T592	RASDTSLTQGIVAFR
Q9H7P9	PLEKHG2	*38.37*			QLLGPNAAALSR	S1278	GPNAAALSRYLAASY
Q86W92	PPFIBP1			*37.39*	SQSTTFNPDDMSEPEFK	S601	GKLRRSQSTTFNPDD
Q6L8Q7	PDE12	*37.36*			CNMSLTHFFK	S533	EEERCNMSLTHFFKL
Q86W92	PPFIBP1	*36.83*			SSSLGNLKK	S466	SSLQKSSSLGNLKKE
Q6UUV9	CRTC1	*36.35*			SQYLQLGPSR	S48	ARLQLQKSQYLQLGP
P62701	RPS4X	*35.82*			LSNIFVIGK	S223	NSFATRLSNIFVIGK
Q96N67	DOCK7	*35.42*			SLSNSNPDISGTPTSPDDEVR	S900	RSRSLSNSNPDISGT
Q15678	PTPN14	*32.83*			GILHTDSQSQSLR	S465	HTDSQSQSLRNLNII
Q8TF72	SHROOM3	*31.85*			SAFSSLQNIPESLR	S664	KTKSAFSSLQNIPES
Q01850	CDR2	*31.02*			SSSETILSSLAGSDIVK	S310	RKPLKRSSSETILSS
Q8IVF2	AHNAK2	*30.7*			TFSTQIVR	S5497	LSVPRTFSTQIVRES
Q9Y305	ACOT9	*29.09*			IAFSSTSLLK	S244	KGRRIAFSSTSLLKM
P15924	DSP	*27.31*			ISTISSVR	S2598	SKISTISSVRNLTIR
P07437	TUBB	*26.7*			ALTVPELTQQVFDAK	T285	SQQYRALTVPELTQQ
Q8IZQ1	WDFY3	*24.05*			CLVSMTTPHDIR	S1027	TRVKCLVSMTTPHDI

APPENDIX III: MS/MS SPECTRA

PPP1R12A S445 (Score: 112.12)

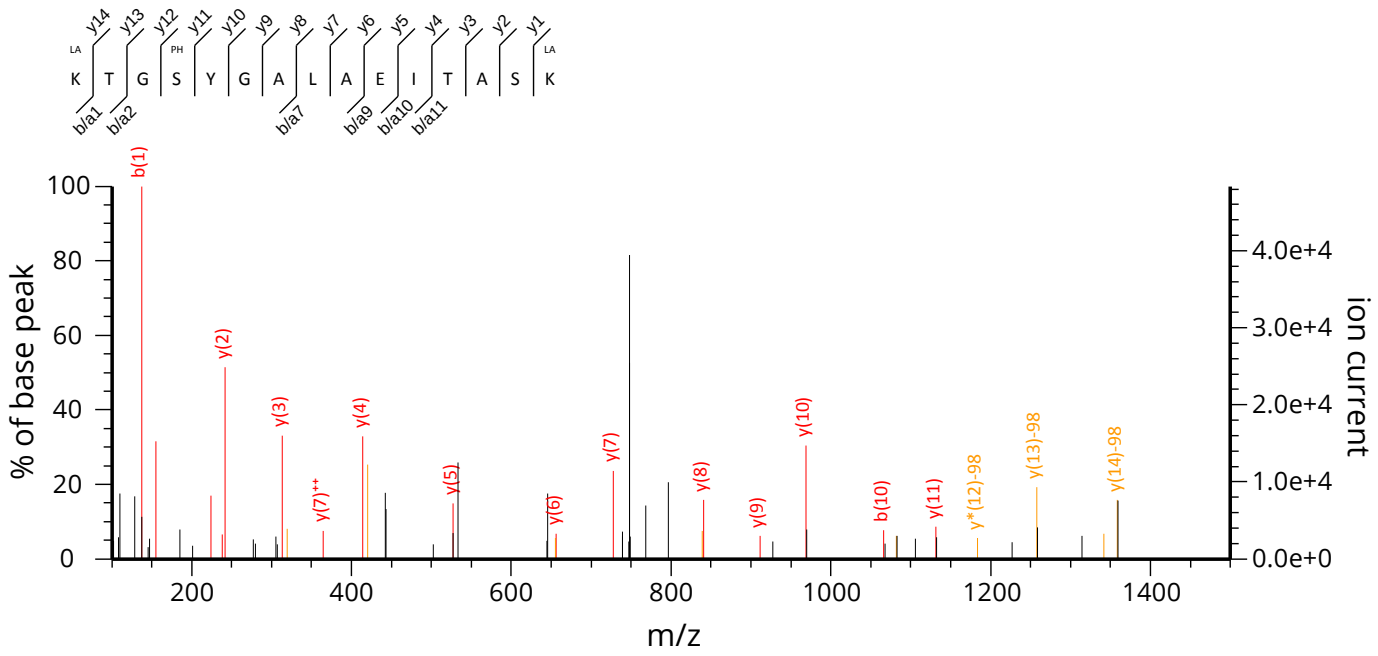

CLASP2 S370 (Score: 86.99)

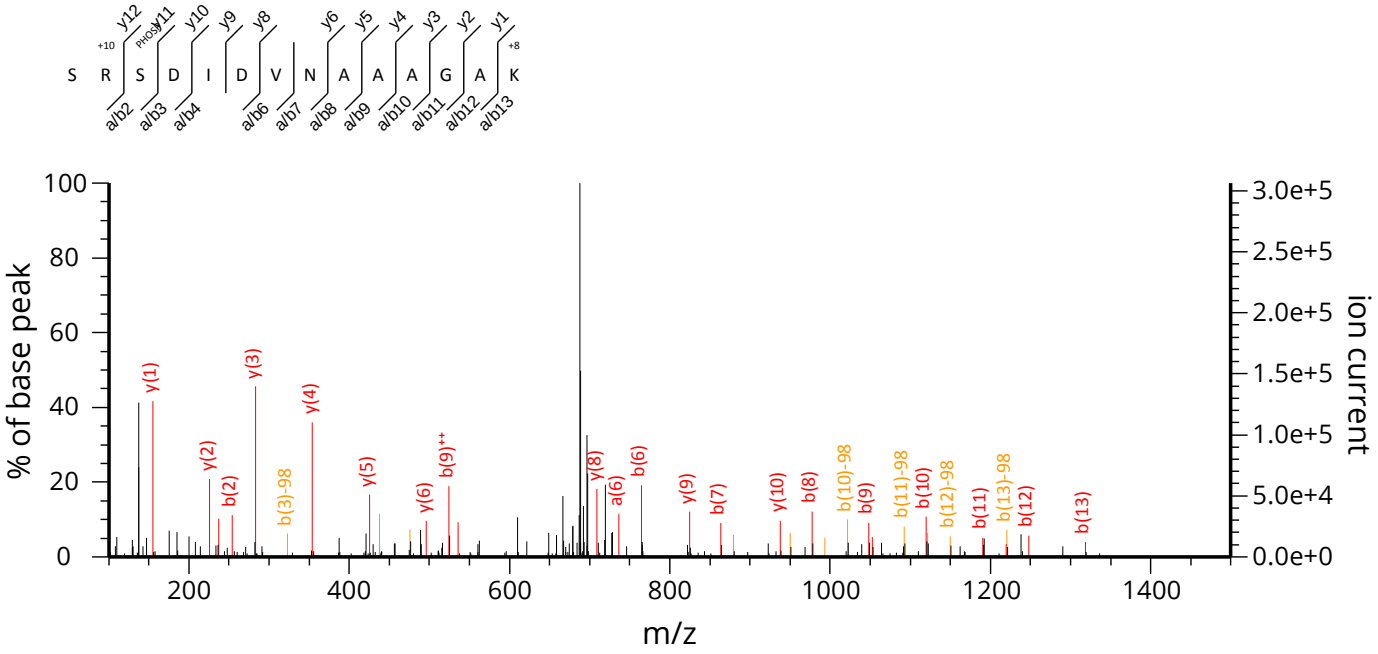

CTNND1 S268 (Score: 84.68)

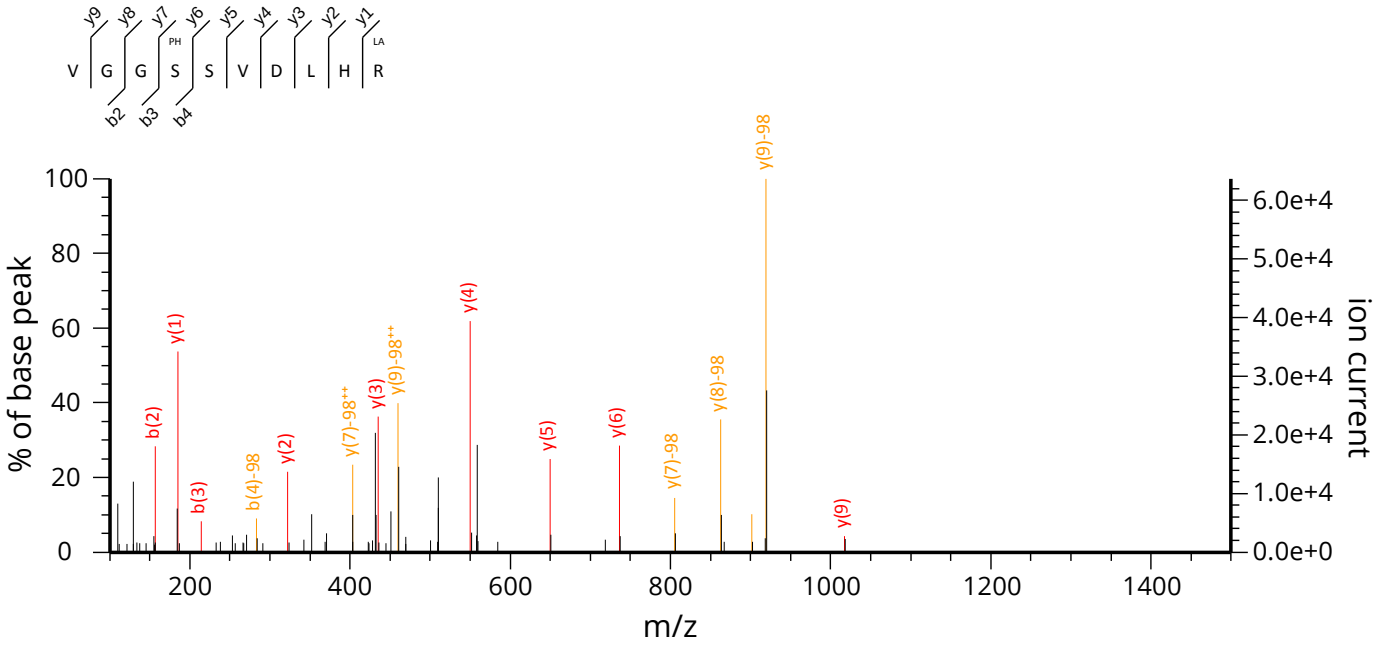

CLASP1 S600 (Score: 73.77)

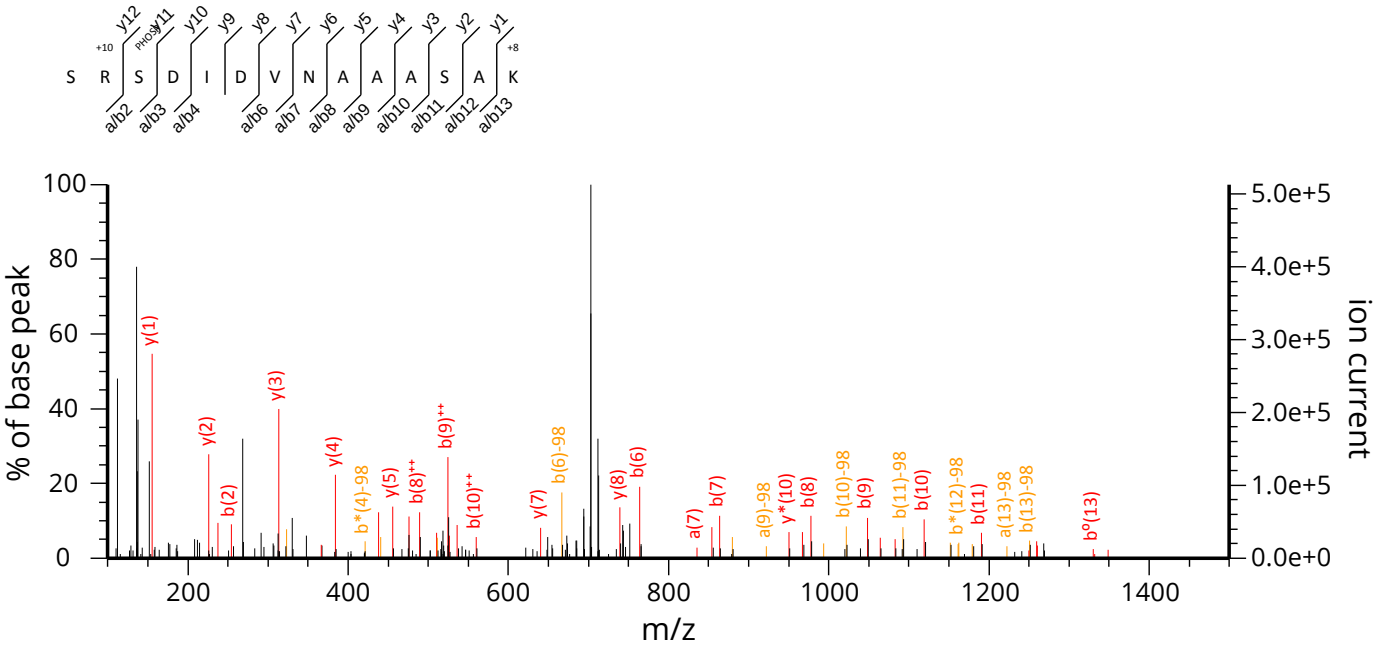

DSP S22 (Score: 64.33)

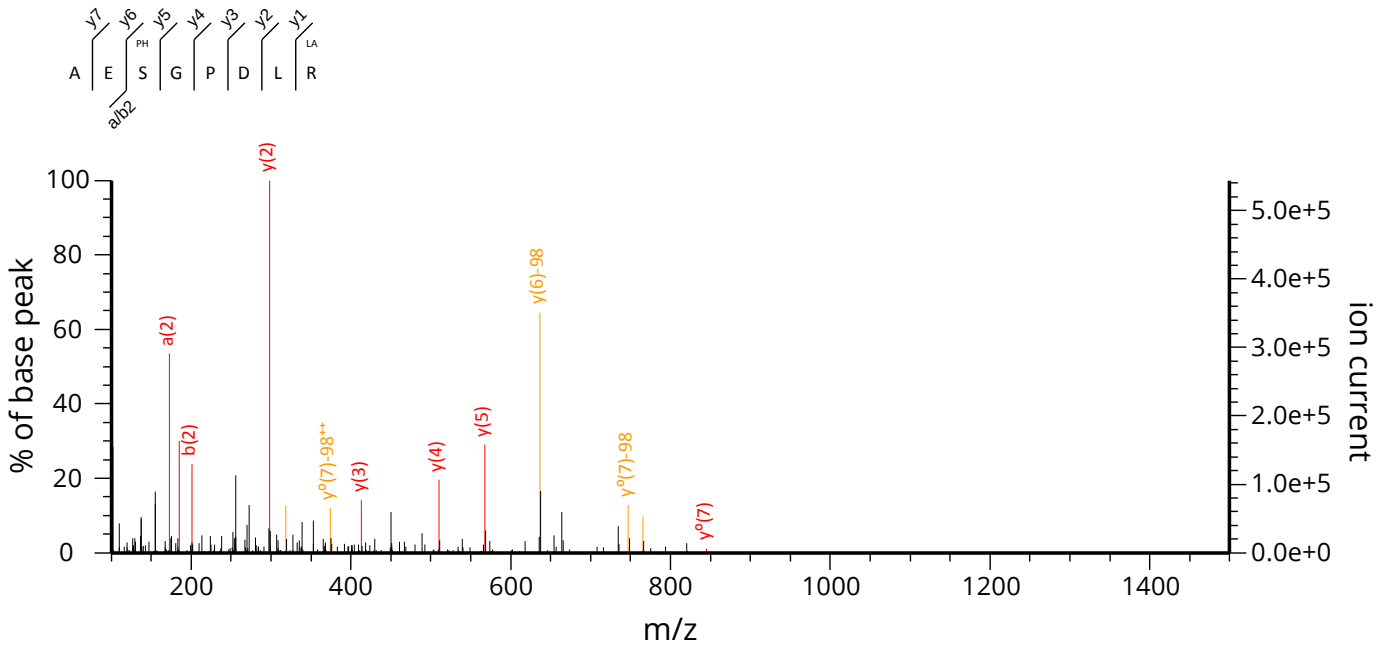

SIK2 S674 (Score: 85.23)

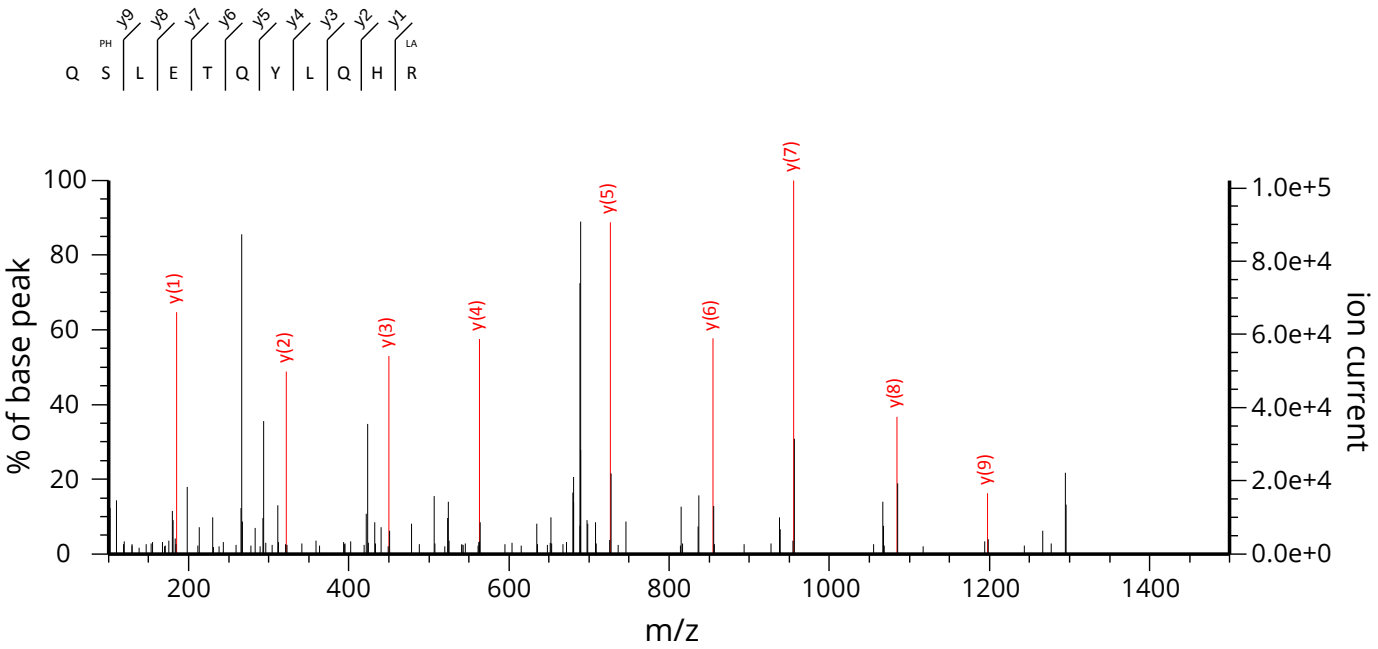

SIK2 S358 (Score: 53.59)

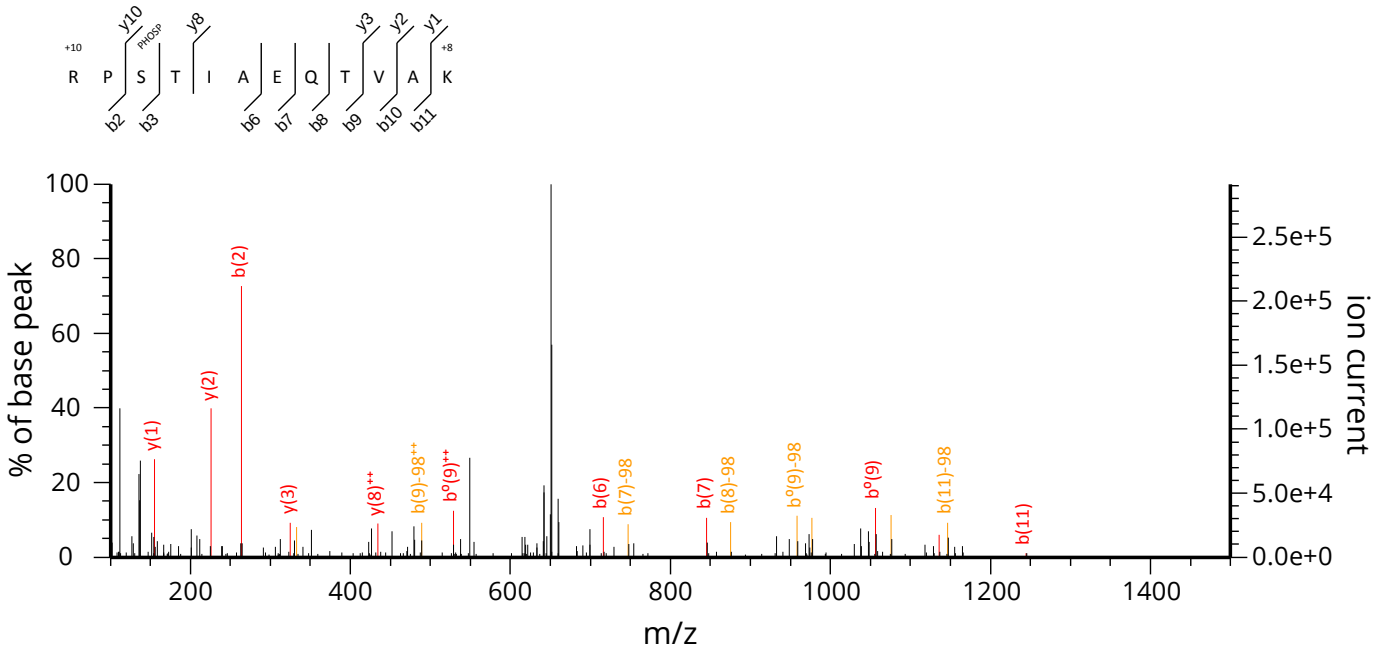

PIK3R1 S154 (Score: 76.43)

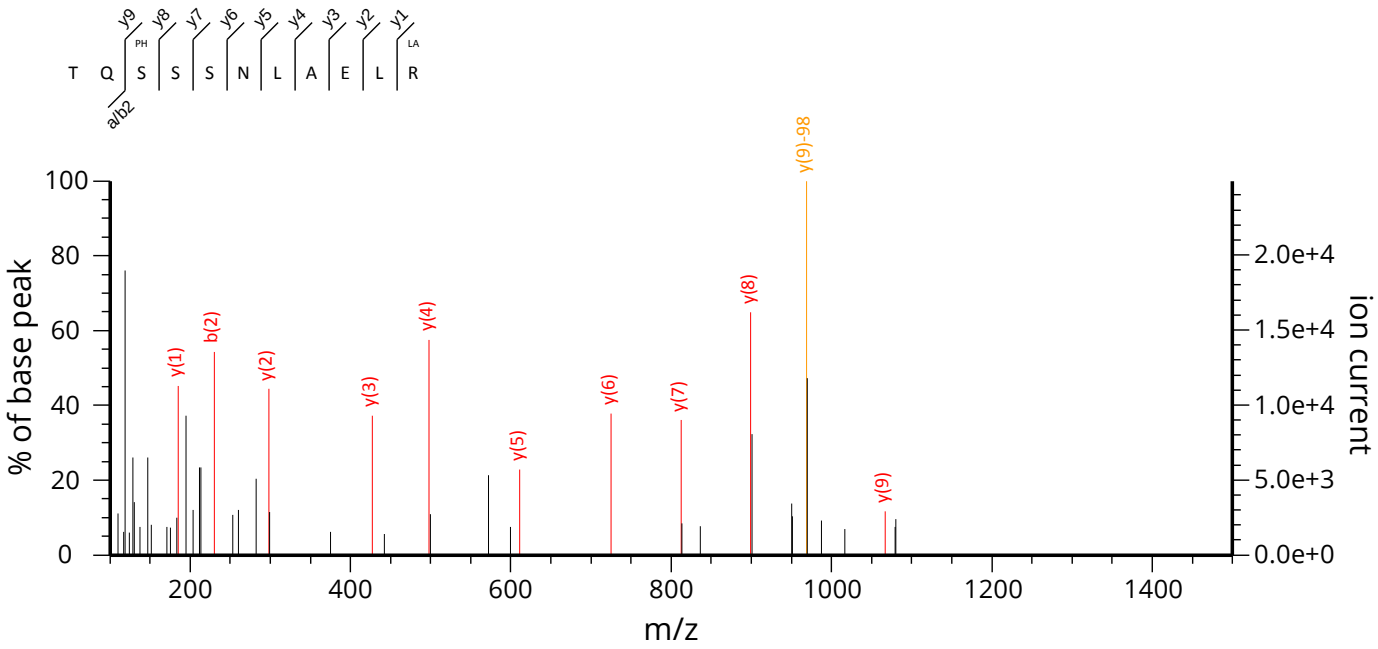

APPENDIX IV: GENE ONTOLOGY ANALYSIS

GO over-representation test (72 proteins)

GO biological process experimental only	Background	Screen	Expected	Fold Enrichment	+/-	*p*-value
regulation of microtubule polymerization or depolymerization	27	4	0.09	> 5	+	9.83E-03
mitotic spindle organization	30	4	0.1	> 5	+	1.49E-02
regulation of microtubule cytoskeleton organization	77	5	0.26	> 5	+	2.82E-02
regulation of microtubule-based process	93	6	0.32	> 5	+	3.40E-03
cell division	82	5	0.28	> 5	+	3.81E-02
microtubule cytoskeleton organization	175	7	0.6	> 5	+	9.44E-03
microtubule-based process	196	7	0.67	> 5	+	1.97E-02
mitotic cell cycle process	238	8	0.81	> 5	+	6.27E-03
mitotic cell cycle	250	8	0.85	> 5	+	9.00E-03
cytoskeleton organization	347	9	1.18	> 5	+	1.12E-02
single-organism organelle organization	832	14	2.84	4.93	+	2.84E-03
organelle organization	1193	19	4.07	4.67	+	4.67E-05
cellular component organization	1792	22	6.11	3.6	+	2.67E-04
cellular component organization or biogenesis	1832	22	6.25	3.52	+	3.94E-04
cellular process	5414	39	18.47	2.11	+	8.46E-04
single-organism process	4758	33	16.23	2.03	+	3.90E-02
biological_process	7531	47	25.69	1.83	+	1.04E-03
Unclassified	13283	24	45.31	0.53	-	0.00E+00

GO molecular function experimental only	Background	Screen	Expected	Fold Enrichment	+/-	*p*-value
microtubule plus-end binding	9	3	0.03	> 5	+	6.19E-03
tubulin binding	103	5	0.35	> 5	+	4.03E-02
poly(A) RNA binding	1106	18	3.77	4.77	+	3.18E-05
RNA binding	1209	19	4.12	4.61	+	2.07E-05
enzyme binding	1088	15	3.71	4.04	+	4.55E-03
nucleic acid binding	1790	19	6.11	3.11	+	8.29E-03
heterocyclic compound binding	2092	20	7.14	2.8	+	2.10E-02
organic cyclic compound binding	2135	20	7.28	2.75	+	2.82E-02
binding	9911	59	33.81	1.75	+	8.86E-07
protein binding	9227	54	31.47	1.72	+	7.40E-05
molecular_function	10809	59	36.87	1.6	+	5.49E-05
Unclassified	10005	12	34.13	0.35	-	0.00E+00

GO cellular component experimental only	Background	Screen	Expected	Fold Enrichment	+/-	*p*-value
ribonucleoprotein granule	70	5	0.24	> 5	+	3.58E-03
microtubule	136	8	0.46	> 5	+	1.88E-05
cytosolic ribosome	85	5	0.29	> 5	+	9.09E-03
ribosomal subunit	102	5	0.35	> 5	+	2.16E-02
ribosome	116	5	0.4	> 5	+	3.96E-02
cytosolic part	149	6	0.51	> 5	+	9.95E-03
focal adhesion	341	11	1.16	> 5	+	1.82E-05
cell-substrate adherens junction	341	11	1.16	> 5	+	1.82E-05
cell-substrate junction	344	11	1.17	> 5	+	1.99E-05
adherens junction	360	11	1.23	> 5	+	3.14E-05
anchoring junction	368	11	1.26	> 5	+	3.91E-05
cell junction	508	14	1.73	> 5	+	1.33E-06
ribonucleoprotein complex	352	8	1.2	> 5	+	2.12E-02
cytoskeletal part	711	11	2.43	4.54	+	2.19E-02
cell periphery	1584	19	5.4	3.52	+	7.68E-04
plasma membrane	1550	18	5.29	3.4	+	2.52E-03
membrane	3361	37	11.46	3.23	+	2.44E-09
intracellular non-membrane-bounded organelle	2024	19	6.9	2.75	+	2.64E-02
non-membrane-bounded organelle	2024	19	6.9	2.75	+	2.64E-02
macromolecular complex	2621	24	8.94	2.68	+	2.51E-03
cytoplasmic part	3320	30	11.33	2.65	+	9.55E-05
intracellular organelle part	4183	37	14.27	2.59	+	1.65E-06
cytoplasm	5114	45	17.44	2.58	+	4.01E-09
organelle part	4239	37	14.46	2.56	+	2.42E-06
nucleus	3933	30	13.42	2.24	+	3.85E-03
intracellular organelle	6316	47	21.54	2.18	+	4.02E-07
intracellular part	7307	53	24.93	2.13	+	9.73E-09
intracellular	7399	53	25.24	2.1	+	1.68E-08
intracellular membrane-bounded organelle	5764	40	19.66	2.03	+	2.90E-04
cell part	8052	54	27.47	1.97	+	1.29E-07
cell	8059	54	27.49	1.96	+	1.34E-07
organelle	7904	50	26.96	1.85	+	2.32E-05
membrane-bounded organelle	7440	47	25.38	1.85	+	1.38E-04
cellular_component	9832	60	33.54	1.79	+	5.91E-08
Unclassified	10982	11	37.46	0.29	-	0.00E+00

GO over-representation test (18 proteins)

GO biological process experimental only	Background	Screen	Expected	Fold Enrichment	+/-	*p*-value
negative regulation of wound healing, spreading of epidermal cells	3	2	0	> 5	+	1.21E-02
positive regulation of extracellular matrix disassembly	4	2	0	> 5	+	2.16E-02
positive regulation of basement membrane assembly involved in embryonic body morphogenesis	5	2	0	> 5	+	3.37E-02
regulation of basement membrane assembly involved in embryonic body morphogenesis	5	2	0	> 5	+	3.37E-02
regulation of wound healing, spreading of epidermal cells	5	2	0	> 5	+	3.37E-02
microtubule nucleation	6	2	0.01	> 5	+	4.85E-02
exit from mitosis	6	2	0.01	> 5	+	4.85E-02
negative regulation of cytoskeleton organization	50	3	0.04	> 5	+	4.21E-02
microtubule organizing center organization	51	3	0.04	> 5	+	4.47E-02
regulation of microtubule-based process	93	4	0.08	> 5	+	4.44E-03
Unclassified	13283	4	11.49	0.35	-	0.00E+00

GO molecular function experimental only	Background	Screen	Expected	Fold Enrichment	+/-	*p*-value
dystroglycan binding	7	2	0.01	> 5	+	2.36E-02
microtubule plus-end binding	9	2	0.01	> 5	+	3.90E-02
poly(A) RNA binding	1106	7	0.96	> 5	+	3.10E-02
Unclassified	10005	2	8.65	0.23	-	0.00E+00

GO cellular component experimental only	Background	Screen	Expected	Fold Enrichment	+/-	*p*-value
basal cortex	5	2	0	> 5	+	6.77E-03
cell cortex region	7	2	0.01	> 5	+	1.33E-02
kinetochore	75	3	0.06	> 5	+	2.82E-02
chromosome, centromeric region	91	3	0.08	> 5	+	4.99E-02
cell junction	508	6	0.44	> 5	+	2.34E-03
protein complex	2229	9	1.93	4.67	+	2.79E-02
macromolecular complex	2621	10	2.27	4.41	+	1.28E-02
intracellular organelle	6316	14	5.46	2.56	+	3.50E-02
intracellular part	7307	15	6.32	2.37	+	2.88E-02
intracellular	7399	15	6.4	2.34	+	3.41E-02
Unclassified	10982	2	9.5	0.21	-	0.00E+00